AD-A041 537 AIR FORCE INST OF TECH WRIGHT-PATTERSON AFB OHIO SCH--ETC F/G 20/6
THE THEORY OF DIFFRACTION FROM A HOLOGRAPHIC LENS.(U)
MAY 77 D D YOUNG

UNCLASSIFIED AFIT/DS/PH/76-4 AFAL-TR-76-270 NL

1 OF 3
AD
A041 537

AFAL-TR-76-270

AD A041537

THE THEORY OF DIFFRACTION FROM A HOLOGRAPHIC LENS

ELECTRO-OPTICS AND RECONNAISSANCE BRANCH
RECONNAISSANCE AND WEAPON DELIVERY DIVISION

MAY 1977

TECHNICAL REPORT AFAL-TR-76-270
FINAL REPORT

AU NO.
DDC FILE COPY

Approved for public release; distribution unlimited

DDC
JUL 11 1977
D

AIR FORCE AVIONICS LABORATORY
AIR FORCE WRIGHT AERONAUTICAL LABORATORIES
AIR FORCE SYSTEMS COMMAND
WRIGHT-PATTERSON AIR FORCE BASE, OHIO 45433

NOTICE

When Government drawings, specifications, or other data are used for any purpose other than in connection with a definitely related Government procurement operation, the United States Government thereby incurs no responsibility nor any obligation whatsoever; and the fact that the government may have formulated, furnished, or in any way supplied the said drawings, specifications, or other data, is not to be regarded by implication or otherwise as in any manner licensing the holder or any other person or corporation, or conveying any rights or permission to manufacture, use, or sell any patented invention that may in any way be related thereto.

This report has been reviewed by the Information Office (OI) and is releasable to the National Technical Information Service (NTIS). At NTIS, it will be available to the general public, including foreign nations.

This technical report has been reviewed and is approved for publication.

David D. Young

DANIEL D. YOUNG, CAPT., USAF
Project Engineer

Ronald N. Hubbard

RONALD N. HUBBARD, Chief
Reconnaissance Systems Group
E-O and Recon Branch

FOR THE COMMANDER

William A. Wallace

WILLIAM A. WALLACE, LT COL, USAF
Chief, Electro-Optics and Recon Branch
Recon and Weapon Delivery Division

Copies of this report should not be returned unless return is required by security considerations, contractual obligations, or notice on a specific document.

AIR FORCE - 28 JUN 77 - 75

SECURITY CLASSIFICATION OF THIS PAGE (When Data Entered)

REPORT DOCUMENTATION PAGE	READ INSTRUCTIONS BEFORE COMPLETING FORM
1. REPORT NUMBER: AFAL-TR-76-270	2. GOVT ACCESSION NO.
3. RECIPIENT'S CATALOG NUMBER	
4. TITLE (and Subtitle): THE THEORY OF DIFFRACTION FROM A HOLOGRAPHIC LENS.	5. TYPE OF REPORT & PERIOD COVERED: Final Report.
6. PERFORMING ORG. REPORT NUMBER: DS/PH/76-4	
7. AUTHOR(s): Daniel D. Young	8. CONTRACT OR GRANT NUMBER(s)
9. PERFORMING ORGANIZATION NAME AND ADDRESS: Air Force Institute of Technology (EFIT-EN) Wright-Patterson AFB, Ohio 45433	10. PROGRAM ELEMENT, PROJECT, TASK AREA & WORK UNIT NUMBERS: Project 20040527
11. CONTROLLING OFFICE NAME AND ADDRESS: Air Force Avionics Laboratory (AFAL/RWI-1) Wright-Patterson AFB, Ohio 45433	12. REPORT DATE: May 1977
	13. NUMBER OF PAGES: 210
14. MONITORING AGENCY NAME & ADDRESS (if different from Controlling Office)	15. SECURITY CLASS. (of this report): UNCLASSIFIED
	15a. DECLASSIFICATION DOWNGRADING SCHEDULE

16. DISTRIBUTION STATEMENT (of this Report)

Approved for public release; distribution unlimited.

17. DISTRIBUTION STATEMENT (of the abstract entered in Block 20, if different from Report)

18. SUPPLEMENTARY NOTES

This dissertation was presented to the Faculty of the School of Engineering of the Air Force Institute of Technology, Air University, in partial fulfillment of the requirements for the Degree of Doctor of Philosophy.

19. KEY WORDS (Continue on reverse side if necessary and identify by block number)

Holography
Diffraction Theory
Coupled Wave Equations
Holographic Lens Design

20. ABSTRACT (Continue on reverse side if necessary and identify by block number)

The objective of this effort was to apply diffraction theory to calculate the diffraction efficiency of a holographic lens in terms of the original geometry, exposure conditions, material parameter, processing effects, and reconstruction geometry.

The analysis was based upon a pair of coupled wave equations with variable coefficients of sufficient generality to permit the determination of the diffraction efficiency in cases where previous theories have been limited.

→ next page

DD FORM 1 JAN 73 1473 EDITION OF 1 NOV 65 IS OBSOLETE

SECURITY CLASSIFICATION OF THIS PAGE (When Data Entered)

012 225

20. ABSTRACT (Cont'd)

cont →

These cases include: (1) spherical object, reference, and reconstruction waves; (2) polarized reconstruction waves; (3) reconstruction wave vectors out of the plane of incidence of the construction wave vectors; (4) thickness changes of the hologram recording material due to processing; (5) gross changes in optical index to processing; (6) variations with position inside the hologram of the hologram parameters such as optical index, index modulation; (7) saturation of the index and absorptance modulation with exposure; and (8) absorption during exposure of the construction waves.

The JWKB approximation is used to solve the coupled wave equations with variable coefficients which describe the diffraction process. The boundary conditions for both a transmission and reflection hologram were applied to obtain particular solutions.

A closed form solution was obtained for the case of a transmission hologram by the trapezoidal approximation. Good agreement was obtained between the experimentally measured diffraction efficiency and the theoretically calculated diffraction efficiency.

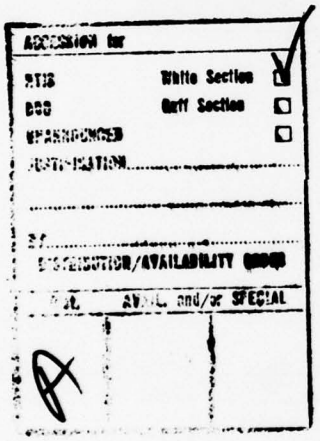

DDC
JUL 11 1977
D

PREFACE

This dissertation represents an effort to relate theoretically the diffraction efficiency of a holographic lens to measurable apriori parameters describing the holographic construction and reconstruction geometry, the construction exposure, and the holographic recording material. The concept has proven to be successful.

The author wishes to thank Dr Harold Rose, of the Air Force Avionics Laboratory (AFAL), who furnished daily guidance and advice during this research effort. His original suggestion, "There is a fruitful area of research here somewhere, go find it!", has proven to be correct. His assistance and timely suggestions are greatly appreciated.

This author's gratitude is extended to Dr Donn G. Shankland, of the Air Force Institute of Technology, who greatly aided this worker during this effort. His suggestion of the JWKB approximation and his reminder, "that only gradients of phase are important (Dummy)", have proved to be invaluable to the accomplishment of this task.

Thanks is also extended to Dr Tom Williamson, of AFAL, whose suggestions and philosophical comments regarding coupled wave theory and holographic recording material parameters were of great aid.

A special note of appreciation is due to Dr B. J. Chang of the Environmental Research Institute of Michigan. His permission to include in this disseration some of his data concerning the diffraction efficiency

of dischromated gelatin holograms was very thoughtful. Also, the several discussions with him concerning processing effects in dichromated gelatin were very enlightening.

Thanks is also extended to my fellow workers at AFAL, who were always found to be willing to listen to ideas presented to them. A partial list of those helpful people includes: Dr Dave Flannery, Dick Lane, Andy Grandjean, and Charlie Bond. Dr Flannery's suggestion that I read a paper on a "Unified Theory of Ultrasonic Light Diffraction" by Klein and Cook (Ref. 20) proved to be extremely helpful. Mr Lane's constant willingness to aid with and make suggestions to improve my programming of the HP 9820 calculator is most appreciated. Mr Grandjean's steady support and encouragement throughout this effort were greatly appreciated, especially on those days when nothing seemed to be going right. Finally, thanks is extended to Charlie Bond, of Systems Research Laboratories, whose outstanding laboratory and experimental abilities are greatly appreciated by this author. Much of the data appearing in Appendix F, concerning the measurement of holographic parameters for bleached Kodak 649-F holograms was taken with Mr Bond's assistance.

Gratitude is also given to the management of AFAL who has supported this effort. Dr William Eppers, Col Charles Hudson, Ed Deal, Harold Geltmacher, and Ronald Hubbard have been most understanding of the unique problems and requirements of the doctoral student.

The author wishes to thank Susan Miller who must be the most competent secretary in the Air Force. Her speedy and accurate typing of this dissertation is greatly appreciated.

This author wishes to express his gratitude to his wife, Sally Sue Young. Her patience, understanding, and encouragement during the many months required to complete this dissertation merit this author's highest expression of appreciation. Finally, thanks is extended to my son, Matthew, who arrived in the middle of this effort and who has, somehow, managed to be patient in his demands for my attention.

Preceding Page BLANK - NOT FILMED

CONTENTS

CONTENTS (Cont'd)

CONTENTS (Cont'd)

LIST OF FIGURES

LIST OF FIGURES (Cont'd)

LIST OF TABLES

SUMMARY

The objective of this effort was to apply diffraction theory to calculate the diffraction efficiency of a holographic lens in terms of the original construction geometry, exposure conditions, material parameters, processing effects, and reconstruction geometry.

The analysis was based upon a pair of coupled wave equations with variable coefficients of sufficient generality to permit the determination of the diffraction efficiency in cases where previous theories have been limited. These cases include: (1) spherical object, reference, and reconstruction waves, (2) polarized reconstruction waves, (3) reconstruction wave vectors out of the plane of incidence of the construction wave vectors, (4) thickness changes of the hologram recording material due to processing, (5) gross changes in optical index due to processing, (6) variations with position inside the hologram of the hologram parameters such as optical index and index modulation, (7) saturation of the index and absorptance modulation with exposure, and (8) absorption during exposure of the construction waves.

The JWKB approximation was used to solve the coupled wave equations with variable coefficients which describe the diffraction process. The boundary conditions for both a transmission and reflection hologram were applied to obtain particular solutions.

A closed form solution was obtained for the case of a transmission hologram by the trapezoidal approximation. Good agreement was obtained between the experimentally measured diffraction efficiency and the theoretically calculated diffraction efficiency as a function of exposure for dichromated gelatin holograms. Also, excellent agreement was obtained between theory and the epxerimentally measured diffraction efficiency response to reconstruction wave polarization changes for Kodak 649-F silver halide holograms. Strikingly different theoretical results were predicted for dichromated gelatin holograms, but experimental verification has not been attempted.

It was concluded that the application of the JWKB approximation to obtain a solution of the equations which describe the diffraction of light by a holographic lens was successful. An equation for the diffraction efficiency in terms of the apriori characteristics of (1) the exposure conditions, (2) the holographic recording material parameters, (3) the construction geometry, (4) the processing effects, and (5) the reconstruction geometry. The theory provides a basis for the capability to perform a holographic lens design starting with the desired operational characteristics of the lens and ending up with the proper construction conditions, exposure conditions, and recording material parameters required to make the lens.

CHAPTER I

INTRODUCTION TO THE THEORY OF THE HOLOGRAPHIC LENS

A. Setting the Perspective - The Holographic Lens

A holographic lens is a diffraction grating created by the holographic process expressly for use as a lens in an optical system. The holographic lens is formed by the exposure of a photo-sensitive recording material to the interference intensity pattern or a spherical wave (the object wave) and another plane of spherical wave (the reference wave). The photo-sensitive material is developed and processed after exposure to become a holographic lens.

The recorded fringe structure present in the hologram acts as a three dimensional diffraction grating. The diffraction efficiency of a holographic lens is the ratio of power diffracted into the object wave measured at the output surface of the hologram to the power in the reconstruction wave incident upon the input surface of the hologram (Ref. 37).

Modern holographic lenses have diffraction efficiencies as high as 95% and offer several unique features in optical designs over conventional optical elements (i.e., refractive or reflective optics composed of planar or spherical surfaces). For example, a conventional convex refractive lens causes an incident plane wave propagating parallel to the optical axis of the lens to be brought to a focus at a focal point on the optical axis. The holographic lens has the

advantage that the focal point need not lie on the optical axis as shown in Figure 1.

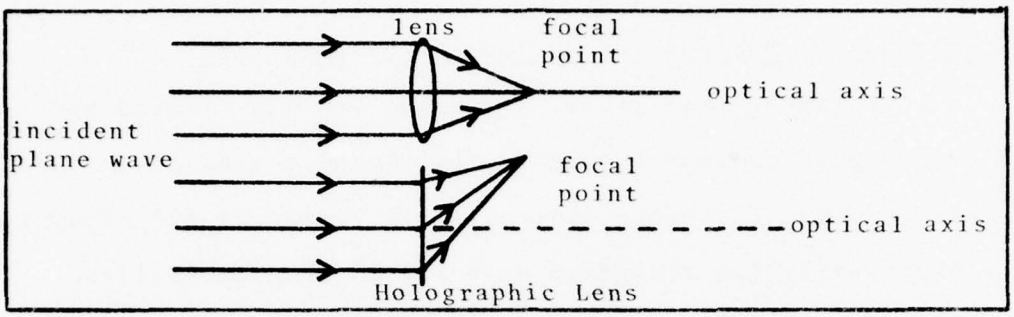

Figure 1. Comparison of Conventional Lens to Holographic Lens

In order to accomplish the same off-axis focal point design with conventional optics, an additional reflective surface or refractive prism would be required. Therefore, the capability to design optical systems using off-axis holographic lenses is a significant advantage if small, compact, short focal length optical systems are of concern.

The holographic lens possesses a greater chromatic dispersion than a conventional refractive lens because of its diffractive nature. Consequently, the holographic lens acts as a chromatic filter bringing to focus only light in a very narrow spectral region. This is an important consideration if the reduction of undesired background radiation is a design goal or if a simple spectral analysis of the collected light is of importance.

B. The Problem

In order to design a conventional optical system, a knowledge of the reflection, refraction, and transmission laws of geometrical optics is required. Based on these laws, the direction of the light rays may be traced throughout the optical system and the optical efficiency of each ray may be determined from the transmission and absorption properties of the optical elements of the system. From this knowledge an optical system design is determined. The situation is not as simple in the case of holographic optics. In this case the propagation of rays through the optical system is based upon the laws of diffraction which are more difficult to apply.

It is often a matter of trial and error to design the appropriate holographic lens for a specific application because of deficiencies in our present capability to theoretically determine the hologram diffraction efficiency. Two parameters are required in order to ray-trace design and determine the optical efficiency of a holographic lens system: (1) the direction of the ray, and (2) the transmission of that ray through each lens of the system. The direction of the ray is determined by Snell's Law and the local Bragg conditions of the ray. The transmission of the ray is determined by the diffraction efficiency of the ray at its coordinates on each holographic lens. What is lacking is an accurate theory for determining the diffraction efficiency

of a ray at a given position on the hologram in terms of the original exposure, construction geometry, recording material parameters, and the reconstruction conditions.

It is the purpose of this work to determine the diffraction efficiency of a holographic lens in terms of the original exposure, construction geometry, recording material parameters, processing effects, and reconstruction geometry. This allows not only an increased capability to design a holographic lens, but the exposure level, the material parameters, and the construction geometry necessary to produce that lens can be determined. A knowledge of these constraints will allow an assessment to be made of the practicability of the lens.

C. Background

Previous theories relating to the determination of the diffraction efficiency of a hologram abound, but they are sufficiently general and limited in their applicability that practical assessments of hologram diffraction efficiency based upon these theories are not possible. A detailed review of previous diffraction theories for the hologram is contained in Chapter II. This section contains a discussion of the limitations and oversights of these theories. These deficiencies are: (1) the spherical nature of the construction and reconstruction waves, (2) the relationship of the diffraction efficiency to the exposure level and construction geometry, (3) the change in emulsion thickness, optical index,

and absorption coefficient due to development processes, (4) the polarization of the construction and reconstruction waves, (5) the reconstruction wave vector being out of the plane of incidence of the construction wave vectors, (6) the absorption of the construction waves, and (7) the saturation of the photo-sensitive response of the recording material to exposure.

1. Spherical Wave Effects. The holographic lens is formed by at least one spherical wave (the object beam) and one plane or spherical wave incident upon the recording material during the construction process. Often the spherical object wave is formed by diffraction through a pin hole located very close to the recording material plate. Therefore, the interference pattern which illuminates the plate during construction possesses a curvature of field and varies in intensity across the surface of the plate and with depth. A holographic lens is not composed of linear, periodic, planar, uniform, fringes as a consequence. For this reason, previous theories which assume planar-sinusoidal gratings for the hologram are only applicable on a localized basis.

In a holographic lens one cannot assume plane waves. Spherical object, reference, and reconstruction waves must be considered which, of course, should reduce to the plane wave case if the radius of curvature is large or if one is sufficiently "localized".

2. Relation to exposure level and construction geometry.

No previous theories have related the final hologram diffraction efficiency to the original exposure level and construction geometry. Most theories relate back to the absorption modulation and index modulation in the hologram, but contain no information as to how this modulation was created. Therefore, the calculation of the diffraction efficiency based upon these theories cannot be related to the exposure and construction conditions. Consequently, the practicability of the construction of a hologram design cannot be assessed.

3. Changes in the emulsion due to development.

Effects upon the holographic recording material due to processing have not been addressed in previous published theories. If the recording material is a photographic emulsion, for example, expansion or shrinkage of the emulsion during processing changes the thickness and orientation of the holographic diffraction grating fringe structure upon reconstruction. In addition, the bulk refractive index and absorptance of the photographic emulsion usually changes during processing due to fixing, hardening, and the removal of photochemical compounds. It may be inferred from these effects that the reconstruction of the object from the original reference beam coordinates cannot be optimum. These effects must be included in any practical theory.

4. Polarization of the reconstruction and construction waves. The polarization of the construction beams must be considered, since only parallel components will interfere during the construction process. The optical index modulation depth will be dependent upon the polarization of the object and reference beams. Also, the polarization of the reconstruction wave must be considered in order to accurately predict the diffraction efficiency of the holographic process.

5. Reconstruction out of the original plane of incidence. The fact that the reconstruction wave vector is not necessarily in the plane of incidence of the original construction wave vectors needs to be considered theoretically. This has been a limitation in all previous published theories. Certainly, this is a severe limitation in terms of holographic lens design and it needs to be corrected.

6. The absorption of the construction waves. According to the photochemical law, known as the Grathus-Draper Law, radiation must be absorbed by any system to produce a photochemical reaction in that system (Ref. 33). In all photochemical processes used in holography, that absorption is quite strong (e.g., 50% absorption in films of 15μ thickness). Therefore, the absorption of the construction beams during the original construction process is very important. The absorption leads to a decrease in both the bulk optical index and the optical index modulation with depth in the processed hologram. Therefore, the characteristics

of the surrounding optical index and the coupling efficiency of the hologram are variable and decrease with depth into the emulsion. Indeed, the processed hologram is inhomogeneous. The same effects occur for the absorption and absorption moduation of the hologram.

The absorption of the construction waves must be accounted for by any accurate theory of hologram diffraction efficiency. It will be seen that this effect leads to a set of coupled differential equations which have variable coefficients.

7. Saturation of emulsion response. Saturation effects are of importance also. In any photochemical process there is a photo sensitive substance in limited quantity (usually <10% by volume), which is typically homogeneously suspended in an emulsion. If the incident light is of sufficient stregnth, the substance is exhausted by the continuous photon absorption and any further exposure is of little consequence. Also, the index modulation may saturate due to physical process, as in dichromated gelatin. The saturation effect must be considered in any event.

In short, the effects listed above have not in totality been considered by any single previously published theory of holographic diffraction. Bits and pieces of many of these effects have been addressed by various workers using a variety of unrelated approaches as is discussed in the next

chapter. The totality of these effects must be addressed in a unified theory.

No theory exists such that in practice one can predict the absolute diffraction efficiency at a given point on the surface of a holographic lens from the known characteristics of the: (1) exposure conditions, (2) the emulsion parameters, and (3) the reconstruction conditions. The purpose of this work is to provide a simple analytical solution which can accurately predict the efficiency of a holographic lens based on measurable exposure, emulsion, and reconstruction parameters. The approach is discussed in the next section.

D. Possible Approaches

Any approach, of necessity, would start from Maxwell's equations since these are the equations which descirbe the diffraction of light. From them, one may proceed in two directions in order to calculate the electric field amplitude of the diffracted light, (1) to an integral equation, or (2) to a differential equation. Both represent solutions to the same problem.

The differential equation approach yields the well known wave equation and ultimately the set of two coupled-wave equations as derived by Kogelnik (Ref. 21). The equations in that form allow for full depletion of the incident light and have previously been successful when applied to the ideal sinusoidally modulated, dielectric grating (Ref. 21).

The wave equation may be changed to an integral equation using Green's functions or Fourier Transforms. These integral equations usually are solved by an approximation technique, such as the first Born approximation, which requires weak depletion of the incident light as a limiting assumption. This limitation clearly does not apply to modern holographic elements for which as much as 95% of the incident light is depleted.

The scattering theory developed by Williamson overcame this limitation of the integral equation approach by considering the emulsion as a volume of small, similar, single particle scatterers which have a probability density function related to the original exposure intensity. The integral equation for the total scattered field became the three-dimensional integral sum of the contributions to the total field of each individual dipole scatterer. Since the contribution of each scatterer was identical except for phase, and since the phase was dependent upon a coordinate-separable, periodic, position probability density function, the three-dimensional integral was separated into the product of three ordinary integrals which were evaluated using the Array Theorem. The result was shown to be equivalent to that of the Kogelnik coupled wave solution for a specific range of particle sizes (Ref. 44).

Therefore, both the integral equation approach and the differential equation approach to the solution of the wave equation have been successful when applied to the ideal, sinusoidally modulated, dielectric grating. This being the case, the choice between the two approaches rests upon matters related to familiarity of mathematical techniques.

E. Choice of Approach

The differential equation approach was chosen as a basis for analyzing holographic diffraction in this dissertation. A set of two coupled wave equations with variable coefficients was derived and shown to be applicable to the diffraction of light by a holographic lens. The choice of the differential equation approach was made because of the applicability of the JWKB approximation to the solution of the equations in differential form.

F. An Overview

The main body of this report is devoted to a derivation and evaluation of the results of the JWKB approximation solution to the set of two coupled wave equations which describe holographic diffraction. An integral equation technique using Green's functions is presented for comparison in Appendix G.

The analysis is sufficiently general and unified to permit the determination of the diffraction efficiency of a

holographic lens for the totality of the cases in which the limitations of previous theories have precluded the calculation.

A detailed review of previous hologram diffraction theories and their assumptions and limiations is presented in Chapter II. Chapter III contains a derivation of a set of two coupled wave equations for the holographic lens. In Chapter IV, these equations are reduced to a single second order differential equation to which the JWKB approximation is applied. This results in a general solution to the holographic lens diffraction problem. Specific boundary conditions for a transmission and a reflection hologram are applied and a comparison is made to previous theories. An evaluation of the theory for a transmission hologram and a comparison to experimental results is contained in Chapter V. It is shown that the theory accurately predicts experimental results for which previous theories have not been sufficiently general to explain. Conclusions and recommendations are in Chapter VI.

CHAPTER II

REVIEW OF THE STATE OF THE ART IN HOLOGRAM DIFFRACTION THEORY

A good review of the state of the art of the diffraction theory of holograms is given by Kogelnik (Ref. 21). This chapter summarizes Kogelnik's review, with additions to include more recent work.

Leith (Ref. 30) and others analyzed the effect of emulsion thickness on the optical characteristics of the reconstructed image. The sensitivity of the image to changes in the reconstruction wave vector angle of incidence and in the reconstruction beam wavelength was determined from the scalar Kirchhoff diffraction integral. A first-order perturbational approach was used in which the diffraction integral was reduced to a line integral. This integral was integrated along a straight line of continuous scattering centers. It was shown that the integral solution was equivalent to a first-order solution of the wave equation by a discrete expansion in plane waves at the Bragg frequency. Experimental verification of these predictions was also published, but no information about the diffraction efficiency was obtained.

Gabor and Stroke (Ref. 15) solved the wave equation in a periodic emulsion possibly formed by the interference of plane waves, (i.e., a holographic grating) by using Green's functions to yield an integral equation. They obtained a

first-order solution by using the first Born approximation. This yielded interfering, secondary, scattered, spherical wavelets from which the angular and wavelength sensitivity of the hologram was investigated.

The theory of Gabor and Stroke, as well as Leith's, yielded no diffraction efficiency information because of the basic assumption that the incident light was weakly depleted by the diffraction process. For high diffraction efficiencies (>95%) observed in modern holograms, the incident wave is strongly depleted and theoretical approaches which allow for incident wave depletion are required.

One such approach is to use the electronic computer to solve the relevant electromagnetic equations accurately. Burckhardt (Ref. 3 and 4) has done this for the diffraction of a plane wave from a sinusoidally stratified dielectric material by an expansion in plane waves after a separation of variables. The expansion was substituted into the wave equation which yielded an infinite set of coupled wave equations. By truncating this set, a matrix eigenvalue problem was obtained. The solution was presented for both types of electric field polarizations. It was shown that the amplitude of the diffracted wave has a maximum if the reconstruction beam is at the Bragg angle. The amplitude of the first-order diffracted wave was computed as a function of

hologram thickness and dielectric modulation depth. It was shown that diffraction efficiencies of 100% are possible for the correct thickness and dielectric modulation depth. This was possible because the theory ignored losses.

The basis of the Burckhardt approach is similar to the generalized theory of Raman and Nath on the ultrasonic diffraction of light (Ref. 38 and 39). An excellent modern review of ultrasonic diffraction if given by Klein and Cook (Ref. 20). Many authors (Ref. 21, 3, 4, 8, 9, 10) have solved the problem of the holographic grating by using the Raman-Nath approach. In these cases, the wave equation is solved by expanding the electric field in the medium in an infinite sum of plane waves which have phase terms which are spatial frequency harmonics of the Bragg frequency. Each harmonic corresponds to a Fraunhoffer diffracted order and the approach leads to a truncated set of coupled linear differential equations. In all cases the equations apply to a dielectric holographic grating (possibly lossy) consisting of fringes which might have been formed originally from plane waves and illuminated by plane waves upon reconstruction.

If two of the wave equations considered in the Raman-Nath approach are kept, it is called coupled wave theory and analytical soultions are possible. Kogelnik (Ref. 21) used coupled wave theory to predict the first-order diffraction efficiency of an ideal, lossy, sinusoidal dielectric grating.

This is the classic paper on the theory of dielectric gratings and explains the sensitivity of hologram diffraction efficiency to changes in the angle of incidence of the reconstruction wave vector and in the wavelength of the reconstruction wave. The diffraction efficiency is related to the refractive index modulation and absorption modulation of the hologram.

In the Kogelnik theory, only two significant light waves are assumed to exist in a sinusoidally modulated medium, an incoming wave and an outgoing wave. The assumption that these waves approximately obey the Bragg condition limits the validity of the theory to thick holograms. The electric field at any point in the emulsion is taken to be the linear sum of the electric field of the two waves. This sum, when substituted into the wave equation, yields two coupled second-order differential equations which are linearized and solved in closed form for the diffracted field amplitude. The resulting general expression is valid for all types of thick, ideal, holographic gratings including cases of off-Bragg incidence, of lossy gratings, and of slanted fringes. This classic theory is a simple technique to predict the intensity and direction of the diffracted wave provided certain conditions and assumptions hold. These are: (1) near-Bragg angle incidence of monochromatic plane waves polarized perpendicular to the plane of incidence of the original object and reference beams, (2) the hologram fringes lie in a plane perpendicular to the plane of incidence

and are represented by a constant fringe-wave-vector lying in the plane of incidence, and (3) the medium in which the waves propagate has a sinusoidally modulated wave propagation constant. No mention was made as to how these assumptions are met in practice.

Carrying the coupled wave approach one step further, Chang and George (Ref. 8, 9, 10) solved four second-order coupled wave equations (via a computer) in order to consider holograms which were too thin to meet the Bragg condition, so that two coupled waves were no longer accurate. They solved for the zero, first, and second-order diffracted field amplitude via the Raman-Nath formalism modified for lossy dielectric periodic gratings. Graphs were prepared showing the diffraction efficiency into the first-order versus the index modulation for a range of thicknesses and losses. Experimental results verified the theory.

Recently, Su and Gaylord (Ref. 41) have extended the coupled wave approach to a method for determining the arbitrary-order diffraction efficiency of thick, lossless transmission gratings with arbitrary periodic grating shapes. That is, their work covers idealistic analytical grating such as saw-tooth gratings (non-sinusoidal but still periodic). The fringe planes were assumed to be perpendicular to the plane of incidence.

Also, Uchida (Ref. 43) has analyzed a sinusoidal grating with an index modulation that exponentially decreases along the direction perpendicular to the grating vector using Kogelnik's coupled wave theory. The general solutions of the coupled waves were given for transmissive and reflective holograms. The solutions were compared to the Kogelnik case in which the index modulation was a constant. Kermish has also derived the expression for the diffraction efficiency of a grating with a decreasing exponential index of refraction (Ref. 19). These derivations were only valid at Bragg angle reconstruction.

Latta (Ref. 26, 27, 28) has used Kogelnik's results to formulate a computer based analysis of thick, periodic holograms using ray tracing. This program allows for the direction and relative phase of any ray to be calculated. Further, the program analyzed up to 5th-order aberration effects of holographic optical elements. The program uses the Kogelnik theory to compute the diffraction efficiency, hence, it is limited to the same constraints as that theory.

Williamson (Ref. 44), and to some extent Matthews (Ref. 32) and Chang and George (Ref. 8, 9), have considered the emulsion as a volume of small, similar, single particle scatterers (i.e., radiating dipoles) with a phase relationship dependent upon their spatial relation to the reconstruction beam. Williamson assumed the position of each particle was a random variable with a three-dimensional probability density

function of the same form as the intensity pattern that was recorded during the exposure. His work holds rigorously only for planar fringes for which the probability density for the position of a scatterer after processing is coordinate separable. In such a case, the total scattered field is the product of the three coordinate integrals from a linear array of scatterers along each coordinate. Provided the effects of particle size are not important, the solution is equivalent to the Kogelnik results. The technique is more powerful in that multiple-exposures are more easily considered. Also, the scattering theory approach allows for the first time the direct inclusion of film parameters into the theory.

Case (Ref. 5) has extended the coupled wave diffraction theory to include double exposure holographic gratings for the geometry in which the two gratings have a common central Bragg angle. This theory involves the solution of three-coupled wave equations. Saturation of the index modulation response to exposure is included in this theory and experimental measurements of this response for dichromated gelatin holograms were obtained.

The method of thin-grating decomposition, based upon concepts used in coherent optics to treat propagation in discrete systems, was used by Alferness as an approach to the wave propagation in periodic modulated media (Ref. 1). In this method, thin gratings were used as building blocks in order to determine the response of thicker gratings.

The approach was similar to that of Williamson. In the Williamson theory, the building block was the diffracted field amplitude from a single particle, in the Alferness theory the building block was the diffraced field amplitude of a thin grating. As a consequence, the Alferness theory of thin-grating decomposition was limited to planar fringes. The concept of propagation in a medium with non-uniform modulation was treated as a sequence of thin gratings each having a constant, but slightly different, index modulation.

Recently, Kogelnik has analyzed the wavelength selectivity of reflection gratings that have a slowly varying modulation or fringe spacing (Ref. 22). His intent was to determine modulation profiles that cause suppression of the high sidelobes characteristics of reflection gratings. Such suppression is significant in applications in which wavelength rejection is a consideration. He showed that the coupled wave equations reduce to a single non-linear Riccati equation which must be evaluated numerically.

In conclusion, it can be said that all published theories of holographic diffraction to date have been limited in their applicability to describe the total holographic process.

Some theories have addressed non-uniform modulation (Ref. 43, 19, 22), but these theories have not related this non-uniform index modulation to the construction geometry or to the absorption in real photographic materials.

Other theories have addressed the polarization of the construction and reconstruction wave (Ref. 22,28), but these theories have been limited to plane of incidence reconstruction. Also, the relationship of the polarization of the diffracted light to the incident wave polarization and wave vector has not been addressed by these theories.

Chang and Case have addressed the saturation effects in dichromated gelatin, but have not included the effects of non-uniform index modulation (Ref. 6, 5). No theory has addressed the inhomogeneity of the bulk refraction index in holograms made from materials like bleached silver halide emulsions.

Williamson has been the only author that has attempted to relate the diffraction efficiency to the photographic properties of the emulsion, the construction geometry, and exposure level. However, his theory was limited to planar fringes because of his use of the array theorem (Ref. 44).

CHAPTER III

GENERAL THEORY OF THE HOLOGRAPHIC LENS

The derivation of a set of two coupled wave equations which describe the propagation of the diffracted light within a holographic lens is presented in this chapter.

The derivation starts with the vector wave equation for an inhomogeneous, isotropic medium. The electric field amplitude within the medium is taken to be the linear sum of the individual electric field amplitudes of the Fraunhoffer diffracted orders. This sum is substituted into the vector wave equation and results in an infinite set of coupled wave equations. A justification for the truncation of this infinite set of coupled wave equations to a set of only two coupled wave equations is given. These two simultaneous, linear, first-order partial differential equations with variable coefficients are solved in Chapter IV using the JWKB approximation.

A. Derivation of the Coupled Wave Equations

The processed holographic lens medium is considered to be locally isotropic, inhomogeneous, and non-magnetic. It is isotropic because any stresses or strains present in the holographic recording medium are relieved by the processing. Although it is recognized the photochemically induced stresses and strains are in large part responsible for the formation of cracking along fringes in dichromated gelatin,

it is assumed that this process does not induce any bulk antisotropy (Ref. 11). The medium is inhomoegneous since the bulk optical index and the index modulation decrease with depth through the emulsion.

The time independent wave equation for monochromatic light in such a medium is given by

$$\nabla^2 \vec{E}(\vec{r}) + k^2(\vec{r}) \vec{E}(\vec{r}) + \vec{\nabla}(\vec{\nabla} \ell n\, \varepsilon(\vec{r}) \cdot \vec{E}(\vec{r}) = 0 \qquad (1)$$

and the wave propagation coefficient, $k(\vec{r})$, is defined by the equation

$$k^2(\vec{r}) = \frac{\varepsilon(\vec{r})\omega^2}{c^2} - i\,\frac{\omega\sigma(\vec{r})}{c^2} \qquad (2)$$

and $\vec{E}(\vec{r})$ is the electric field amplitude in the medium. $\varepsilon(\vec{r})$ and $\sigma(\vec{r})$ are respectively the dielectric constant and the conductivity of the medium. The coordinate system, geometrical conventions, physical units, and the derivation of Eqs (1) and (2) from Maxwell's equations are presented in Appendix A.

The first two terms in Eq (1) represent a description of wave propagation according to the laws of geometrical optics and scalar diffraction theory. The third term describes the effects upon wave propagation of polarization and is significant if $\vec{\nabla} \ell n\, \varepsilon(\vec{r})$ is of the order of $k(\vec{r})$. This occurs in regions of high optical index gradients or near edges.

In the next few paragraphs, $\vec{\nabla} \ell n\, \varepsilon(\vec{r})$ is shown to be of little significance in a holographic medium.

The polarization term is small compared to the other terms and will be ignored. The justification of that statement is based upon the fact that the maximum variation in the dielectric constant occurs from fringe to fringe. If the slower gross variations in dielectric constant with position are ignored temporarily, the dielectric constant for an ideal sinusoidal hologram as derived by Kogelnik is valid (Ref. 21). It is given by

$$\varepsilon(\vec{r}) = \varepsilon_o + \varepsilon_1 \cos \phi(\vec{r}) \tag{3}$$

where ε_o is the average bulk dielectric constant, ε_1 is the amplitude of the dielectric modulation and $\phi(\vec{r})$ is the phase difference between the object and reference waves in construction. It is assumed that $\varepsilon_1 << \varepsilon_o$. Taking the natural logarithm of Eq (3) one obtains

$$\ell n \varepsilon(\vec{r}) = \ell n \varepsilon_o + \ell n \left(1 + \frac{\varepsilon_1}{\varepsilon_o} \cos \phi(\vec{r})\right) \tag{4}$$

since $\varepsilon_1 << \varepsilon_o$, the approximation $\ell n(1+x) \simeq x$ for $x << 1$ is valid and Eq (4) becomes

$$\ell n \varepsilon(\vec{r}) \simeq \ell n \varepsilon_o + \frac{\varepsilon_1}{\varepsilon_o} \cos \phi(\vec{r}) \tag{5}$$

Therefore, the gradient of $\ell n\varepsilon(\vec{r})$ appearing in Eq (1) is given by

$$\vec{\nabla}\ell n\varepsilon(\vec{r}) \simeq -\frac{\varepsilon_1}{\varepsilon_o}\sin(\phi(\vec{r}))\vec{\nabla}\phi(\vec{r}) \tag{6}$$

The polarization term in Eq (1) can safely be ignored, if

$$\frac{|\vec{\nabla}\ell n\varepsilon(\vec{r})|}{k(\vec{r})} << 1 \tag{7}$$

The conductivity, σ, representing the losses in the processed hologram, appearing in Eq (2), is small for typical holographic materials and can be ignored in this analysis. Therefore, the wave propagation coefficient determined from Eqs (2) and (3) is

$$k(\vec{r}) = \frac{2\pi}{\lambda_o}\sqrt{\varepsilon_o}\left[1 + \frac{1}{2}\frac{\varepsilon_1}{\varepsilon_o}\cos\phi(\vec{r})\right] \tag{8}$$

which can be approximated for use in Eq (7) since $\varepsilon_1 << \varepsilon_o$ as

$$k(\vec{r}) \simeq \frac{2\pi\sqrt{\varepsilon_o}}{\lambda_o} \tag{9}$$

Substitution of Eqs (6) and (9) into Eq (7) yields

$$\frac{|\vec{\nabla}\ell n\varepsilon(\vec{r})|}{k(\vec{r})} \simeq \frac{\lambda_o\varepsilon_1|\sin\phi(\vec{r})\ \vec{\nabla}\phi(\vec{r})|}{2\pi(\varepsilon_o)^{3/2}} << 1 \tag{10}$$

using the fact that

$$|\sin\phi(\vec{r})| \leq 1 \tag{11}$$

and

$$|\vec{\nabla}\phi(\vec{r})| = |\vec{k}(\vec{r})| = \frac{2\pi}{\Lambda_o(\vec{r})} \tag{12}$$

Where $\vec{k}$ is the fringe wave vector normal to the fringes of the hologram, and Λ_o is the spacing between fringes, the inequality (10) becomes

$$\frac{\lambda_o \varepsilon_1}{\Lambda_o \varepsilon_o^{3/2}} \ll 1 \tag{13}$$

The minimum value of Λ_o is $\frac{1}{2}\lambda o$, therefore, Eq (13) in the worst case is

$$\frac{2\varepsilon_1}{\varepsilon_o^{3/2}} \ll 1 \tag{14}$$

Eq (14) is always true for holographic materials since $\varepsilon_1 \ll \varepsilon_o$ due to limitations in the physical processes used to modulate the dielectric constant. For example, the most highly modulatable holographic material known to date is dichromated gelatin, for which (Ref. 6, 7)

$$\varepsilon_1 = .192 \tag{15}$$

and

$$\varepsilon_o = 2.25 \tag{16}$$

Based upon the above analysis, the third term in Eq (1) will be ignored and the vector wave equation becomes

$$\nabla^2 \vec{E}(\vec{r}) + k^2(\vec{r})\vec{E}(\vec{r}) = 0 \tag{17}$$

The electric field inside the emulsion, as a result of the superposition principle, is take to be the linear sum of the individual complex electric field amplitudes of the Fraunhoffer diffracted orders

$$\vec{E}(\vec{r}) = \sum_{m=-\infty}^{\infty} V_m(\vec{r}) e^{i\phi_m(\vec{r})} \hat{e}_m \tag{18}$$

$\hat{e}_m$ is a unit polarization vector of the mth diffracted order and is derived in Appendix H. $V_m(\vec{r})$ is the amplitude of the mth diffracted wave and ϕ_m is the associated phase. ϕ_m is given by the equation

$$\phi_m(\vec{r}) = \phi_{c2}(\vec{r}) + m\phi(\vec{r}) \tag{19}$$

$\phi(\vec{r})$ is the phase difference between the object and reference waves during construction, and $\phi_{c2}(\vec{r})$ is the phase of the incident reconstruction wave.

In Appendix B it is shown that the wave propagation coefficient, $k(\vec{r})$, for a holographic lens is described

by the equation

$$k^2(\vec{r}) = k_2^2(\vec{r}) + k_1^2(\vec{r})\cos\phi(\vec{r}) \tag{20}$$

for which

$$\phi(r) = \phi_{r_2} - \phi_{o_2} \tag{21}$$

$k_2(\vec{r})$ is related to the bulk optical index of refraction and absorption of the processed emulsion, $k_1(\vec{r})$ is related to the depth of index and absorption modulation in the processed emulsion. If there is no hologram, then $k_1 = 0$. The specific equations for k_1, k_2 and $\phi(\vec{r})$ are in Appendix B. Substitution of Eqs (18) and (20) into Eq (17) yields

$$\nabla^2\left[\sum_m V_m e^{i\phi_m}\hat{e}_m\right] + \left[k_2^2(\vec{r}) + k_1^2(\vec{r})\cos\phi(\vec{r})\right]\cdot\left[\sum_m V_m e^{i\phi_m}\hat{e}_m\right] = 0 \tag{22}$$

The terms in Eq (22) can be evaluated individually as follows. Expanding the first term yields,

$$\nabla^2\left[\sum_m V_m(\vec{r})e^{i\phi_m}\hat{e}_m\right] = \sum_m \nabla^2(V_m(\vec{r})e^{i\phi_m})\hat{e}_m + \sum_m V_m(\vec{r})e^{i\phi_m}(\nabla^2\hat{e}_m) \tag{23}$$

The last term in Eq (23) is negligible since variations in $\hat{e}_m$ with respect to position are small because the medium is isotropic. Continuing the expansion of Eq (23) yields

$$\sum_m \nabla^2 (V_m e^{i\phi_m})\hat{e}_m =$$

$$\sum_m e^{i\phi_m}\left[2i\vec{\nabla}V_m\cdot\vec{\nabla}\phi_m + iV_m(\nabla^2\phi_m + i(\vec{\nabla}\phi_m)^2)\right]\hat{e}_m \qquad (24)$$

where second-order gradients of amplitude have been neglected. This is allowable since the gradients of phase are large compared to gradients of amplitude.

The second term in Eq (22) is expanded as follows:

$$k_2^2\sum_m V_m e^{i\phi_m}\hat{e}_m + \frac{k_1^2}{2}\left[\sum_m (e^{i\phi} + e^{-i\phi})V_m e^{i\phi_m}\hat{e}_m\right] =$$

$$k_2^2\sum_m V_m e^{i\phi_m}e_m + \frac{k_1^2}{2}\left[\sum_m (e^{i(\phi+\phi_m)}V_m\hat{e}_m + e^{-i(\phi-\phi_m)}V_m\hat{e}_m)\right] \qquad (25)$$

The dummy variables may be redefined in the last part of Eq (25) by use of the equations

$$\phi_{m+1} = \phi_m + \phi \qquad (26)$$

$$\phi_{m-1} = \phi_m - \phi \qquad (27)$$

By using Eqs (26) and (27) in the equation for the second term in Eq (22), one obtains,

$$\left[k_2^2 + k_1^2\cos\phi\right]\left[\sum_m V_m e^{i\phi m}\hat{e}_m\right] = k_2^2\sum_m V_m e^{i\phi_m}\hat{e}_m +$$
$$\frac{k_1^2}{2}\left[\sum_m (e^{i\phi_m}V_{m+1}\hat{e}_{m+1} + e^{i\phi_m}V_{m-1}\hat{e}_{m-1})\right] \qquad (28)$$

Inserting Eqs (28) and (24) into Eq (22) and collecting coefficients of equal phase terms, it is found that

$$\sum_m e^{i\phi_m}\left(\left[2i\vec{\nabla}V_m\cdot\vec{\nabla}\phi_m+V_m(i\nabla^2\phi_m-(\vec{\nabla}\phi_m)^2+k_2^2)\right]\hat{e}_m+\frac{k_1^2}{2}\left[V_{m+1}\hat{e}_{m+1}+V_{m-1}\hat{e}_{m-1}\right]\right)=0 \tag{29}$$

which implies,

$$\left[\frac{\partial V_m(\vec{r})}{\partial z}+V_m(\vec{r})C_m(\vec{r})\right]\hat{e}_m=Q_m(\vec{r})[V_{m+1}(\vec{r})\hat{e}_{m+1}(\vec{r})\ \hat{e}_{m-1}] \tag{30}$$

$$C_m(\vec{r})=\frac{-i}{2}\left[\frac{k_2^2(\vec{r})-(\vec{\nabla}\phi_m)^2+i\vec{\nabla}\cdot\vec{\nabla}\phi_m}{\vec{\nabla}\phi_m\cdot\hat{z}}\right] \tag{31}$$

$$Q_m(\vec{r})=\frac{i\,k_1^2(\vec{r})}{4\vec{\nabla}\phi_m\cdot\hat{z}},\quad m=0,\pm1,\pm2,\ \ldots\ \pm \tag{32}$$

The derivatives of V_m with respect to x and y have been deleted, since they are small compared to the derivative of V_m with respect to z. This is justified physically by the fact that holographic diffraction efficiency is particularly sensitive to hologram thickness, but varies slowly in the x, y directions across the surface of the hologram.

The physical significance of the coefficient $C_m(\vec{r})$ is more clearly understood by assuming that $Q_m(\vec{r})$ equals zero for the moment. Under such conditions, the solution to Eq (30) becomes

$$V_m(d)=V_m(o)e^{\int_o^d C_m(x,y,z)dz} \tag{33}$$

If C_m is written as the sum of real part ($R[C_m]$) and an imaginary part ($I[C_m]$), Eq (33) is written as

$$V_m(d) = V_m(o)\, e^{\int_o^d R[C_m(\vec{r})]dz}\, e^{i\int_o^d I[C_m(\vec{r})]dz} \qquad (34)$$

It is concluded from Eq (34) that $R[C_m]$ represents the amplitude loss coefficient of the mth diffracted wave and that $I[C_m]$ represents the associated phase. If $C_m(\vec{r})$ is a constant, then the integrals in Eq (34) are easily performed and $R[C_m]$ and $I[C_m]$ reduce to the conventional definitions of amplitude loss coefficient and of phase, respectively.

The physical significance of Q_m is interpreted directly from Eq (30). If Q_m is not zero, then there is a coupling of energy between the complex amplitudes of the mth diffracted wave and the adjacent m-1 th and m+1 th waves. Therefore, Q_m is interpreted as a coupling coefficient representing in some sense the magnitude of the coupling between the waves as they propagate through the hologram.

In the next section, a more detailed discussion of the physical significance of $C_m(\vec{r})$ and $Q_m(\vec{r})$ is presented.

B. Physical Interpretation of the Coefficients of Coupled Waves

The coupled waves represented by Eq (30) have been derived by an expansion in spherical waves representing the order of Fraunhoffer diffraction by a holographic lens.

This expansion is similar to an expansion in plane waves described by Klein and Cook (Ref. 20) for ultrasonic diffraction of light. In the case of the holographic lens, an expansion in spherical waves is more physically appealing since the diffracted waves propagate as spherical waves. The interpretation of the coefficients C_m and Q_m can be adapted from the work of Klein and Cook with modifications in syntax for the hologram.

By observation of the right hand side of Eq (30), it is clear that only adjacent modes (diffraction orders) couple electromagnetic energy directly between each other. This is shown schematically in Figure 2. An arrow sloping upward represents a coupling or transition of energy from a lower-order mode to a higher-order mode. An arrow sloping downward indicates a transition of energy from a higher-order mode to a lower-order mode. A horizontal arrow represents no coupling of energy. Figure 2 indicates that according to Eq (30) energy cannot transition to a higher-order mode without first having been through its adjacent lower-order mode. The zero order mode represents the incident light.

The amount of energy transfer between adjacent modes depends upon the magnitude of the two coefficients in Eq (30), C_m and Q_m. Q_m depends on k_1^2, which is related to the amount of index modulation and absorption modulation present in the processed holographic lens. The amount

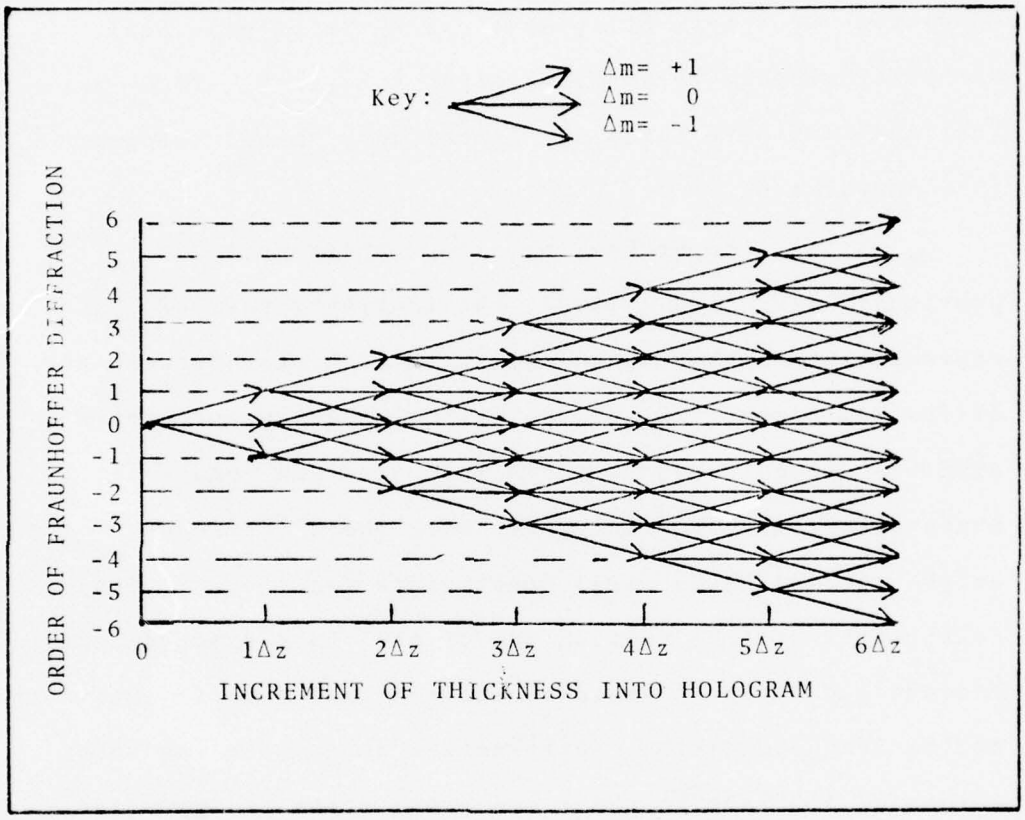

Figure 2. Schematic of Coupling Order
The arrows represent merely the transition of energy to an adjacent order as indicated by Eq (30). The ordinate represents the order of Fraunhoffer diffraction into which energy is coupled. The abscissa is the increment of thickness into the hologram.

of modulation determines the strength of adjacent mode coupling and must be non-zero if a hologram is to exist. As a consequence, Q_m is called the "coupling coefficient". If Q_m is totally imaginary, the hologram is an index modulation or "phase hologram". If Q_m is totally real, then the hologram is an "absorption hologram". If Q_m has real and imaginary parts, it is called a "mixed hologram" (see Appendix B).

C_m may also be broken into its complex parts as previously described. $I[C_m]$, the imaginary part of C_m, represents the phase synchronization parameter between the diffracted orders. Since the various modes propagate in different directions, two adjacent modes can remain in phase synchronization only over very short distances unless special geometrical constraints are obeyed. These constraints will be derived out of the phase synchronization concept and it is shown in Appendix B that this is equivlaent to the Bragg condition. Diffraction modes with the same values of $I[C_m]$are in phase synchronization in space and time as they propagate. Under the conditions of phase synchronization energy is constructively transferred directly between two adjacent modes.

The $R[C_m]$, the real part of C_m, represents an amplitude loss coefficient which accounts for all losses and gains occurring to the mth mode. It contains terms representing the absorption of the wave by the medium and the divergence

of the spherical wave which may contribute to an increase in intensity in the case of a converging wave or a decrease in intensity for a diverging wave.

Therefore, the coefficients in Eq (30) have real physical significance when described in the context of a holographic lens. But, Eq (30) is an infinite set of coupled waves and cannot be solved in closed form. It is not soluble even on a computer without truncation. In the next section, a physical and mathematical argument for reducing the number of coupled equations to be solved to two is presented based upon the interpretation of the coefficients just discussed. This will allow a closed form approximate solution to be obtained.

C. Justification for Truncation to Two-Coupled Waves

Kogelnik used a theory including only two-coupled waves to describe the diffraction from a thick, uniformly, sinusoidally modulated medium, but he did not justify his mathematical choice rigorously (Ref. 21). This section contains a justification for the use of only two-couled waves.

To digress briefly, for Bragg type holograms, the diffraction efficiency between the zero order and m=-1 diffracted order is experimentally found to be large ($\geq$95%). This in itself suggests the use of only two coupled waves to describe the diffraction process since little energy is coupled to other orders. However, a further analysis of $I[C_m]$ leads

to a more accurate physical understanding of why only two equations need to be retained in thick holograms.

The transfer of energy from the existing zero-order mode (the incident reconstruction wave) can only occur initially into the $m=\pm 1$ orders as has previously been argued by observation of the form of Eq (30) (see Figure 2). In order that this occur efficiently, phase synchronization between the modes must occur. If the energy is to remain confined between the zero-order mode and one or the other of the $m=\pm 1$ modes, then another physical conditions has to occur. The higher-order modes must be significantly out of phase synchronization with the m=0, and m=-1 mode or the m=+1 mode, so that energy is not transferred to them. The conditions for efficient trapping of energy between the m=0 and m=-1 modes is shown in Table 1.

TABLE I

CONDITIONS FOR TRAPPING OF ENERGY BETWEEN THE m=0 and m=-1 MODES

(D = hologram thickness)

1.	$Q_o d,\ Q_{-1} d \neq 0$	(The trivial condition, some material medium modulation exists)
2.	(a) $\lvert I[C_o]-I[C_{-1}]\rvert d \ll \pi$	(Phase synchronization between two orders - thick grating)
	or (b) $\lvert I[C_o]-I[C_m]\rvert d \ll \pi$	(No dephasing exists over the thickness of the hologram and all modes are in phase - thin grating)
3.	$\lvert I[C_o]-I[C_m]\rvert d \gg \pi$	(All higher orders rapidly desynchronize - thick grating)

If conditions 1, 2a, and 3 exist, then all orders except m=0,-1 decouple rapidly because of phase desynchronization. Energy is transferred from the zero order mode to the m=-1 order and back and forth throughout the thickness of the material as shown schematically in Figure 3. The energy is in effect trapped between the first two adjacent modes.

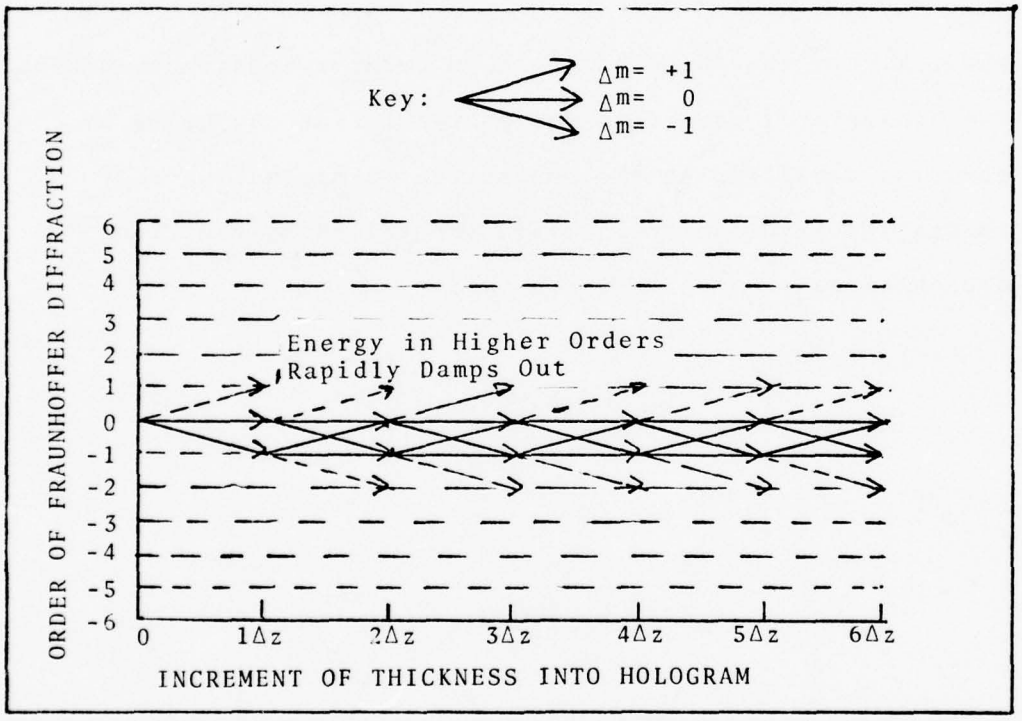

Figure 3. Schematic of Energy Trapping between m=0,m=-1 Modes

The conditions for efficient energy transfer between the first two modes hold for a holographic lens when the reconstruction wave vector is along or near the original reference wave vector. (It also occurs near the object wave vector.) This may be seen by analysis of the $I[C_m]$ for reconstruction near the original reference wave vector.

Recall Eq (19), rewritten as

$$\phi_m = \phi_{c2} + m(\phi_{r2} - \phi_{o2}) \tag{35}$$

where ϕ_{c2} is the phase of the zero-order reconstruction beam. The subscript 2 refers to the phases inside the hologram emulsion according to the convention in Appendix A. By taking the gradient of Eq (35), the following equations are obtained

$$\bar{\nabla}\phi_m = \bar{\nabla}\phi_{c2} + m(\bar{\nabla}\phi_{r2} - \bar{\nabla}\phi_{o2}) \tag{36}$$

or

$$\vec{k}_m(\vec{r}) = \vec{k}_{c2} + m\,(\vec{k}_{r2}(\vec{r}) - \vec{k}_{o2}(\vec{r})) \tag{37}$$

Eq (37) is obtained, because the gradient of the phase is the wave propagation vector. $\vec{k}_m$ is the wave propagation vector of the mth diffracted mode. One can write the reconstruction wave vector as the vector sum

$$\vec{k}_{c2} = \vec{k}_{r2} + \vec{\Delta} \tag{38}$$

where $\vec{\Delta}$ represents any changes of the reconstruction wave vector from that of the original reference wave vector. These changes may arise from (1) angular position changes of the reconstruction wave vector; (2) wavelength changes, (3) optical index changes of the emulsion due to processing, and (4) radius of curvature changes of the reconstruction wave from that of the reference wave. Substitution of Eqs (37) and (38) into Eq (31) yields

$$C_m(\vec{r}) = \frac{1}{2}\left[\frac{\bar{\nabla}\cdot([m+1]\vec{k}_{r2}-m\vec{k}_{o2}+\vec{\Delta}) + k_c^2\,\alpha}{[(m+1)\vec{k}_{r2}-m\vec{k}_{o2}+\vec{\Delta}]\cdot\hat{z}}\right] +$$

$$-\frac{i}{2}\left[\frac{k_2^2(\vec{r})(1-[m+1]^2-m^2)+2\vec{\Delta}\cdot(-m\vec{k}_{o2}+[m+1]\vec{k}_{r2})-2(m+1)\vec{k}_{r2}\cdot\vec{k}_{r2}+\vec{\Delta}^2}{[(m+1)\vec{k}_{r2}-m\vec{k}_{o2}+\vec{\Delta}]\cdot\hat{z}}\right] \tag{39}$$

where it has been assumed $\vec{k}_{r2}\cdot\vec{k}_{r2}=\vec{k}_{o2}\cdot\vec{k}_{o2}=\vec{k}_{c2}\cdot\vec{k}_{c2}=k_2^2(\vec{r})$. The imaginary part of C_m reduces to the following when $\vec{\Delta}\simeq 0$ (i.e. when reconstruction is nearly identical to the construction conditions).

$$I[C_m] \simeq -\frac{1}{2}\left[\frac{k_2^2(1-(m+1)^2-m^2) - 2m(m+1)\vec{k}_{r2}\cdot\vec{k}_{o2}}{[(m+1)\vec{k}_{r2} - m\vec{k}_{o2}]\cdot z}\right] \tag{40}$$

From Eq (40) is it possible to show the conditions for trapping of energy between the m=0 and m=-1 orders as enumerated in Table I hold for a thick hologram for reconstruction along or near the reference wave vector.

The first condition in Table I is the trivial condition that some form of modulation must exist in the emulsion. The second condition in Table I is the phase synchronization condition between the m=0 and m=-1 orders. That condition is

$$|I[C_o] - I[C_{-1}]|d \ll \pi \tag{41}$$

$I[C_o]$ and $I[C_{-1}]$ are evaluated using Eq (40) for m=0 and m=-1, these results, when substituted into Eq (41), yield the condition

$$0 \ll \pi \tag{42}$$

which is true. Therefore, condition 2a of Table I holds. By use of Eq (40), condition 3 is written as

$$\frac{1}{2}\left|\frac{k_2^2(1-(m+1)^2-m^2)-2m(m+1)\vec{k}_{r2}\cdot\vec{k}_{o2}}{[(m+1)\vec{k}_{r2}-m\vec{k}_{o2}]\cdot\hat{z}}\right| d \gg \pi \;;\forall m\neq 0,-1 \tag{43}$$

The left side of the inequality (43) is of the order $mk_2 d$ where k_2 is the wave propagation coefficient of the hologram. Since $k_2 d >> \pi$, inequality (43) holds. Consequently, the conditions of Table I for trapping of energy between the m=0 and m=-1 diffracted modes holds rigorously for the case of a thick, holographic medium for reconstruction wave vectors similar to the original reference wave vector (i.e., $\vec{\Delta}=o$).

Because the energy diffracted by a thick hologram is trapped between the first two orders (m=0 and m=-1) only two of the infinite set of coupled wave equations is required to describe the wave propagation in the medium. This is the justification for the truncation of Eq (30) to a set of two coupled wave equations, the m=0, and m=-1 equations. Such a truncation holds rigorously for $\vec{\Delta}$ near zero. The question remains as to how large $\vec{\Delta}$ may be before this truncation is invalid. As $\vec{\Delta}$ becomes large, $I[C_m]$ approaches

$$I[C_m] = -\frac{1}{2}\left[\frac{2\vec{\Delta}\cdot(-m\vec{k}_{o2}+(m+1)\vec{k}_{r2}) + \vec{\Delta}^2}{[(m+1)\vec{k}_{r2} - m\vec{k}_{o2} + \vec{\Delta}]\cdot\hat{z}}\right] \qquad (44)$$

Eq (44) is valid only for m=0,-1; it may be substituted into the phase synchronization condition (2a) of Table I, to yield

$$\frac{1}{2}\left|\frac{2\vec{\Delta}\cdot\vec{k}_{r2}+\vec{\Delta}^2}{[\vec{k}_{r2}+\vec{\Delta}]\cdot\hat{z}} - \frac{2\vec{\Delta}\cdot\vec{k}_{o2}+\vec{\Delta}^2}{[\vec{k}_{o2}+\vec{\Delta}]\cdot\hat{z}}\right| \quad d << \pi \qquad (45)$$

which may be rewritten as

$$|\vec{\Delta} \cdot \vec{\ell}(\vec{\Delta})| \; d << \pi \tag{46}$$

where

$$\vec{\ell}(\vec{\Delta}) = \frac{\vec{k}_{r2} + \frac{\vec{\Delta}}{2}}{(\vec{k}_{r2}+\vec{\Delta}) \cdot \hat{z}} - \frac{\vec{k}_{o2} + \vec{\Delta}/2}{(\vec{k}_{o2} \cdot \vec{\Delta}) \cdot \hat{z}} \tag{47}$$

$\vec{\ell}(\vec{\Delta})$ is a weak function of $\vec{\Delta}$ since $|\vec{k}_{r2}|$ and $|\vec{k}_{o2}|$ are much larger than $|\vec{\Delta}|$. Therefore inequality (46) can be used to estimate the range of $|\vec{\Delta}|$ over which phase synchronization holds if written as

$$|\vec{\Delta}| << \frac{\pi}{|\vec{\ell}| d \cos(\vec{\ell}, \vec{\Delta})} \tag{48}$$

$|\vec{\ell}|$ is of the order $\frac{\lambda_o}{\Lambda_o}$, where Λ_o is the interfringe spacing, λ_o is the free space wavelength of the construction (object or reference)light, and $\cos(\vec{\ell}, \vec{\Delta})$ hence, inequality Eq (48) becomes approximately

$$|\vec{\Delta}| << \frac{\pi \Lambda_o}{\lambda_o d} \tag{49}$$

Inequality (49) implies that thick holograms are much more sensitive to reconstruction wave vector changes than thin holograms. It also implies that holograms constructed at short wavelengths are much more sensitive to reconstruction wave vector changes than holograms constructed at long

wavelengths. Also, holograms with large fringe spacing are less sensitive to changes in the reconstruction wave vector than holograms with small fringe spacings. These conclusions agree with the commonly expected facts about hologram reconstruction sensitivity.

Once inequality (49) is no longer true, then phase synchronization between the m=0 and m=-1 orders is disrupted. Energy is not transferred between the m=0 and m=-1 orders. This desynchrnoization also means that energy cannot be transferred to any of the more negative-order modes since energy must first be transferred to the m=-1 mode in order to reach the more negative-order modes. Therefore, the use of two coupled wave equations remains valid as $|\vec{\Delta}|$ gets arbitrarily larger, unless a reconstruction wave vector position is reached for which phase synchronization occurs for the chain of positive diffraction orders. This occurs when $\vec{k}_{c2}$ approaches a position for which reconstruction occurs along or near the original object wave vector (creating the reference wave). This can be described by an analogous set of two coupled wave equations in which the names of the object and reference waves are switched.

Therefore, it is concluded that a set of two coupled wave equations reliably describes the diffraction process in thick holograms for reconstruction wave vectors along or near the original reference wave vector.

The coupled wave equations to be used throughout the remainder of this dissertaion are those between the zero-order and -1 order diffracted waves, given by Eq (30) as

$$\left[\frac{\partial V_o}{\partial z} + V_o C_o\right] \hat{e}_o = Q_o V_{-1} \hat{e}_{-1} \tag{50}$$

$$\left[\frac{\partial V_{-1}}{\partial z} + V_{-1} C_{-1}\right] \hat{e}_{-1} = Q_{-1} V_o \hat{e}_o \tag{51}$$

The terms involving V_{+1} are neglected since $I[C_{+1}]$ is very large and rapid dephasing damps out any m=1 or higher $\pm$ orders. C_o and C_{-1} are described by Eq (31) and Q_o and Q_{-1} are given by Eq (32). One reduces Eqs (59) and (51) to a set of scalar equations by taking the dot product of $\hat{e}_o$ along $\hat{e}_{-1}$ since this is the component of the individual polarizations which will couple. This yields,

$$\frac{\partial V_o}{\partial z} + V_o C_o = Q_o V_{-1} \hat{e}_{-1} \cdot \hat{e}_o \tag{52}$$

$$\frac{\partial V_{-1}}{\partial z} + V_{-1} C_{-1} = Q_{-1} V_o \hat{e}_{-1} \cdot \hat{e}_o \tag{53}$$

It is shown in Appendix H that $\hat{e}_{-1}\ \hat{e}_o = |\sin\Psi_{-1}|$ where Ψ_{-1} is the angle between the incident polarization and the diffraction direction. Therefore, the coupled wave equations reduce to

$$\frac{\partial V_o}{\partial z} + C_o V_o = Q_o V_{-1} |\sin\Psi_{-1}| \tag{54}$$

$$\frac{\partial V_{-1}}{\partial z} + C_{-1} V_{-1} = Q_{-1} V_o |\sin\Psi_{-1}| \tag{55}$$

C_o and C_{-1} are given by Eq (31) for m=0, -1, respectively; and Q_o, Q_{-1} are given by Eq (32) for m=0, -1, respectively.

In the case of constant coefficients, the solution to Eqs (54) and (55) is straight forward, identical to the Kogelnik result for an ideal, uniformly, sinusoidally modulated, planar fringe grating. However, the coefficients $C_o(\vec{r})$, $C_{-1}(\vec{r})$, $Q_o(\vec{r})$, and $Q_{-1}(\vec{r})$ are not constants for a more realistic material. The exact functional dependency upon position of these coefficients for the case of the holographic lens is derived in Appendix B. The solution to the variable coefficient, coupled wave equations (Eqs (54) and (55)) is the subject of the next chapter. A closed form solution is derived using the JWKB approximation.

CHAPTER IV

THE JWKB SOLUTION

The solution to the coupled wave equations with constant coefficients has been obtained using standard differential equation techniques for the ideal sinusoidal plane wave grating by Kogelnik (Ref. 21). The assumption of constant coefficients limits his theory to media in which the grating parameters are not dependent upon position inside the holographic material.

In practical materials, absorption of the object and reference beams during construction of the hologram causes the optical index and the amplitude of index modulation to vary with position inside the hologram. In this case, the coefficients of the coupled wave equations (Eqs (54) and (55)) describing the diffraction process are variable and a new solution must be obtained.

In this chapter, the pair of variable-coefficient, coupled-wave equations derived in Chapter III is transformed into a single second-order differential equation with variable coefficients to which the JWKB approximation is applied yielding a general, closed form solution. By imposing the appropriate boundary conditions, the particular solutions for a transmission and reflection hologram are obtained. A comparison is made to the Kogelnik results. It is shown that the JWKB solution reduces to that of Kogelnik for plane waves and constant coefficients. Finally, the significance

of the JWKB terms is emphasized by an example. Section A contains the JWKB solution and an evaluation of the validity of this solution. In Section B, the particular solution for the transmission hologram is derived. In an analogous manner, the result for the reflection hologram is obtained in Section C. A comparison of the JWKB solution to previous theories is presented in Section D.

A. The JWKB Solution

In this section the general solution to the coupled wave equations with variable coefficients (Eqs (54) and (55)) derived in Chapter III is obtained by applying the JWKB approximation. An inequality is derived which bounds the applicability of the JWKB technique. Finally, these bounds are determined for typical holographic materials and it is shown that the approximations involved in the use of the JWKB techniques are valid.

Recall that the variable coefficient, coupled wave equations derived in Chapter III were

$$\frac{\partial V_o}{\partial z} + C_o V_o = Q_o V_{-1} \left|\sin\Psi_{-1}\right| \qquad (56)$$

$$\frac{\partial V_{-1}}{\partial z} + C_{-1} V_{-1} = Q_{-1} V_o \left|\sin\Psi_{-1}\right| \qquad (57)$$

$V_o(\vec{r})$ is the amplitude of the incident wave, $V_{-1}(\vec{r})$ is the amplitude of the diffracted light, and $C_o(\vec{r})$, $C_{-1}(\vec{r})$, $Q_o(\vec{r})$ and $Q_{-1}(\vec{r})$ are the variable coefficients defined by Eqs (31) and (32). Taking the derivative of Eq (57) (where $' \equiv \frac{\partial}{\partial z}$ and $'' \equiv \frac{\partial^2}{\partial z^2}$), one obtains

$$V''_{-1}+V'_{-1}C_{-1}+V_{-1}C'_{-1}=Q_{-1}V'_o|\sin\psi_{-1}|+V_oQ'_{-1}|\sin\psi_{-1}| \qquad (58)$$

which may be solved for V'_o to yield

$$V'_o = \frac{1}{Q_{-1}|\sin\psi_{-1}|}\left[V''_{-1}+V'_{-1}C_{-1}+V_{-1}C'_{-1} - V_o|\sin\psi_{-1}|Q'_{-1}\right] \qquad (59)$$

into which $V_o|\sin\psi_{-1}|$ may be substituted from Eq (57) to yield

$$V'_o=\frac{1}{Q_{-1}\sin_{-1}}\left[V''_{-1}+V'_{-1}C_{-1}+V_{-1}C'_{-1} - \frac{Q_{-1}}{Q_{-1}}(V'_{-1}+C_{-1}V_{-1})\right] \qquad (60)$$

Eqs (60) and (57) may be substituted for V_o and V'_o in Eq (56), resulting in

$$\frac{1}{Q_{-1}|\sin\psi_{-1}|}\left[V''_{-1}+V'_{-1}C_{-1}+V_{-1}C'_{-1} - \frac{Q'_{-1}}{Q_{-1}}(V'_{-1}+C_{-1}V_{-1})\right]+ \frac{C_o}{Q_{-1}|\sin\psi_{-1}|}\left[V'_{-1}+C_{-1}V_{-1}\right]=Q_oV_{-1}|\sin\psi_{-1}| \qquad (61)$$

which can be rearranged to form a second-order differential equation, determined to be

$$V''_{-1}+V_{-1}[C_o+C_{-1}-\frac{Q'_{-1}}{Q_{-1}}]+V_{-1}[C_oC_{-1}-Q_oQ_{-1}\sin^2\psi_{-1}+C'_{-1}-\frac{C_{-1}Q'_{-1}}{Q_{-1}}]=0 \qquad (62)$$

Eq (62), which is the equation for the complex amplitude of the light diffracted as the output of the hologram, is of the form (where $y = V_{-1}$)

$$y'' + f(z)\, y' + g(z)\, y = 0 \tag{63}$$

where,

$$f(z) = C_o + C_{-1} - \frac{Q'_{-1}}{Q_{-1}} \tag{64}$$

and

$$g(z) = C_o C_{-1} - Q_o Q_{-1} \sin^2 \Psi_{-1} + C'_{-1} - \frac{C_{-1} Q'_{-1}}{Q_{-1}} \tag{65}$$

Eq (63) can be transformed to yield

$$V'' + \left(\frac{2p'}{p} + f \right) V' + \left(\frac{p'' + fp' + gp}{p} \right) V = 0 \tag{66}$$

which was obtained by substitution of

$$y(z) = V(z)\, p(z) \tag{67}$$

into Eq (63).

p is a function which is forced to obey the equation

$$\frac{2p'}{p} + f = 0 \tag{68}$$

such that

$$p(z) = \exp\left[-\frac{1}{2}\int_0^z f(\xi)d\xi\right] \tag{69}$$

As a result of Eq (68), Eq (66) becomes

$$V''(z) + F(z)V(z) = 0 \tag{70}$$

where

$$F(z) = \frac{p''(z)+f(z)p'(z)+g(z)p(z)}{p(z)} \tag{71}$$

Eq (70) can be solved by the JWKB Approximation (Ref. 14, Page 10) by writing Eq (70) as

$$V''(z) + \frac{F(z)}{\lambda^2} V(z) = 0 \tag{72}$$

where λ is a "smallness parameter" which later can be set equal to unity. Assume, V(z) is of the form

$$V(z) = \exp\left\{\frac{1}{\lambda}\int_0^z \sum_{\nu=0}^{\infty} \chi_\nu(\xi)\lambda^\nu d\xi\right\} \tag{73}$$

Substitution of Eq (73) into Eq (72) and collection of terms in successive powers of $\frac{1}{\lambda}$ yields the following set of equations

$$\nu = o \; ; \quad \chi_o(z) = \pm i \sqrt{F(z)} \tag{74}$$

$$\nu = 1,2,3,\ldots\infty; \; \chi'_\nu(z) = -\sum_{\mu=o}^{\nu} \chi_\mu \chi_{\nu-\mu} \tag{75}$$

from which the series $\sum_{n=0}^{\infty} X_n(z)\lambda^n$ can be determined (Ref. 14).

From Eqs (75) and (75)

$$\chi_1 = \frac{-1}{2\chi_o}\frac{d\chi_o}{dz} = -\frac{1}{4}\frac{F'}{F} \tag{76}$$

$$\chi_2 = \frac{-1}{2\chi_o}\left[\frac{d\chi_1}{dz}+\chi_1^2\right] = \frac{\pm iF^{-3/2}}{8}\left(\frac{5}{4}\frac{F'^2}{F}-F''\right) \tag{77}$$

Substitution of Eqs (74), (76), and (77) into Eq (73) and neglecting higher order terms yields the approximate solution

$$V_\pm(z) = EXP\left[\int_o^z \left[\pm i\sqrt{F(\xi)} - \frac{1}{4}\frac{F'(\xi)}{F(\xi)} \pm \frac{iF(\xi)^{-3/2}}{8}\left(\frac{5}{4}\frac{F'^2(\xi)}{F(\xi)} - F''(\xi)\right)d\xi\right]\right. \tag{78}$$

which can be written as

$$V_\pm(z) = \frac{1}{\sqrt{F(z)}}\, e^{\pm i\int_o^z F(\xi)\,d\xi}\, e^{\pm\int_o^z \frac{F(\xi)^{-3/2}}{8}\left[\frac{5}{4}\frac{F'^2(\xi)}{F(\xi)} - F''(\xi)\right]d\xi} \tag{79}$$

Eq (79) represents the two particular solutions to the coupled wave equation; the constants of integration will be accounted for by the coefficients in the general solution of the form:

$$V(z) = C_+V_+(z) + C_-V_-(z) \tag{80}$$

A further simplification to Eq (79) is expected to be valid provided the contributions from the higher order integrals in Eq (79) are small (Ref. 14, Page 11). This simplification is

$$V_{\pm}(z) = \frac{1}{\sqrt[4]{F(z)}}\, e^{\pm\int_o^z F(\xi)\, d\xi} \tag{81}$$

Eq (81) is the well known first-order JWKB approximation and is valid provided (Ref. 14, Page 11),

$$\left|\int_o^z \sqrt{F(\xi)}\, d\xi\right| >> \left|\frac{1}{4}\int_o^z \frac{F'(\xi)}{F(\xi)}\, d\xi\right| >> \left|\frac{1}{8}\int_o^z F(\xi)^{-3/2}\left[\frac{5}{4}\frac{F'^2(\xi)}{F(\xi)} - F''(\xi)\right] d\xi\right| \tag{82}$$

which may be rewritten using the Triangle Inequality (Ref. 36, Page 178).

$$\left|\int_o^z \sqrt{F(\xi)}\, d\xi\right| >> \frac{1}{4}\left|\int_o^z \frac{F'(\xi)}{F(\xi)}\, d\xi\right| >> \frac{1}{8}\left\{\frac{5}{4}\left|\int_o^z F^{-\frac{5}{2}} F'^2 d\xi\right| + \left|\int_o^z F^{-\frac{3}{2}} F'' d\xi\right|\right\} \tag{83}$$

The inequalities given in Eq (83) may be evaluated to determine the validity of applying the first-order JWKB approximation to the problem of the holographic lens. To accomplish the evaluation, the magnitude of F must be determined. From Eq (69)

$$p'(z) = -\frac{1}{2} f(z)\, e^{-\frac{1}{2}\int_o^z f(\xi)\, d\xi} = -\frac{1}{2} f(z)p(z) \qquad (84)$$

and

$$p''(z) = -\frac{1}{2}f' e^{-\frac{1}{2}\int_o^z f d\xi} - \frac{1}{2}f(z)\left[-\frac{1}{2}f e^{-\frac{1}{2}\int_o^z f d\xi}\right] \qquad (85)$$

$$p''(z) = -\frac{1}{2}f'p + \frac{1}{4}f^2 p = \left[-\frac{1}{2} f' + \frac{1}{4}f^2\right] p \qquad (86)$$

Substitution of Eqs (84) and (86) into Eq (71) results in

$$F(z) = g(z) - \frac{1}{4}f^2(z) - \frac{1}{2}f'(z) \qquad (87)$$

Substitution of Eqs (64) and (65) into Eq (87) yields

$$F(z) = C_o C_{-1} - Q_o Q_{-1} \sin^2 \Psi_{-1} + C'_{-1} - \frac{C_{-1} Q'_{-1}}{Q_{-1}} - \frac{1}{4}\left(C_o + C_{-1} - \frac{Q'_{-1}}{Q_{-1}}\right) - \frac{1}{2}\left(C'_o + C'_{-1} - \frac{\partial}{\partial z}\left(\frac{Q'_{-1}}{Q_{-1}}\right)\right) \qquad (88)$$

Collecting terms yields,

$$F(z) = -\frac{1}{4}(C_o - C_{-1})^2 - Q_o Q_{-1} \sin^2 \Psi_{-1} + \frac{1}{2}(C_o - C_1)\frac{Q'_{-1}}{Q_{-1}} - \frac{1}{2}\frac{\partial}{\partial z}\left[C_o - C_{-1} - \frac{Q'_{-1}}{Q_{-1}}\right] - \frac{1}{4}\left(\frac{Q'_{-1}}{Q_{-1}}\right)^2 \qquad (89)$$

F(z), given by Eq (89), is a complicated complex function of z. In order to evaluate the inequality, Eq (83), which determines the validity of the JWKB approximation, certain integrals of F(z), F'(z), and F''(z) must be determined. In the following paragraph, the function F(z) is estimated from the magnitude of the largest term in Eq (89). Then the inequality given by Eq (83) is determined in an approximate manner.

F(z) is composed of the following individual functions derived in Appendix B

$$C_o(\vec{r}) = \frac{k_o \alpha_b(\vec{r})}{2k_c \cos\theta_c} + \frac{\vec{\nabla}\cdot\vec{k}_{2c}(\vec{r})}{2k_c \cos\theta_c} \frac{1}{n_b(\vec{r})} + \frac{i}{2k_c \cos\theta_c}\left[\frac{\alpha_b^2(\vec{r})}{4n_b(\vec{r})} - \Delta k^2 n_b^2(\vec{r})\right] \tag{90}$$

$$C_{-1}(\vec{r}) = \frac{1}{2}\left[\frac{i\left(-\frac{\alpha_b^2(\vec{r})}{4} - \Delta k^2 n_b^2(\vec{r}) + \vec{K}'\cdot\vec{K}' - 2\vec{k}_{2c}\cdot\vec{K}'\right) + n_b(\vec{r})\alpha_b(\vec{r})k_o + \vec{\nabla}\cdot(\vec{k}_{2c}-\vec{K}')}{k_c n_b(r)\cos\theta_c - K_z'}\right] \tag{91}$$

$$Q_o(\vec{r}) = \frac{i\, k_1^2(\vec{r})}{4k_c n_b(\vec{r})\cos\theta_c} \tag{92}$$

$$Q_{-1}(\vec{r}) = \frac{i\, k_1^2(\vec{r})}{4(k_c n_b(\vec{r})\cos\theta_c - K_z')} \tag{93}$$

$k_o = \frac{2\pi}{\lambda_o}$, where λ_o is the construction wavelength,
$k_c = \frac{2\pi}{\lambda_c}$, where λ_c is the reconstruction wavelength;
$\alpha_b(\vec{r})$ is the absorption coefficient of the processed hologram, $\vec{k}_{2c}(\vec{r})$ is the reconstruction wave vector, $n_b(\vec{r})$ is the optical index of the hologram, θ_c is the angle between $\vec{k}_{2c}(\vec{r})$ and $\hat{z}$,

Δk^2 is the difference between k_o^2 and k_c^2, $\vec{K}'$ is the fringe wave vector derived in Appendix C, $\vec{K}'_z$ is the z-component of $\vec{K}'$, Ψ_{-1} is the angle between the incident polarization and the diffraction direction, derived in Appendix H, and $k_1^2(\vec{r})$, for a phase hologram, is given by the equation

$$k_1^2(\vec{r}) = 2k_o^2 n_b(\vec{r})\Delta n(\vec{r}) \qquad (94)$$

derived in Appendix B. $\Delta n(\vec{r})$ is the amount of index modulation present in the hologram.

The dominant terms in Eq (89) are the first two. This may be determined from the knowledge of the fact $k_o >> \alpha_b(\vec{r})$ for holographic materials in the optical frequencies. The first term is small for reconstruction wave vectors near the original reference wave vector, because the quantity

$$\vec{K}' \cdot \vec{K}' - 2\vec{k}_{2c} \cdot \vec{K}' \approx 0 \qquad (95)$$

as mentioned in Chapter III. Therefore, the difference $(C_o - C_{-1})$, appearing in Eq (89), is approximately zero for practical reconstruction geometries. The quantity $\frac{Q'_{-1}}{Q_{-1}}$ is of the order of α, where α is the absorption during construction. Again, $k_o >> \alpha$ for holographic emulsions.

Therefore, since $Q_o Q_{-1}$ is of the order of $\Delta n^2 k_o^2$, it is the dominant term in Eq (89) for the values of index modulation, Δn, in holographic materials.

Therefore, at least to first-order, F(z) may be represented as

$$F(z) \simeq - Q_o Q_{-1} \sin^2 \Psi_{-1} \qquad (96)$$

For the case of unslanted fringes, $K'_z = 0$, with reconstruction at the construction wavelength, $\Delta k^2 = 0$, Eq (94) can be substituted into Eqs (94) and (93) to yield

$$Q_o = Q_{-1} = \frac{.5i\ k_o \Delta n(\vec{r})}{\cos \theta_c} \qquad (97)$$

For the general case of slanted fringes $K'_z \neq 0$, Q_o and Q_{-1} would not be equal, but would be approximately the same order of magnitude.

Consequently, the following analysis would not change much. It is shown in Appendix B that $\Delta n(\vec{r})$ is of the form

$$\Delta n(\vec{r}) = \Delta n_o (E(x,y)) e^{-\frac{\alpha}{2}(L_o + L_r)z} \qquad (98)$$

$\Delta n_o(E(x,y))$ is derived in Appendix D for bleached Kodak 649-F holograms and in Appendix E for dichromated gelatin holograms. $E(x,y)$ is the exposure, α is the absorption coefficient of the emulsion during construction, $L_o = \frac{1}{\cos\theta_o}$, $L_r = \frac{1}{\cos\theta_r}$, where θ_o and θ_r are, respectively, the angles with respect to the normal of the hologram of the object and reference wave vectors. Substitution of Eq (97) and Eq (98) into Eq (96) implies

$$F(z) = F_o(x,y)e^{-\alpha(L_o+L_r)z} \tag{99}$$

$$F_o(x,y) = \frac{\pi^2\Delta n_o^2(x,y)}{\lambda_o\cos\theta_c} \sin^2\Psi_{-1} \tag{100}$$

Eq (99) implies

$$F'(z) = -\alpha(L_o+L_r)F_o e^{-\alpha(L_o+L_r)z} \tag{101}$$

and

$$F''(z) = +\alpha^2(L_o+L_r)\ F_o e^{-\alpha(L_o+L_r)z} \tag{102}$$

Using Eqs (99) through (102), the JWKB inequalities, Eq (83), which must hold for the JWKB approximation to be valid, become,

$$1 >> \frac{1}{\delta}\frac{\lambda_o\cos\theta_c\alpha^2(L_o+L_r)^2}{\pi\Delta n_o\sin\Psi_{-1}}\ z >> \frac{\delta}{32}\frac{\lambda_o^2\cos^2\theta_c\alpha^2(L_o+L_r)}{\pi^2\Delta n_o^2\sin^2\Psi_{-1}}\ \frac{\left|1 - e^{\frac{\alpha(L_o+L_r)z}{2}}\right|}{\left|1 - e^{\frac{-\alpha(L_o+L_r)z}{2}}\right|} \tag{103}$$

Some approximations have been made to derive inequality (103) such that the inequalities are valid only to first-order. The terms which have been neglected have been shown to be at least an order of magnitude smaller than the terms retained, hence, Eq (103) is a reasonable estimate of the validity of the JWKB approximation. Inequality (103) determines the bound of the parameters: (1) the absorption coeffficient of the emulsion during construction, α, (2) the amplitude of the index modulation, $\Delta n_o(E)$, and (3) the thickness of the emulsion, z, for which the JWKB approximation is valid.

Clearly, if the emulsion becomes too thick, the thickness dependent terms will cause the inequality to be invalid. Similarly, if the absorption during exposure becomes extreme, the inequality becomes invalid. One cannot arbitrarily put bounds on these parameters, but α, Δn_o, and z can be determined for each type of holographic material to which the theory derived in this disseration is to be applied and the inequality (103) can be checked.

A typical holographic material to be examined extensively in the next chapter is dichromated gelatin for which $z = 13\mu$, $\alpha = 2.75 \times 10^4\ m^{-1}$, $\lambda_o = .5\mu$, $\theta_o = \theta_r = \theta_c = 45°$ and $\Delta n_o(E) \simeq .08$. For this typical material, inequality (103) becomes

$$1 >> .015 >> .001 \qquad (104)$$

The first inequality in Eq (104) represents the relative magnitude of the terms kept by the first-order JWKB approximation. The second inequality represents the relative magnitude of the last term retained compared to the first term neglected by the first-order JWKB approximation.

These inequalities indicate that the JWKB approximation is valid for the typical holographic material, dichromated gelatin. The reader is cautioned that inequalities (103) should be checked for each new material to which the JWKB approximation is applied.

In summary, the first-order JWKB approximation has been used to solve for the electric field amplitude of the first-order diffracted wave from a holographic lens. Inequalities were derived to estimate the validity of the JWKB approximation and evaluated for a typical holographic material. The final result for that amplitude of the diffracted wave is obtained by substitution of Eqs (81) and (87) into Eq (80), which becomes

$$V_{-1}^{JWKB}(d) = \sqrt{\frac{2i}{\gamma_+(d)-\gamma_-(d)}}\left[C_+ e^{\int_o^d \gamma_+(z)dz} + C_- e^{\int_o^d \gamma_-(z)dz}\right] \qquad (105)$$

where

$$\gamma_{\pm}(z) = -\frac{1}{2}f(z) \pm i\sqrt{F(z)} \qquad (106)$$

d is the thickness of the hologram, f(z) is given by Eq (64) and F(z) by Eq (89). C_+ and C_- are complex constants to be determined by the boundary conditions of the specific hologram. In the next sections, these constants are determined for a transmission and reflection hologram.

B. The Transmission Holographic Lens

For a transmission holographic lens, both the incident and diffracted waves have the same sense to their z-components of propagation through the hologram. The boundary conditions in transmission are

$$V_{-1}(0) = 0 \tag{107}$$

and

$$V_o(0) = 1 \tag{108}$$

using Eq (107), $C_+ = -C_-$ such that Eq (105) becomes

$$V_{-1}(z) = \sqrt{\frac{2i}{\Delta\gamma(z)}}\, C_+ e^{-\frac{1}{2}\int_o^z f(\xi)d\xi} \left[e^{\frac{1}{2}\int_o^z \Delta\gamma(\xi)d} - e^{-\frac{1}{2}\int_o^z \Delta\gamma(\xi)\, d\xi} \right] \tag{109}$$

where

$$\Delta\gamma(z) = \gamma_+ - \gamma_- = 2i\sqrt{F(z)} \tag{110}$$

The application of the second boundary condition involves using one of the original coupled differential equation, Eq (50), since the second boundary condition is not a direct condition upon V_{-1}, but rather applies to V_o. From Eq (57)

$$V_o(z)\Big|_o = \frac{1}{Q_{-1}(z)|\sin\Psi_{-1}|}\left(\frac{\partial V_{-1}}{\partial z} + C_{-1}V_{-1}\right)\Big|_o \qquad (111)$$

Using both boundary conditions, Eq (111) yields

$$1 = \frac{1}{Q_{-1}(0)|\sin\ _{-1}|}\left(\frac{\partial V_{-1}}{\partial z}\right)\Big|_o \qquad (112)$$

By taking the derivative of Eq (109), it can be shown that

$$\frac{\partial V_{-1}}{\partial z}\Big|_o = \sqrt{2i\Delta\gamma(0)}\ C_+ \qquad (113)$$

From Eqs (112) and (113)

$$C+ = \frac{Q_{-1}(o)|\sin\Psi_{-1}|}{\sqrt{2i\Delta\gamma(o)}} \qquad (114)$$

Hence, evaluation of Eq (109) using Eq (114) with z=d, the thickness of the hologram, yields

$$V_{-1}(d) = \frac{Q_{-1}(0)|\sin\Psi_{-1}|}{\sqrt{\Delta\gamma(z)\Delta\gamma(0)}}\ e^{-\frac{1}{2}\int_o^d f(z)dz}\left[e^{\frac{1}{2}\int_o^d \Delta\gamma(z)dz} - e^{-\frac{1}{2}\int_o^d \Delta\gamma(z)dz}\right] \qquad (115)$$

Inserting f(z) from Eq (64), one sees that Eq (115) becomes

$$V_{-1}^{JWKB}_{TRANS}(d) = |\sin\Psi_{-1}| \sqrt{\frac{Q_{-1}(d)Q_{-1}(0)}{\Delta\gamma(d)\Delta\gamma(0)}}\, e^{-\frac{1}{2}\int_o^d (C_o(z)+C_{-1}(z))dz} \left\{ e^{\frac{1}{2}\int_o^d \Delta\gamma(z)dz} - e^{-\frac{1}{2}\int_o^d \Delta\gamma(z)dz} \right\} \quad (116)$$

$V_{-1}^{JWKB}_{TRANS}$ is the complex electric field amplitude of the wave diffracted by a holographic transmission lens. Eq (116) is one of the primary results of this chapter. From it, the intensity of the diffracted wave and the diffraction efficiency of the holographic lens are determined. An analogous equation for the diffracted field amplitude for the case of a reflection hologram is obtained in the next section.

C. The Reflective Holographic Lens

For a reflection hologram, the incident and diffracted waves have the opposite sense to their z-components of propagation through the hologram. Thus, on reconstruction the hologram's output wave is on the same side as its input wave. The output wave appears to be a reflection of the input wave off the surface of the hologram (it is really a diffraction of the input wave). The boundary conditions in the case of reflection are

$$V_o(0) = 1 \quad (117)$$

$$V_{-1}(d) = 0 \quad (118)$$

The application of Eq (118) to the general solution, Eq (105), implies

$$C_- = -C_+ \, e^{\int_o^d \Delta\gamma(z)dz} \tag{119}$$

which, when substituted into Eq (105), yields

$$V_{-1}(z) = \sqrt{\frac{2iQ_{-1}(\xi)}{\Delta\gamma(z)Q_{-1}(0)}} \; e^{-\frac{1}{2}\int_o^z (C_o + C_{-1} + \Delta\gamma)d\xi} C_+ \left[e^{\int_o^z \Delta\gamma(\xi)d\xi} - e^{\int_o^d \Delta\gamma(\xi)d\xi} \right] \tag{120}$$

In order to evaluate C_+, the original differential equation, Eq (57), is solved for $V_o(z)$ to yield

$$V_o(z) = \frac{1}{Q_{-1}|\sin\Psi_{-1}|}\left[\frac{\partial V_{-1}}{\partial z} + C_{-1}V_{-1}\right] \tag{121}$$

Application of Eq (117) results in

$$1 = \frac{1}{Q_{-1}(0)|\sin_{-1}|}\left[\left.\frac{\partial V_{-1}}{\partial z}\right|_o + C_{-1}(0)V_{-1}(0)\right] \tag{122}$$

The $\left.\frac{\partial V_{-1}}{\partial z}\right|_o$ is found by differentiation of Eq (120) and evaluation at z=0 to be

$$\left.\frac{\partial V_{-1}}{\partial z}\right|_o = \sqrt{\frac{2i}{\Delta\gamma(0)}}\, C_+ \left\{ \Delta\gamma(0) + \frac{1}{2}(1 - e^{\int_o^d \Delta\gamma(z)dz}) \left[\frac{Q'_{-1}(0)}{Q_{-1}(0)} - \frac{\Delta\gamma(0)}{\Delta\gamma(0)} - (C_o(0) + C_{-1}(0) + \Delta\gamma(0))\right]\right\} \tag{123}$$

and $V_{-1}(0)$ is given by

$$V_{-1}(0) = \sqrt{\frac{2i}{\Delta\gamma(0)}}\, C_+ (1 - e^{\int_o^d \Delta\gamma(z)dz}) \tag{124}$$

C_+ is found by substituting Eqs (123) and (124) into Eq (124) to be

$$C_+ = \frac{Q_{-1}(0)\,|\sin\Psi_{-1}|}{\sqrt{\frac{2i}{\Delta\gamma(0)}}\left[\Delta\gamma(0)+\frac{1}{2}(1-e^{\int_o^d \Delta\gamma(z)dz})\,[C_{-1}(0)-C_o(0)-\Delta\gamma(0)+\frac{Q'_{-1}(0)}{Q_{-1}(0)}-\frac{\Delta'\gamma(0)}{\Delta\gamma(0)}]\right]} \tag{125}$$

Since the output of a reflection hologram occurs at z=0, the complex amplitude of the diffracted wave as a function of hologram thickness, d, is given by substitution of Eq (125) into Eq (124). This yields

$$V_{-1}^{\substack{JWKB\\TRANS}}(d) = \frac{2\,Q_{-1}(0)\,|\sin\Psi_{-1}|}{\Delta\gamma(0)\left[\frac{1+EXP(\int_o^d\Delta\gamma(z)dz)}{1-EXP(\int_o^d\Delta\gamma(z)dz)}\right]+\left[C_{-1}(0)-C_o(0)+\frac{Q'_{-1}(0)}{Q_{-1}(0)}-\frac{\Delta'\gamma(0)}{\Delta\gamma(0)}\right]} \tag{126}$$

Eq (126) is another of the primary results of this chapter. It contains an expression for the complex amplitude of the light diffracted by a reflection type holographic lens and can be used to calculate the diffraction efficiency of a reflective holographic lens.

In the next section, the JWKB solutions for the diffracted field amplitude for a reflection and transmission hologram are compared to previous theories.

D. Comparison of the JWKB Solution to Other Theories and Interpretation of the JWKB Terms

In this section, it is shown that the JWKB solution reduces to the Kogelnik results (Ref. 21) for a transmission and reflection hologram in the case of plane waves and constant coefficients. This is to be expected since plane waves are a special case of spherical waves and constant coefficients are a sub-set of variable coefficients. Also, the JWKB theory is shown to reduce to Uchida's results (Ref. 43) for the special case in which the amplitude of the index modulation is an exponentially decreasing function of thickness.

The JWKB theory should reduce to the Kogelnik results in the case of plane waves and constant coefficients. The ideal, lossless, sinusoidal grating with unslanted fringes is considered for comparison. It is assumed that reconstruction is at the Bragg angle in the plane of incidence of the original object and reference beams. In this case using Eqs (89) and (110) Eq (106) becomes,

$$\Delta\gamma = 2i\sqrt{-Q_o Q_{-1}} = 2i\sqrt{F_o} = \frac{2i\pi\Delta n_o(E)}{\lambda_o \cos\theta_c} \qquad (127)$$

The amplitude of the diffracted light is given by Eq (116), which yields, upon substitution of Eq (127), the following result

$$V_{-1}(d) = i \sin\left(\frac{\pi\Delta n_o d}{\lambda_o \cos\theta_c}\right) \qquad (128)$$

The diffraction efficiency of a holographic lens has previously been defined in Chapter I as the ratio of the diffracted output power at the output surface of the hologram to the incident power at the input surface of the hologram. This efficiency is given by

$$\eta(d)=(1-\Omega)F\ \frac{V_{-1}(d)V_{-1}^{*}(d)}{V_{o}(0)V_{o}^{*}(0)}=(1-\Omega)FV_{-1}(d)V_{-1}^{*}(d) \qquad (129)$$

$(1-\Omega)$ is a normalization factor to correct for changes in intensity caused by the fact that the diffracted wave can have a different projected area upon the front surface than does the incident light. $F(\vec{K}_{c},\vec{K}')$ is a normalization factor to correct for intensity changes caused by the convergence or divergence of the diffracted and incident light.

In the case of the ideal lossless sinusoidal transmission grating with unslanted fringes $F=(1-\Omega)=1$, and Eq (129), yields

$$\eta(d)=\underset{\text{TRANS}}{\sin^{2}\left[\frac{\pi\Lambda n_{o}d}{(\lambda_{o}\cos\theta_{c})}\right]} \qquad (130)$$

Eq (130) is the familiar Kogelnik result for an ideal, lossless unslanted transmission grating (Ref. 21).

The equations for a reflection hologram may be evaluated in a similar manner. In such a case, however, $Q_o=-Q_{-1}$, because the incident wave travels in the opposite sense in the hologram during reconstruction. Using Eq (97), Eq (127) for a reflection hologram becomes

$$\Delta\gamma = 2i\sqrt{Q_{-1}^2} = \frac{2\pi\Delta n_o}{\lambda_o \cos\theta_c} \tag{131}$$

Substitution of Eq (131) into Eq (126) yields the field amplitude diffracted from a reflective hologram,

$$V_{-1}(d) = -i\left[\frac{1 - e^{\Delta\gamma d}}{1 + e^{\Delta\gamma d}}\right] \tag{132}$$

which can be rewritten as

$$V_{-1}(d) = i \tanh\left(\frac{1}{2}\Delta\gamma d\right) \tag{133}$$

Again, using Eq (95) and the definition of efficiency, Eq (93), modified for a reflection hologram, one gets

$$\eta_{REF}^{(d)} = \tanh^2\left(\frac{\pi\Delta n_o d}{\lambda_o \cos\theta_c}\right) \tag{134}$$

Again a familiar Kogelnik result is obtained (Ref. 21).

The fact that the JWKB equations reduce to the Kogelnik results in these ideal cases is a good benchmark in the sense that there would have been an obvious flaw in the theory had that not occurred. However, this fact is not very instructive in terms of examining what the JWKB terms mean or in terms of explaining their effect upon the diffraction efficiency.

In order to gain some insight into the significance of the JWKB terms, consider the ideal, lossless, transmission grating again. Allow the index modulation to decrease exponentially as in Eq (98), repeated here

$$\Delta n(z) = \Delta n_o(F) e^{\frac{-\alpha (L_o+L_r) z}{2}} \qquad (135)$$

In this case, Eq (129), for the diffraction efficiency of a transmission grating is easily seen to reduce to

$$\eta^{JWKB}_{TRANS}(d) = \sin^2\left(\frac{\pi}{\lambda_o \cos\theta_c} \int_o^d \Delta n_o(F)\, e^{\frac{-\alpha (L_o+L_r) z}{2}} dz \right) \qquad (136)$$

which, after integration becomes

$$\eta^{JWKB}_{TRANS}(d) = \sin^2\left(\frac{2\pi \Delta n_o}{\alpha \lambda_o \cos\theta_c (L_o+L_r)} \left[1 - e^{\frac{-\alpha (L_o+L_r) d}{2}}\right] \right) \qquad (137)$$

Eq (137) has been derived previously by Uchida from the original coupled wave equations without the use of the JWKB approximation (Ref. 43). This is possible because of the exponential dependency of the amplitude of the index modulation upon distance into the emulsion. Uchida's result is a special limited case of the general JWKB theory derived in this disseration. He obtained closed form results only for reconstruction at the Bragg angle for a sinusoidally modulated planar fringe grating. However, Uchida's result, while limited, exhibits a characteristic of the effect of the JWKB terms on the solution. That characteristic, in general, is to retard the phase of the $\sin^2$ function when compared to the ideal hologram with constant index modulation. Furthermore, the magnitude of the phase retardation is dependent upon the absorption coefficient of the emulsion (α) during the construction process. Similar characteristics will be noted again in the next chapter, in which the JWKB theory is compared to experimental results.

In summary, the complex field amplitude, $V_{-1}^{JWKB}(d)$, of the diffracted wave emitted by a transmission holographic lens and a reflection holographic lens have been derived. These results are given by Eq (116) for the transmission case and by Eq (126)for the reflection case. The results are more general than previous theories, but reduce to the same for the identical conditions. Furthermore, the inequalities

which specify the regions validity of the more general JWKB results have been determined.

CHAPTER V

EVALUATION OF THE JWKB THEORY FOR A TRANSMISSION HOLOGRAM AND COMPARISON TO EXPERIMENTAL RESULTS

In this chapter the JWKB solution for the diffraction efficiency of a transmission hologram is derived and compared to experimental data. The choice of a transmission hologram is based upon the availability in the literature of more experimental transmission hologram data than is available for reflection holograms. Furthermore, the evaluation of the JWKB solution for a transmission hologram should be just as valid a measure of the usefulness of the JWKB theory as an evaluation based upon a reflection hologram.

In the beginning of this chapter, the general solution for the diffraction efficiency of a transmission hologram is derived. The JWKB integrals contained in the general solution are integrated using the trapezoidal rule. The error associated with this integration is estimated. The integration of the JWKB terms yields a closed form solution for the diffraction efficiency of a transmission hologram. The remainder of the chapter contains the results of the evaluation of this closed form solution for several specific hologram configurations.

The holograms chosen for evaluation illustrate particular effects which are predicted by the theory developed in this dissertation which previous theories do not explain. The effects upon hologram diffraction efficiency of variations in reconstruction wave vector angle of incidence, hologram thickness, and exposure are included. In addition, the hologram diffraction efficiency is evaluated for changes in the following parameters: (1) reconstruction polarization, (2) emulsion expansion or contraction, (3) optical index, (4) absorption during exposure, and (5) reconstruction out of the original construction plane of incidence. Also, the effect of the JWKB terms upon the hologram efficiency is demonstrated.

A. Derivation of the JWKB Solution for the Efficiency of a Tranmission Hologram

Before a comparsion to experimental results is made, the equation for the diffraction efficiency is derived. This section contains that derivation starting with the Eqs (129) and (116) repeated for convenience,

$$\eta_{\text{TRANS}}^{\text{JWKB}}(d) = (1-\Omega)F\, V_{-1}(d)V_{-1}^{*}(d) \tag{138}$$

$$V_{-1}(d)=\left|\sin\Psi_{-1}\right|\sqrt{\frac{Q_{-1}(0)Q_{-1}(d)}{\gamma(0)\,\gamma(d)}}\; e^{-\frac{1}{2}[\tilde{C}_{o}(d)+\tilde{C}_{-1}(d)]}\left[\, e^{\frac{1}{2}\tilde{\Delta}\gamma(d)} - e^{-\frac{1}{2}\tilde{\Delta}\gamma(d)}\,\right] \tag{139}$$

where,

$$\tilde{\Delta\gamma}(d) = \int_o^d \Delta\gamma(z)\, dz \tag{140}$$

and,

$$\tilde{C}_o(d) = \int_o^d C_o(z)dz \tag{141}$$

$$\tilde{C}_{-1}(d) = \int_o^d C_{-1}(z)dz \tag{142}$$

The efficiency is calculated by substitution of Eq (139) into Eq (138), which yields,

$$\eta = \frac{(1-\Omega)F\sin^2\psi_{-1}\left|Q_{-1}(0)Q_{-1}(d)\right|}{\left|\Delta\gamma(0)\Delta\gamma(d)\right|} e^{-[\tilde{C}_{0R}+\tilde{C}_{-1R}]} \cdot \left[e^{\tilde{\Delta\gamma}_R} - e^{i\tilde{\Delta\gamma}_I} - e^{-i\tilde{\Delta\gamma}_I} + e^{-\tilde{\Delta\gamma}_R}\right] \tag{143}$$

R and I indicate real and imaginary parts, respectively. Using hyperbolic and trigonometric definitions and identities, Eq (143) is rewritten as

$$\eta(d)_{\text{TRANS}}^{\text{JWKB}} = \frac{4(1-\Omega)F\sin^2\psi_{-1}\left|Q_{-1}(0)Q_{-1}(d)\right|}{\left|\Delta\gamma(0)\Delta\gamma(d)\right|} \cdot e^{-[\tilde{C}_{0R}(d)+\tilde{C}_{-1R}(d)]} \cdot \left\{\sinh^2\left(\frac{\tilde{\Delta\gamma}_R(d)}{2}\right)+\sin^2\left(\frac{\tilde{\Delta\gamma}_I(d)}{2}\right)\right. \tag{144}$$

where the operator $\sim \equiv \int_o^d dz$ represents a JWKB integral.

Eq (144) is the JWKB solution for the diffraction efficiency of a general mixed transmission hologram. It is similar to the Kogelnik solution in that the diffraction efficiency is proportional to the sum of $\sin^2$ function and $\sinh^2$ funtion. The $\sin^2$ component represents the contribution from a phase hologram; the $\sinh^2$ component represents the contribution from an absorption hologram. Therefore, as in the Kogelnik

case, the diffraction efficiency for a mixed hologram is the sum of the diffraction efficiencies of the absorption and phase holograms present in the medium. However, in the JWKB theory, the $\sin^2$ and $\sinh^2$ arguments are replaced by JWKB integrals. These integrals reduce to the Kogelnik arguments in the case of the ideal sinusoidal grating. However, in the general case, the JWKB integrals must be evaluated in order to compare Eq (144) to experimental results. This integration is performed by the trapezoidal rule in the next section.

B. Integration of the JWKB Integrals by the Trapezoidal Rule

A summary of the integration of the JWKB integrals appearing as arguments in Eq (144) is contained in this section. The assumptions and approximations are discussed and an estimate of the error associated with the trapezoidal rule is given. The primary result in this section is a closed form equation for the diffraction efficiency of a holographic lens. This equation can easily be evaluated on a desk calculator. In the rest of this chapter, the results of the calculator evaluation are compared to experimental measurements of the diffraction efficiency of a hologram available in the literature.

Two of the JWKB integrals appearing in Eq (144) are given by

$$\Delta\tilde{\gamma}_R(d) = R[\Delta\tilde{\gamma}(d)] = R\left[\int_o^d \Delta\gamma(z)dz\right] \tag{145}$$

$$\Delta\tilde{\gamma}_I(d) = I[\Delta\tilde{\gamma}(d)] = I\left[\int_o^d \Delta\gamma(z)dz\right] \tag{146}$$

$\Delta\gamma(z)$ is determined by substitution of Eq (89) into Eq (110) to yield,

$$\Delta\gamma(z) = \sqrt{\frac{1}{4}[C_o(z)-C_{-1}(z)]^2+Q_o(z)Q_{-1}(z)\sin^2\Psi_{-1}} + \frac{1}{2}\frac{\partial}{\partial z}\left[C_o - C_{-1} - \frac{Q'_{-1}}{Q_{-1}}\right] + \frac{1}{4}\left(\frac{Q'_{-1}}{Q_{-1}}\right) \tag{147}$$

The functional dependence ot $\Delta\gamma(z)$ upon the coordinate z is determined by substitution of the following individual functions into Eq (147). It is shown in Appendix B that

$$C_o(z) = \frac{k_o\alpha_b(z)}{2k_c\cos\theta_c} + \frac{\vec{\nabla}\cdot\vec{k}_{2c}(z)}{2k_c\cos\theta_c}\frac{1}{n_b(z)} + \frac{i}{2k_c\cos\theta_c}\left[\frac{\alpha_b^2(z)}{4n_b(z)} - \Delta k^2 n_b^2(z)\right] \tag{148}$$

$$C_{-1}(z) = \frac{1}{2}\left[\frac{i\left(-\frac{\alpha_b^2}{4} - \Delta k^2 n_b^2(z) + \vec{K}'\cdot\vec{K}' - 2\vec{k}_{2c}(z)\cdot\vec{K}'\right) + n_b(z)\alpha_b(z)k_o + \vec{\nabla}\cdot(\vec{k}_{2c}(z)-\vec{K}')}{k_c n_b(z)\cos\theta_c - K'_z}\right] \tag{149}$$

$$Q_o(z) = \frac{i\,k_1^2(z)}{4(k_c n_b(z)\cos\theta_c)} \tag{150}$$

$$Q_{-1}(z) = \frac{i\, k_1^2(z)}{4(k_c n_b(z)\cos\theta_c - K_z')} \tag{151}$$

where,

$$k_1^2(z) = 2k_o^2\, n_b(z)\Delta n(z) \tag{152}$$

$n_b(z)$ is the optical index of the hologram and $\Delta n(z)$ is the optical index modulation which are derived in Appendix B to be,

$$n_b(z) = n_o + \delta n_{max}\left(1 - e^{\frac{-E_{bo}A(z)}{D}}\right) \tag{153}$$

$$\Delta n(z) = \delta n_{max}\left(1 - e^{\frac{-E_{bo}M(z)}{D}}\right) \tag{154}$$

where,

$$A(z) = \frac{R_o^2}{|\vec{r}-\vec{R}_o|}\left[\frac{e^{-\alpha L_o z} + \kappa(x,y)\, e^{-\alpha L_r z}}{1+\kappa_o}\right] \tag{155}$$

and,

$$M(z) = \frac{2\sqrt{\kappa_o}}{1+\kappa_o}\,\frac{R_o R_r \hat{e}_o\cdot\hat{e}_r}{|\vec{r}-\vec{R}_o|\,|\vec{r}-\vec{R}_r|}\, e^{-\frac{\alpha}{2}(L_o+L_r)z} \tag{156}$$

The symbols appearing in Eqs (148) through (156) are defined in the respective appendices in which the functions are derived. Eqs (148) through (156) can be substituted into Eqs (147), (148) and (149) to obtain the functions $\Delta\gamma(z)$, $C_o(z)$, and $C_{-1}(z)$.

The main reason for listing Eqs (148) through (156) is to emphasize the complicated functional dependency of $\Delta\gamma(z)$, $C_o(z)$, and $C_{-1}(z)$ upon z. Consequently, the JWKB integrals are difficult to perform. Indeed, no exact solutions to any of the JWKB integrals could be found by this worker. Consequently, however, the following approximation technique is shown to be very effective.

The JWKB integrals were performed using the trapezoidal approximation. The trapezoidal rule is defined as (Ref. 18),

$$\int_o^d U(z)dz = \frac{d}{2}[U(o)+U(d)] - \frac{d^3}{12}U''(\xi) \qquad (157)$$

Where ξ is some value of z between o and d, the thickness of the hologram. It is important to note that Eq (157) is an exact equation in that it holds without any error for some particular value of ξ as a consequence of the Theorem of the Mean (Ref. 18). If the last term in Eq (157) is dropped, the Eq (157) is called the trapezoidal approximation. The last term can be used to estimate of the maximum error involved in the use of the trapezoidal approximation. This error is given by

$$\varepsilon \leq \frac{d^3}{12} |U''_{max}| \qquad (158)$$

The application of the trapezoidal approximation to the JWKB integrals in Eq (144) yields the following closed form equation for the diffraction efficiency of a transmission holographic lens.

$$\eta(d)=\left[\frac{4F(1-\Omega)\sin^2\Psi_{-1}\left|Q_{-1}(0)Q_{-1}(d)\right|e^{-\frac{d}{2}[C_{0R}(0)+C_{0R}(d)+C_{-1R}(0)+C_{-1R}(d)]}}{\left|\Delta\gamma(0)\Delta\gamma(d)\right|}\right]\cdot$$

$$\cdot\left[\sinh^2\left(\frac{d}{4}[\Delta\gamma_R(0)+\Delta\gamma_R(d)]\right)+\sin^2\left(\frac{d}{4}[\Delta\gamma_I(0)+\Delta\gamma_I(d)]\right)\right] \qquad (159)$$

Eq (159) is the primary result of this chapter. It is the theoretical result from which a comparison between experimental measurements and theoretical predictions for the diffraction efficiency is to be made. Before this comparison is discussed, an error analysis based upon Eq (158) is presented in order to determine the error involved in the use of the trapezoidal approximation.

C. Error Analysis of Trapezoidal Approximation

The objective of this section is to determine an estimate of the order of magnitude of the error associated with the use of the trapezoidal approximation. One approach to this objective would be the evaluation of Eq (158) for the

functions $\Delta\gamma(z)$, $C_o(z)$, and $C_{-1}(z)$. Such an evaluation would be exact, but entirely too lengthy for our purposes. Instead, a less complicated, but realistic approach to the error evaluation, which will provide the reader with an understanding of the order of magnitude of the error associated with the application of the trapezoidal approximation, is taken.

The approach is to analyze the error associated with the trapezoidal approximation applied only to the dominant terms in the argument of the JWKB integrals. The trapezoidal rule is shown to be accurate for the integral of dominant terms. From this it is concluded that contributions to the error associated with the trapezoidal approximation are negligible when less dominant terms are included in the argument of the integral.

First, consider the error associated with the trapezoidal integration of JWKB integral $\tilde{\Delta\gamma}(d)$, Eq (147). It has been argued in Chapter IV that the dominant term is $Q_o(z)Q_{-1}(z)\sin^2\Psi_{-1}$. Therefore, if only dominant terms are considered, $\tilde{\Delta\gamma}(d)$ becomes

$$\tilde{\Delta\gamma}(d) \simeq \left|\sin\Psi_{-1}\right| \int_o^d \sqrt{Q_o(z)Q_{-1}(z)}\, dz \qquad (160)$$

It has previously been shown in Chapter IV that for the case of unslanted fringes, $Q_o(z)$ and $Q_{-1}(z)$ are equal, and become

$$Q_o(z) = Q_{-1}(z) = \frac{.5i\ k_o \Delta n(z)}{\cos\theta_c} \qquad (161)$$

For the general case of slanted fringes, $Q_o(z)$ and $Q_{-1}(z)$ would not be equal, but their magnitudes would be of the same order. Consequently, the limitations associated with using Eq (161) in Eq (160) for the purposes of error analysis is not significant. Substitution of Eq (161) into Eq (160) results in

$$\Delta\gamma\ (d) = \frac{ik_o}{2\cos\theta_c} \int_o^d \Delta n(z)dz \qquad (162)$$

The error associated with the use of the trapezoidal rule is obtained from Eq (158). The function U(z) becomes,

$$U(z) = \frac{ik_o}{2\cos\theta_c}\ \Delta n(z) \qquad (163)$$

where $n(z)$ is given by (see Appendix B) Eq (98) from Chapter III, repeated here,

$$\Delta n(z) = \Delta n_o(E)\ e^{-\frac{\alpha}{2}(L_o+L_r)z} \qquad (164)$$

and $L_o = \frac{1}{\cos\theta_o}$ and $L_r = \frac{1}{\cos\theta_r}$ as previously explained.

$$U(z) = \frac{ik_o \Delta n}{2\cos\theta_c} e^{-\frac{\alpha}{2}(L_o+L_r)z} \tag{165}$$

for which U"(z) becomes

$$U''(z) = \frac{ik_o \Delta n_o \alpha^2 (L_o+L_r)^2}{8\cos\theta_c} e^{-\frac{\alpha}{2}(L_o+L_r)z} \tag{166}$$

Substitution of the maximum value U"(z) into inequality (158) yields,

$$\varepsilon \leq \frac{d^3 k_o \Delta n_o \alpha^2 (L_o+L_r)^2}{96\cos\theta_c} \tag{167}$$

The inequality, (167), provides an estimate of the upper bound for the error associated with the use of the trapezoidal approximation. The relative percent error is defined as

$$EFF(\%) = \frac{\varepsilon \times 100\%}{|\Delta\gamma(d)|} \tag{168}$$

For this case, $|\Delta\gamma(d)|$ can be integrated exactly to yield

$$|\Delta\gamma(d)| = \frac{k_o \Delta n_o (1-e^{-\frac{\alpha}{2}(L_o+L_r)d})}{\alpha(L_o+L_r)\cos\theta_c} \tag{169}$$

AD-A041 537 AIR FORCE INST OF TECH WRIGHT-PATTERSON AFB OHIO SCH--ETC F/G 20/6
THE THEORY OF DIFFRACTION FROM A HOLOGRAPHIC LENS.(U)
MAY 77 D D YOUNG

UNCLASSIFIED AFIT/DS/PH/76-4 AFAL-TR-76-270 NL

2 OF 3
AD
A041537

Inequality (167) and Eq (169) are substituted into Eq (168) to derive an inequality for the upper bound of the percent error associated with the use of the trapezoidal approximation, which is

$$EFF(\%) \leq \frac{[\,d(L_o+L_r)\,]^3 \times 100\%}{96\left[1 - e^{-\alpha(L_o+L_r)d}\right]} \qquad (170)$$

By observation of inequality (170), it is concluded that the upper bound for the percent error associated with the trapezoidal rule grows as the cube of the absorption coefficient of the emulsion during exposure and as the cube of the thickness of the processed hologram. Clearly, if either of these parameters grows without bound, the percent error would become unacceptable at some point.

While certain terms have been neglected in the derivation of the upper bound in inequality (170), the terms neglected are relatively small as argued in Chapter IV.

Inequality (170) presents an upper bound on the limit of the usefulness of the trapezoidal approximation. The magnitude of this upper bound must be checked before the trapezoidal approximation is applied to specific holographic materials.

If inequality (170) is evaluated for the typical holographic material, dichromated gelatin ($d=13\mu$, $\alpha=2.75\times 10^{4}m^{-1}$; $L_o=L_r=\frac{1}{\sqrt{2}}$), the upper bound for the percent error associated with the use of the trapezoidal approximation is

$$\text{EFF } (\%) \leq .6\% \qquad (171)$$

This relative percent error is indeed small and it appears reasonable to use the trapezoidal approximation for this particular material.

The dominant term approach for the analysis of the percent error associated with the trapezoidal approximation has determined the approximate order of magnitude of the errors to be expected. Similar orders-of-magnitude (<1%) in the percent errors associated with C_o and C_{-1}, JWKB integrals, have been determined by this author, but these results are not presented because it is the objective of this section to merely provide the reader with the order-of-magnitude of the error to be expected. The reader is cautioned to check the validity of the use of the trapezoidal approximation for each type of holographic material considered.

D. Evaluation of Theory

The efficiency for a transmission holographic lens given by Eq (159) was programmed on a Hewlett-Packard Model 9820 desk calculator with plotter. The program was formatted so that the diffraction efficiency could be plotted as a function of "angle-off-Bragg" or as a function of total exposure (measured in millijoules/cm^2) during construction.

The term "angle-off-Bragg" (δ) has a specific meaning in the context of a hologram to be defined in this paragraph. The Bragg angle is the angle between the normal to the hologram surface and the wave vector of the reference beam during construction (Ref. 21). If, after processing of the hologram, the thickness of the medium and fringe structure remain unchanged from what they were during construction, then the maximum diffraction efficiency occurs for a reconstruction wave vector parallel to the original reference wave vector. This is termed "Bragg-reconstruction". However, if the wave vector of the reconstruction beam is not parallel to the original reference wave vector direction, an angle exists between the wave vectors. The angle (δ) between the reference wave vector and the reconstruction wave vector is called the "angle-off-Bragg". The geometrical relation of δ to the various wave vectors is shown in Figure 4.

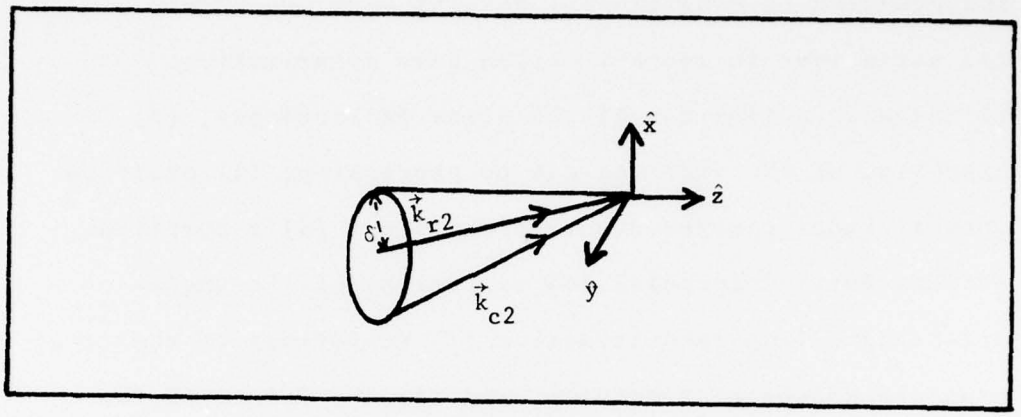

Figure 4. Cone of Possible "angle-off-Bragg"
δ is the angle-off-Bragg, the angle between the reconstruction wave vector, $\vec{k}_{c2}$, and the reference wave vector $\vec{k}_{r2}$. There is a cone about $\vec{k}_{r2}$ of half angle δ of possible locations of $\vec{k}_{c2}$.

If $\vec{k}_{c2}$ lies in the plane of incidence (the plane formed by the $\vec{k}_{o2}$ and $\vec{k}_{r2}$), the angle-off-Bragg is positive ($\delta \geq 0$) when the angle measured from the reference wave vector to the reconstruction wave vector is determined by a clockwise rotation about the normal to the plane of incidence, the angle-off-Bragg is negative ($\delta < 0$) when this rotation is counter-clockwise. For reconstruction wave vectors lying out of the plane of incidence, the sign of the angle-off-Bragg is determined by an appropriate transformation to the plane of incidence.

The following effects will be examined in this section and compared to experimental results when possible: (1) variations in reconstruction beam polarization, (2) reconstruction out of the plane of incidence, (3) expansion of the emulsion due to processing, (4) emulsion optical index changes due to processing, (5) absorption effects during exposure, (6) variations of the angle-off-Bragg during reconstruction, (7) variations of the total exposure during construction, and (8) the effect of the JWKB terms.

In order to illustrate these effects, two hologram construction geometries for which experimental data is available in the literature are considered. The first is a hologram made by Rose and Willimason referred to as the "45° x 45° hologram" (Ref. 40). It is used to illustrate the first two effects mentioned above: (1) variations in reconstruction beam polarization and (2) reconstruction out of the plane of incidence.

The second hologram considered is a hologram made by Chang known as the "ERIM Hologram" (Ref. 6,7). It is used to illustrate the remaining effects previously listed.

These holograms are used throughout the rest of this chapter and serve as a basis for comparison of the JWKB theory to experimental data. In the following paragraphs these holograms are described in greater detail because of their importance to the evaluation. After this description, the holograms are referred to by name only in the remaining sections of this chapter.

1. Description of Holograms used for Experimental and Theoretical Comparison. The "45° x 45° hologram" was constructed using a helium neon laser (λ_o=6328Å) for an experiment by Rose and Williamson in order to determine the reconstruction sensitivity to variations in incident beam polarization. This construction geometry is shown in Figure 5. The "45° x 45° hologram" was recorded on Kodak 649F high resolution silver halide emulsion (described in Appendix D) using plane waves. The object and reference beams were incident at 45° with respect to the normal to the emulsion as measured inside the liquid gate, such that the beams were 90° apart. The liquid inside the gate was used to index match the surfaces of the emulsion and glass substrate in order to eliminate surface reflections and surface relief which would create noise upon reconstruction, and to allow entrance into the emulsion at 45°. During the experiment, reconstruction occurred along the original reference beam wave vector direction; the polarization during reconstruction was

varied from vertical to horizontal in steps of 10° measured with respect to the plane of incidence. For each change in polariztion, the intensity of the reconstructed image was recorded (Ref. 40).

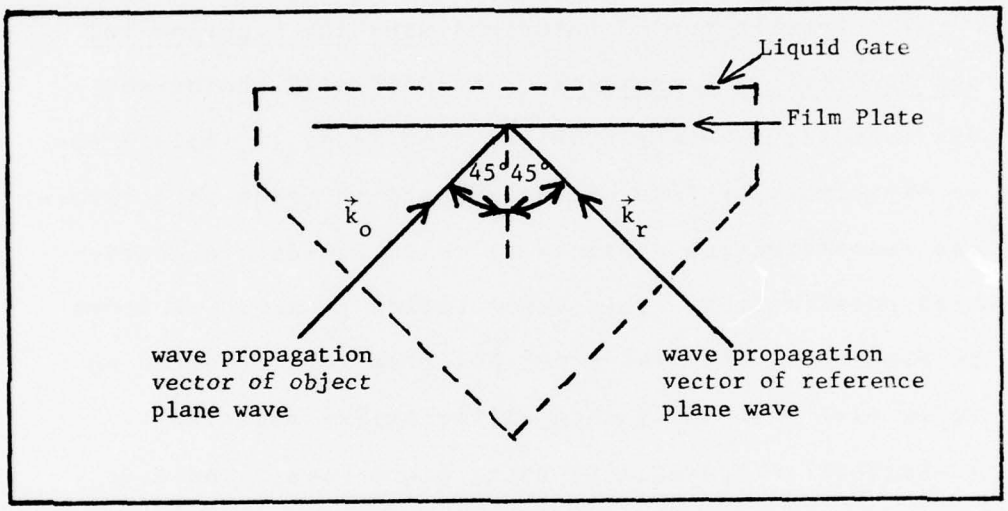

Figure 5. 45° x 45° Construction Geometry

The "45° x 45° hologram" is used to illustrate the effect of reconstruction beam polarization upon the hologram efficiency. The predictions of the theory developed in Appendix H are compared to the experimental results obtained by Rose for "45° x 45° hologram". Good agreement is found for low exposure levels, but significant differences occur

for high exposure levels. Also, the effects on the diffraction efficiency for reconstruction out of the original construction plane of incidence are demonstrated using the "45° x 45° hologram". Experimental and theoretical comparisons are not made in this case because of the lack of such information in the literature.

The second hologram used for the comparison purposes in the evaluation of the JWKB hologram efficiency is the "ERIM hologram". The construction geometry for this hologram is shown in Figure 6. Several holograms were recorded on dichromated gelatin (5% dichromate by volume) using an Argon Laser (λ_o=5145Å) for the construction in geometry in Figure 6. Dichromated gelatin as a recording material of transmission holograms is described in Appendix E. A series of holograms was made, each having a different exposure. Chang recorded the exposure for each hologram and processed the series of holograms in simultaneous identical steps. The diffraction efficiency was measured as a function of angle-off-Bragg for each exposure level.

In the later sections of this chapter, the diffraction efficiency calculated by the JWKB method is compared to the experimental diffraction efficiency measured by Chang for the "ERIM Hologram". Excellent agreement is obtained between the experimental and theoretical predictions for

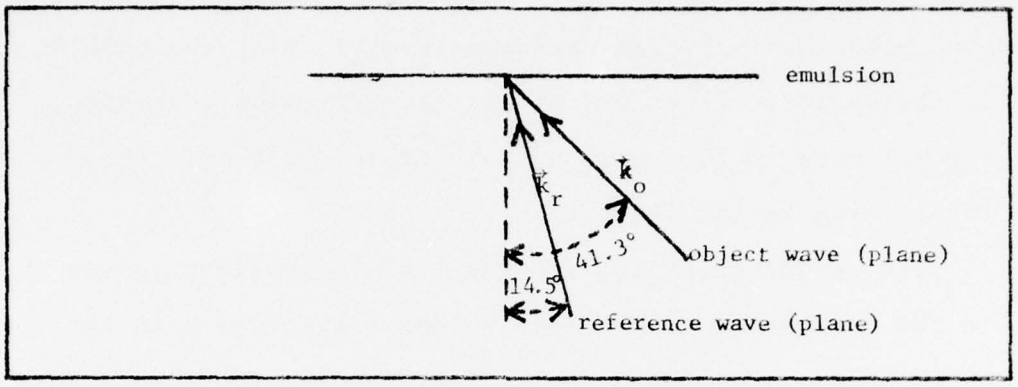

Figure 6. Recording Geometry for "ERIM Hologram" (Ref. 6, 7)

the diffraction efficiency. Variations in the hologram diffraction efficiency as a function of changes in (1) emulsion expansion, (2) optical index, (3) absorption during exposure, (4) angle-off-Bragg, (5) total exposure, and the JWKB terms are evaluated by comparison to the data available for the "ERIM Hologram".

2. Polarization Effects during Reconstruction. The reconstruction efficiency of a hologram is dependent upon the polarization of the reconstruction beam as derived by several authors (Ref. 3, 4, 13, 21, 40, 44). These authors have predicted that the efficiency at Bragg reconstruction should be proportional to $\sin^2\psi_{-1}$, where

Ψ_{-1} is the angle between the polarization of the incident wave and the diffraction direction (derived in Appendix H). Indeed, Rose and Williamson have confirmed such a response for a Kodak 649F hologram. However, it is the contention of this author that such a response is only a consequence of the relatively weak coupling characteristics of 649F holograms.

This may be more easily understood by considering Eq (159) in the lossless, Kogelnik case, for which

$$\eta = \frac{4(1-\Omega)Q_{-1}^2 \sin^2\Psi_{-1}}{|\Delta\gamma|^2} \sin^2\left(\frac{\Delta\gamma_I d}{2}\right) \tag{172}$$

For Bragg reconstruction $|\Delta\gamma| = |\Delta\gamma_{\pm}|$, where

$$|\Delta\gamma_I| = |2\sqrt{Q_o Q_{-1}}\sin\Psi_{-1}| \tag{173}$$

using the relation for transmission holograms that

$$Q_{-1} = \frac{Q_o}{1-\Omega} \tag{174}$$

and substitution of Eqs (173) and (174) into Eq (172).

$$\eta = \sin^2[\sqrt{1-\Omega}\, Q_{-1} d|\sin\Psi_{-1}|] \tag{175}$$

Therefore, the efficiency is not proporational to $\sin^2\psi_{-1}$. However, for the case of weak coupling, where the $Q_{-1}d$ product is small, the argument of the sine may be substituted for the sine, which yields

$$\eta = (1-\Omega)|Q_{-1}|^2 d^2 \sin^2\psi_{-1} \qquad (176)$$

Therefore, for weak coupling, the efficiency of a hologram is proportional $\sin^2\psi_{-1}$, where $Q_{-1}=ik_o\gamma_n E_b M/(2\cos\theta_c(1-\Omega))$ and γ_n is the slope of the optical index versus exposure curve in the linear region (see Appendix B), $k_o = \frac{2\pi}{\lambda_o}$, E_b is the total exposure, M is the construction beam interference modulation, and θ_c is the angle between the construction wave vector and the normal to the emulsion. Eq (159) was evaluated for the Kogelnik, ideal-hologram case using the construction geometry of the "45° x 45° hologram" (shown in Figure 5) for reconstruction at the Bragg angle for various polarizations of the incident light. The diffraction efficiency for each polarization angle was normalized with respect to the maximum value and plotted as a function of $\sin^2\psi_{-1}$. Figure 7 is a graph of the normalized diffraction efficiency versus $\sin^2\psi_{-1}$. It shows the theoretical predictions of Eq (159) for for the case of weak coupling (γ_n = .000069) and strong

coupling (γ_n = .00023). Also plotted in Figure 5 is the experimental data taken by Rose and Williamson (Ref. 40)

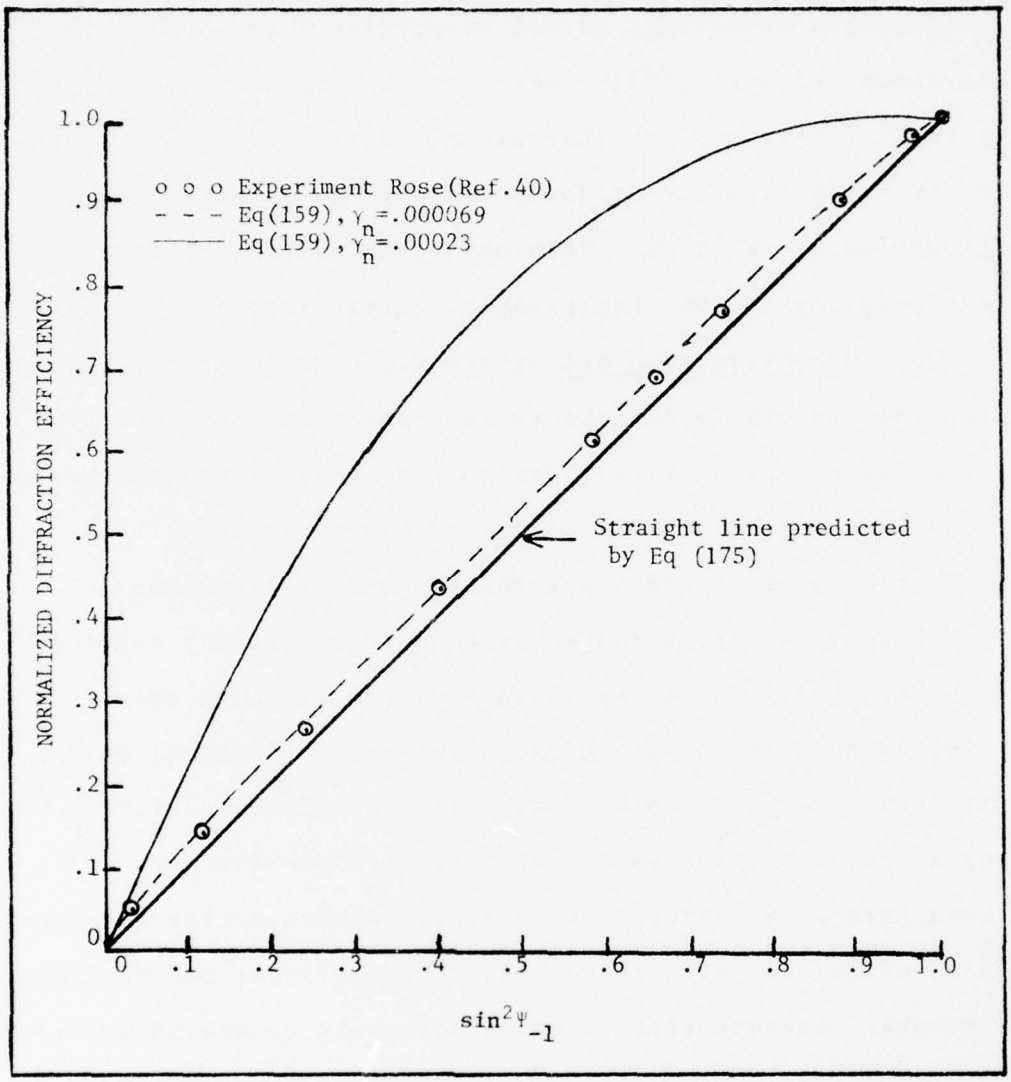

Figure 7. Normalized Diffraction Efficiency versus $\sin^2\psi_{-1}$ for "45° x 45° Hologram"

The theoretical data in Figure 7 indicates that for the case of weak coupling the diffraction efficiency is in very close agreement with the experimental data taken by Rose. For the case of strong coupling, the theoretical diffraction efficiency is not proportional to $\sin^2\psi_{-1}$ in agreement with Eq (174). Both the experimental data points of Rose and the theoretical data points for the case of weak coupling lie slightly above the straight line predicted by Eq (175). This may be an indication that the coupling is just beginning to become strong.

3. Reconstruction out of the Plane of Incidence. The Kogelnik theory is limited to reconstruction wave vectors lying in the plane of incidence of the object and reference beam wave vectors. This is one of the fundamental assumptions of the Kogelnik theory (Ref. 21) and the equations are derived based upon this geometrical limitation.

The theory developed in this dissertation is not limited to reconstruction in the plane of incidence for two reasons: (1) the reconstruction is accounted for by a reconstruction wave vector $\vec{k}_{c2}$ and the fringe structure is accounted for by a fringe wave vector (see the $\vec{K}'\,\vec{K}' - 2\vec{k}_{2c}\cdot\vec{K}'$ term in Eq (149)), and (2) the polarization vectors. Because these vectors are three dimensional, the

diffraction efficiency equations developed in this dissertation are not limited to wave vectors lying in the plane of incidence.

The effect upon the diffraction efficiency of reconstruction wave vectors lying out of the plane of incidence is shown in Figure 9 for the "45° x 45° hologram". The plane in which the rotation of the angle-off-Bragg occurs is specified by the angle p, where p is the angle that the plane of rotation of the reconstruction wave vector makes with respect to the normal to plane of incidence(See Fig 8). If p = 0, for example, then the plane of rotation is perpendicular to the plane of incidence. The reconstruction wave vector starts out 10° below the original reference wave vector and moves to +10° above the original wave vector as the angle-off-Bragg changes from -10° to +10°. In each case, when the angle-off-Bragg is zero, reconstruction occurs for a wave vector parallel to the original reference wave vector. The geometry for the p = 0 case is shown in Figure 8 in which $\vec{k}_o$, and $\vec{k}_r$ are contained in the (y, z) plane.

The angular sensitivity of a hologram is determined by the $\eta(\delta)$ plots. The angular bandwidth of a hologram is the number of degrees between the primary zeros of the $\eta(\delta)$, δ being the angle-off-Bragg. The angular sensitivity

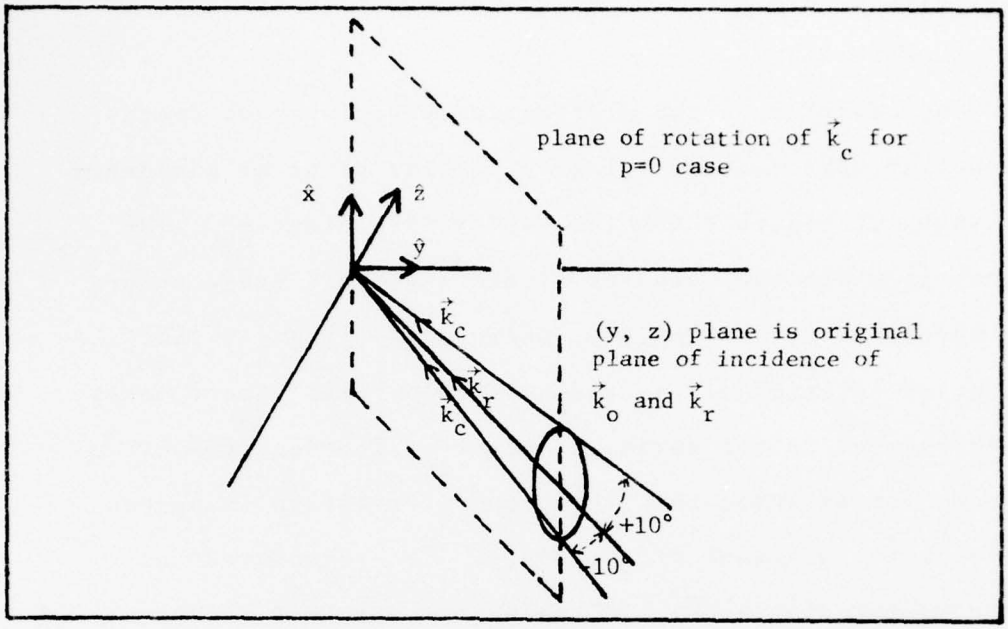

Figure 8. Case for which p=0 showing rotation of $\vec{k}_{2c}$ from δ=-10° to δ=+10° in a plane perpendicular to ($\vec{k}_o$, $\vec{k}_r$)

decreases from about 20° for the p=0 case to about 3° for the p =45° case. This is caused by the fact that the diffraction efficiency of the 45° x 45° hologram is particularly sensitive to variations in the y-component of the reconstruction wave vector because the wave vector for the fringes, $\vec{K}$, is totally in the y-direction.

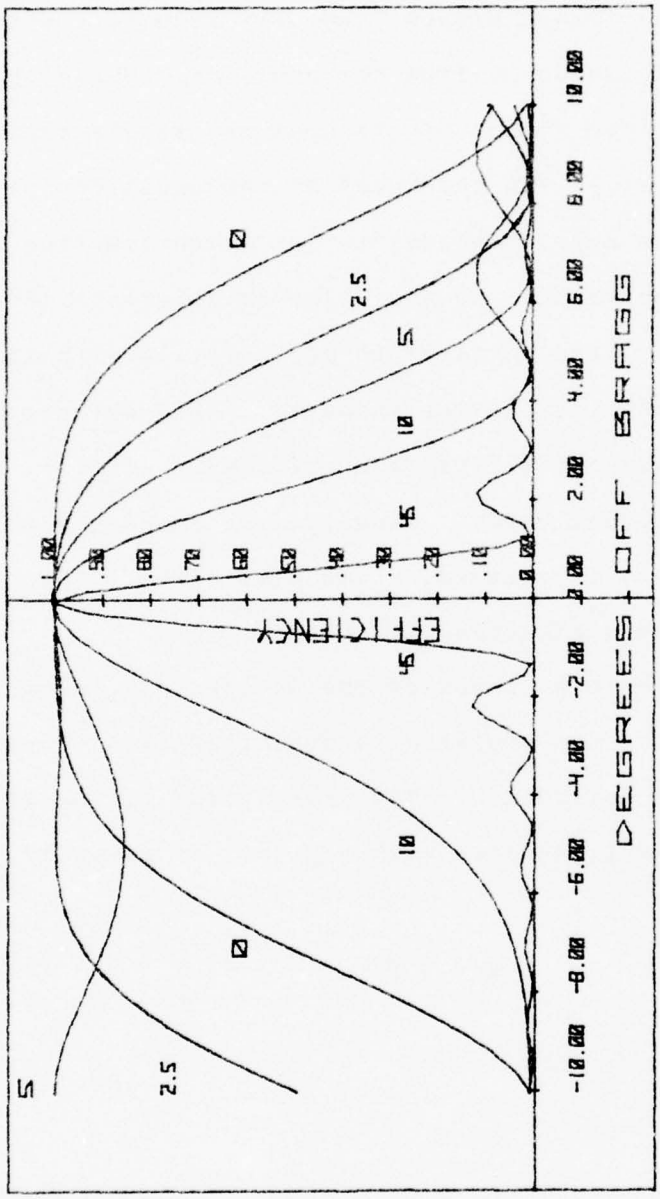

Figure 9. Diffraction Efficiency versus Angle off Bragg for a Reconstruction Wave Vector out of the Plane of Incidence. The numbers associated with each curve denote the angle that the plane of motion of the reconstruction wave vector makes with respect to normal to the plane of incidence, Hologram Geometry defined by the "45° x 45° Hologram".

4. Expansion and Shrinkage of the Emulsion. During processing, the exposed emulsion may expand or contract due to chemically induced changes in the emulsion structure, cracking along fringe planes, humidity induced changes, or removal of compounds from the emulsion. These changes in thickness have three effects upon the reconstruction process. Firstly, the thickness of the emulsion is different; the angular bandwidth for reconstruction is inversely proportional to the hologram thickness (Ref. 32). Secondly,the fringe surfaces rotate position with respect to their orientation during exposure. This changes the position of maximum diffraction efficiency of $\eta(\delta)$, from $\delta=0$, to some other value. Finally, the spacing between fringe surfaces is changed, which also affects the position of the maximum diffraction efficiency.

The change in position of the fringes due to expansion or shrinkage of the emulsion is described by a transformation, T, derived in Appendix C. The wave vector of the fringes after processing, denoted with a prime, is given by

$$\vec{K}' = \underline{T}\,\vec{K}' \qquad (177)$$

and the thickness of the emulsion, denoted by d', is given by

$$d' = S_z d \tag{178}$$

S_z is the thickness factor representing the relative change in emulsion thickness caused by processing. If expansion occurs during processing $S_z > 1$; if shrinkage occurs $S_z < 1$.

Figure 10 shows the theoretically predicted diffraction efficiency versus δ curves for the "ERIM hologram", previously described, with expansion and shrinkage accounted for in this manner. The ordinate is the diffraction efficiency (η) given by Eq (159), and the abscissa is the angle-off-Bragg (δ) previously defined.

If a change in thickness does not occur, then $\vec{K}' = \vec{K}$ and the maximum diffraction efficiency occurs when the reconstruction beam wave vector is parallel to the reference beam wave vector ($S_z = 1$ curve in Figure 10). This occurs at zero "degrees off Bragg", since the angle between the reconstruction wave vector and the reference beam wave vector is zero. If $S_z \neq 1$, then $\vec{K}' \neq \vec{K}$ and the maximum diffraction efficiency occurs for a reconstruction wave vector not parallel to the original reference wave vector, that is, at some $\delta \neq 0$.

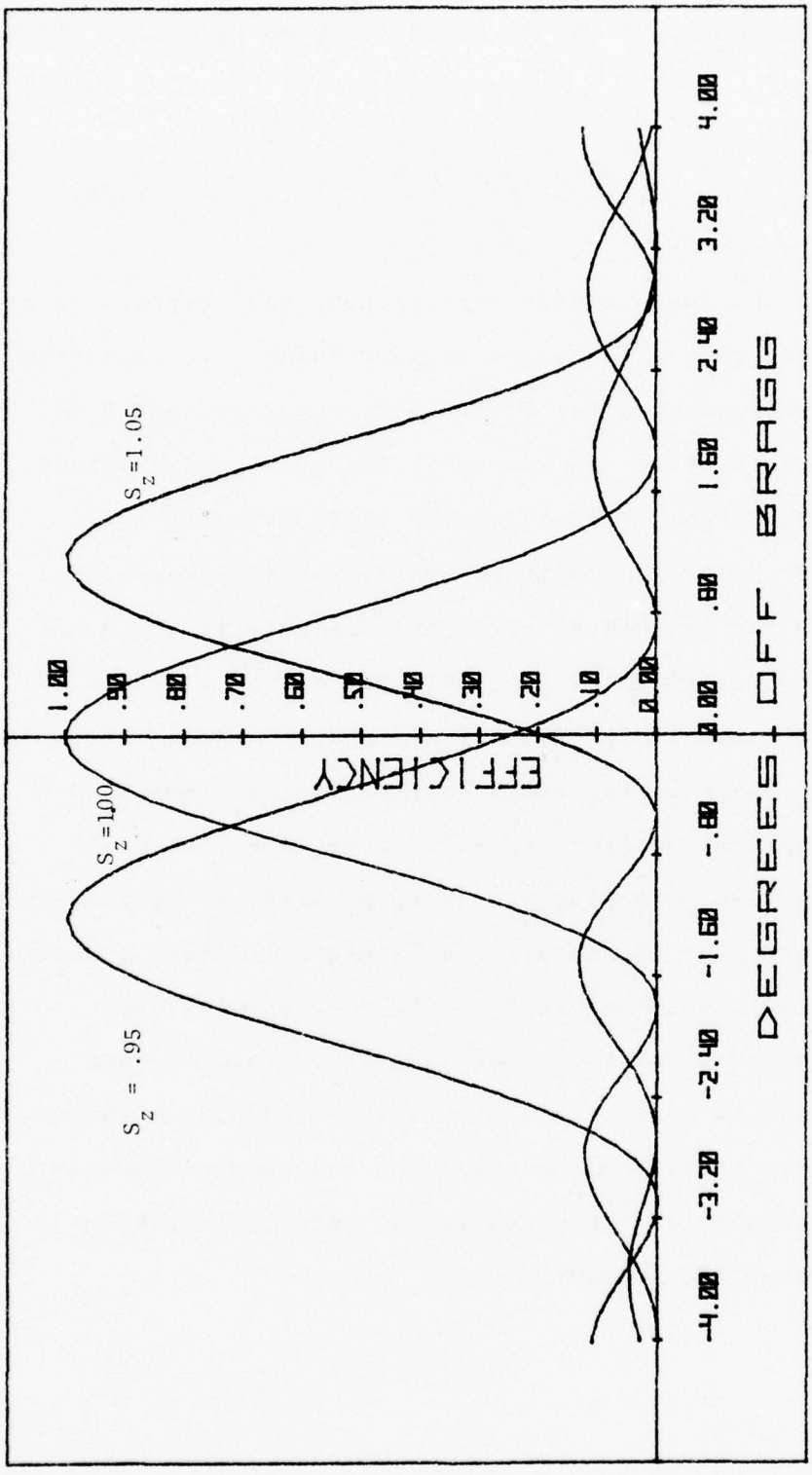

Figure 10. Diffraction Efficiency versus angle-off-Bragg for the ERIM Hologram Shows effect of shrinkage (S_z=.95) and expansion (S_z=1.05) compared to no change in thickness (S_z=1.00). Efficiency is calculated from Eq (159) for the Kogelnik ideal hologram. Sz is the change in thickness factor defined by Eq (178).

Two results can be obtained from Figure 10. First, the position of the diffraction efficiency maximum moves from positive to negative angles-off-Bragg as the change in thickness moves from expansion ($S_z > 1$) to shrinkage ($S_z < 1$). This position is consistent with the Bragg condition given by

$$\vec{K}' \cdot \vec{K}' - 2\vec{k}_{2c} \vec{K}' = 0 \qquad (179)$$

Second, the diffraction efficiency, $\eta(\delta)$, is proportional to $(\frac{\sin\delta}{\delta})^2$ as previously predicted by Kogelnik theory (Ref. 21).

The effects of thickness changes upon the diffraction efficiency and the angular sensitivity is later shown to agree well with the experimental work obtained by Chang (see Figure 12).

5. Optical Index Change due to Processing. The optical index of the emulsion after processing is usually not the same as the optical index of the emulsion during exposure. The reasons for the change in optical index is due to the removal or addition of substances during processing (Ref. 33). Upon reconstruction, the maximum diffraction efficiency does not occur for reconstruction wave vectors along the original reference wave vector.

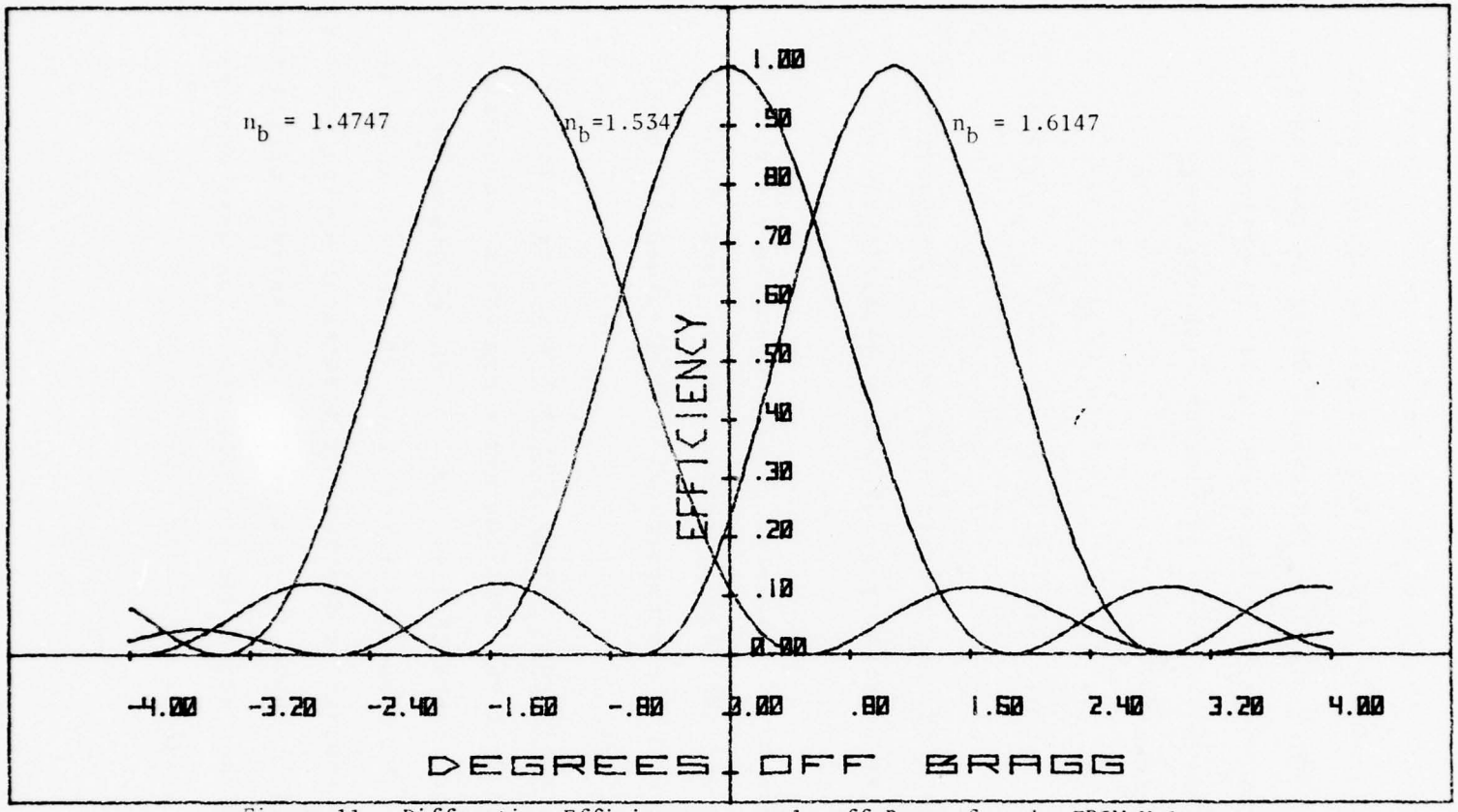

Figure 11. Diffraction Efficiency vs angle-off-Bragg for the ERIM Hologram Shows effects of optical index changes due to processing which cause the optical index of the emulsion to be different than the optical index of the emulsion during exposure. n_b=1.5347 is the case of no change in optical index due to processing. The diffraction efficiency is calculated from Eq (159) for the ideal Kogelnik hologram.

The change in optical index after processing is accounted for theoretically by changing the optical index in the reconstruction wave vector to the optical index after processing.

The effect upon the diffraction efficiency of optical index changes during processing was evaluated using Eq (159) for the Kogelnik case using the ERIM Hologram. The results are presented in Figure 11. The position of maximum diffraction efficiency shifts from positive to negative angles-off-Bragg as the index varies from lower to higher values than the index of the emulsion during exposure. This shift is consistent with the Bragg condition given by Eq (179).

6. Comparison of the JWKB Theory to Experimental Measurements. In this section the JWKB theory is compared to the experimental measurement made by Chang (Ref. 6, 7). The effects upon the diffraction efficiency of (1) absorption during exposure, (2) variations in angle-off-Bragg, (3) variations in exposure, and (4) the physical significance of the JWKB terms is discussed. In all cases, the construction geometry is that of the "ERIM Hologram" described in Figure 4.

The experimental results which Chang obtained are most interesting in that the Kogelnik theory for the diffraction efficiency fails to predict the experimentally measured diffraction efficiency. It will be shown in this section that the JWKB theory developed in this dissertation does predict the experimentally measured diffraction efficiency.

Chang exposed a series of plane wave holograms according to the geometry in Figure 6. The total exposure (measured in millijoules/cm^2) was increased for each successive hologram. The object and reference beams were of equal intensity. The range of exposure was from 24 mj/cm^2 up to 1069 mj/cm^2.

After processing the series of holograms under identical conditions, the diffraction efficiency of each hologram was measured as a function of angle-off-Bragg. From this data the angular sensitivity and angular bandwidth of the hologram as a function of exposure was determined. Also, the diffraction efficiency at the center of the angular bandwidth as a function of exposure could be obtained.

The experimental data obtained by Chang for a total of 24 mj/cm^2 is shown in Figure 12. The solid line through the data is the theoretically predicted efficiency using the theory of Kogelnik based upon a linear response of

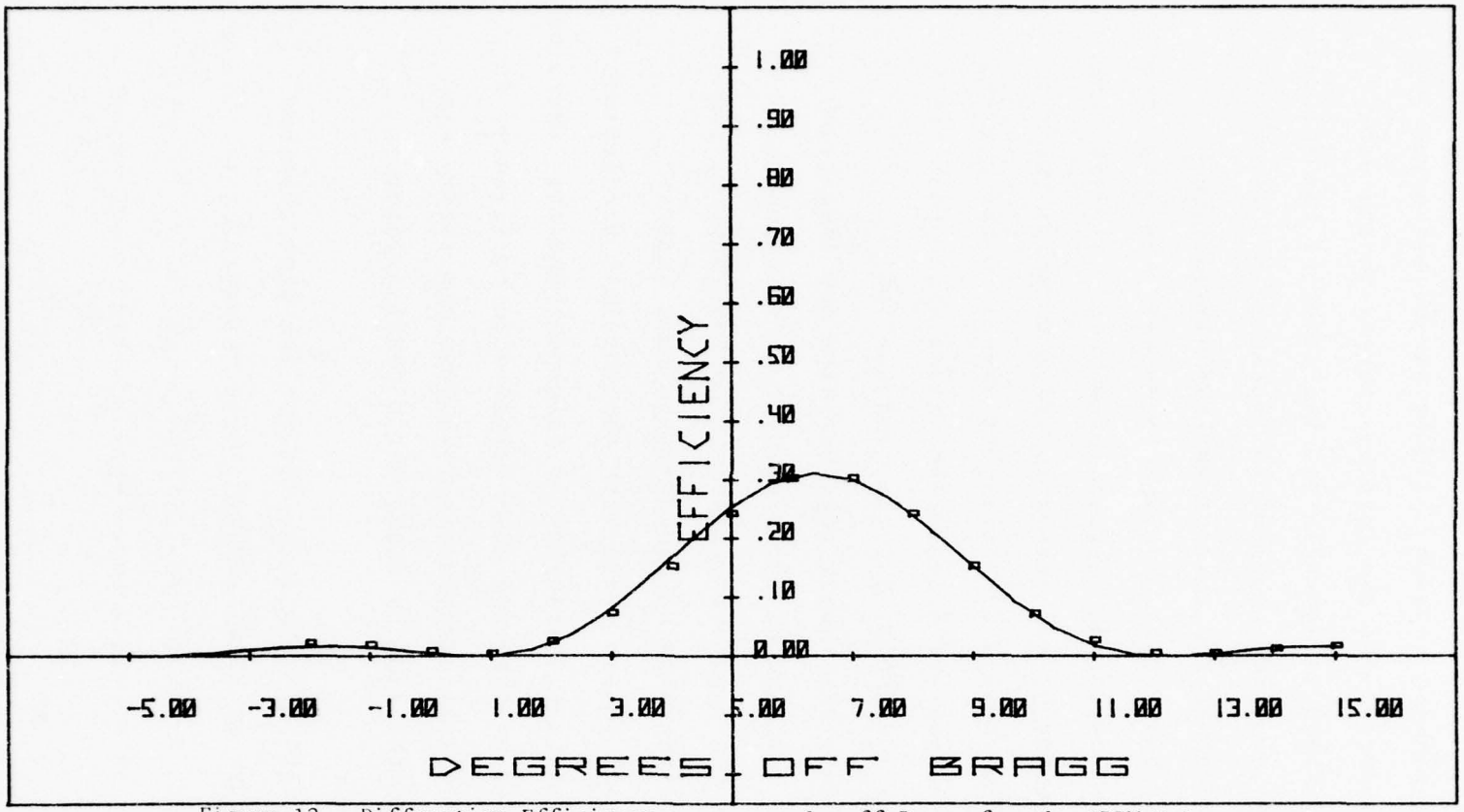

Figure 12. Diffraction Efficiency versus angle-off-Bragg for the ERIM Hologram The diffraction efficiency is calculated from Eq (159) for the ideal Kogelnik hologram. The parameters γ_n=.00023, d=12.4μ,and S_z=1.353 were used to curve fit the data. The data (represented by squres) is provided by Dr. Chang and used by permission (Ref. 6). The total exposure is 24 millijoules/cm^2. A linear index modulation response to exposure is assumed.

index modulation to exposure. Three parameters were varied in order to fit the Kogelnik theory to the data. First, γ_n (defined in Appendix B), the slope of the optical index response of the emulsion to exposure, was varied in order to obtain the correct maximum diffraction efficiency (about 30%). The thickness was varied in order to determine the correct angular bandwidth. Finally, the expansion factor S_z was varied in order to shift the position of maximum diffraction efficiency to the correct number of degrees-off-Bragg. The values which best fit the data are γ_n=.00023, d=12.4μ, and S_z=1.353.

If the Kogelnik theory together with the assumption of a linear response of index modulation to exposure is valid, then these parameters should be constants of the material and the data obtained at the next highest exposure level should agree with the Kogelnik prediction. (Of course, slight variations in thickness and the expansion factor should be expected from hologram to hologram.) In order to check this hypothesis, the Kogelnik theory was curve fit to the data by Chang for a total exposure of 73 mj/cm^2.

The results of this curve fit for the data obtained at an exposure of 73 mj/cm^2 appear in Figure 13.

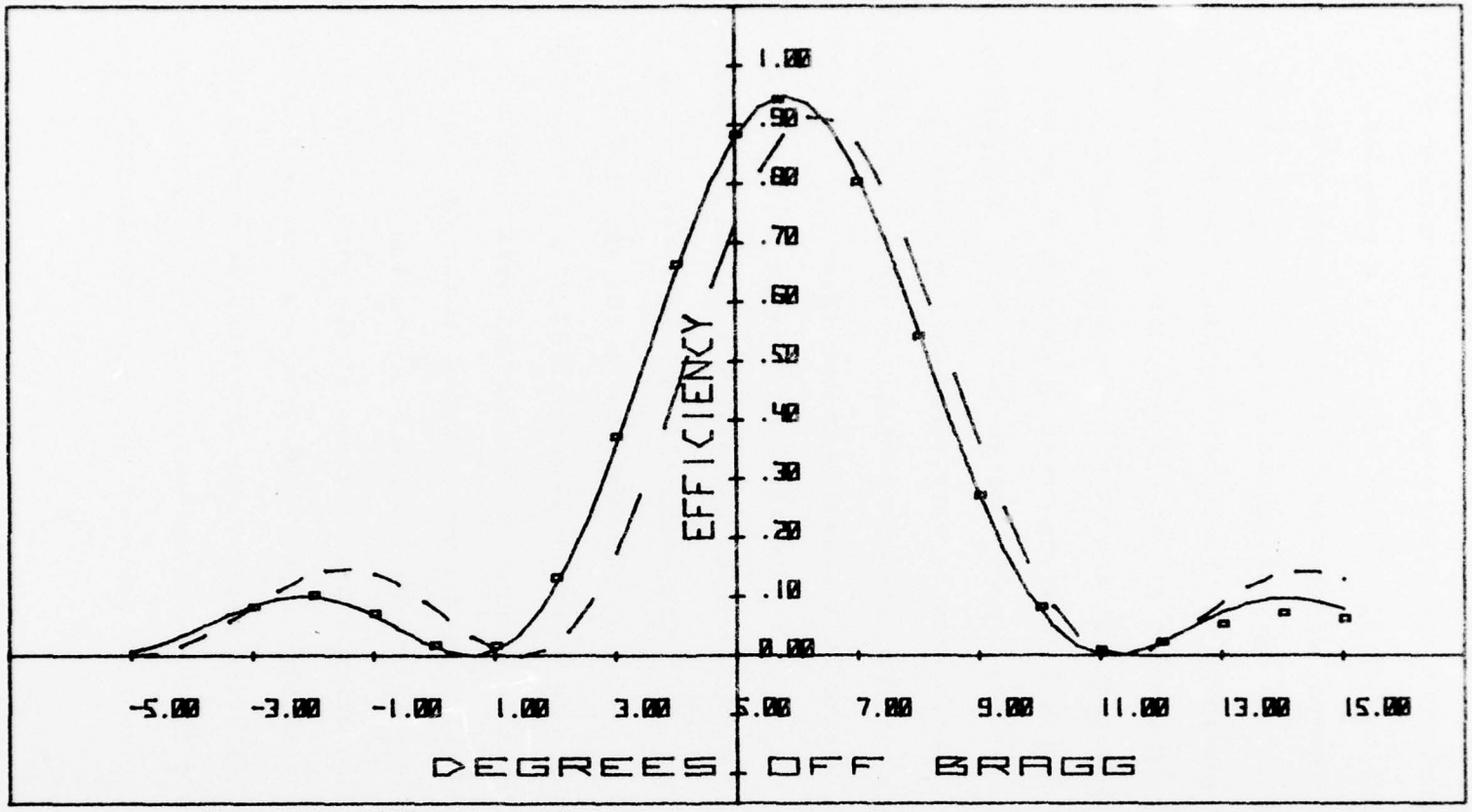

Figure 13. Diffraction Efficiency versus angle-off-Bragg for the ERIM Hologram
The solid line is the theoretical diffraction efficiency calculated from Eq (159) for the ideal Kogelnik case for the parameters. γ_n=.00019, d=12.75μ, and S_z=1.316. The dashed line is the same calculation for the parameters determined in Figure 12. The data (represented by squares) is for a total exposure of 73 millijoules/cm^2 (Ref. 6, 7, use by permission). A linear optical index modulation response to exposure is assumed.

It is noted that excellent agreement is obtained for the parameter values of γ_n=.00019, d=12.75μ and S_z=1.316, but poor agreement is obtained for the parameters of Figure 12. It is obvious that the value of γ_n required to obtain agreement of the linear Kogelnik theory has changed a significant amount. A comparison between the optimum parameters for the 24 mj/cm^2 exposure and the 73 mj/cm^2 exposure indicates that γ_n changed by 17.4%, d changed by 2.82%, and S_z changed by 2.73%. The percentage change in d and S_z can be attributed to experimental variations, but the large percentage change in γ_n indicates that there exists an inadequacy in the theory.

There are several effects which explain why the Kogelnik theory with a linear index modulation response to exposure is not adquate. First, saturation of the optical index modulation response of the emulsion to the exposure is known to occur in dichromated gelatin (Ref. 5). Secondly, the variations with depth of the optical index modulation and the optical index are not included in the Kogelnik theory.

The theory developed in this dissertation accounts for both saturation and variations of the optical properties of the emulsion with depth. The detailed equations relating to saturation with exposure are described more fully in Appendices B and E. The variations of the optical properties of the hologram with depth are included in the JWKB theory, Eq (159).

The diffraction efficiency at the center of the angular bandwidth obtained experimentally by Chang is plotted as a function of total exposure in Figure 14. Also plotted in Figure 14, for comparison, are the Kogelnik theory based upon a linear index modulation response to exposure and the JWKB theory based upon a saturating response of index modulation to exposure. (See Appendix B for more explanation of the linear and saturation responses.) Both the Kogelnik and JWKB theories are initially parameterized by the constants obtained by the curve fit shown in Figure 12 (γ_n=.00023, d=12.4μ, S_z=1.353). This was done because it is assumed that at the low exposure of 24 mj/cm^2 that very little saturation occurs and the two theories should agree well in this region. The results illustrated in Figure 14 indicate that the JWKB theory including saturation effects agrees with the experimental data much better than the linear exposure-response Kogelnik theory.

If the effect of saturation is combined with the Kogelnik theory, one obtains the results appearing in Figure 15. The dashed curve in Figure 15 is the Kogelnik theory including saturation. The solid line is the JWKB theory including saturation. It is concluded that saturation effects are stronger for this particular hologram than the effects caused by the variation of the optical index modulation with depth. However, these effects

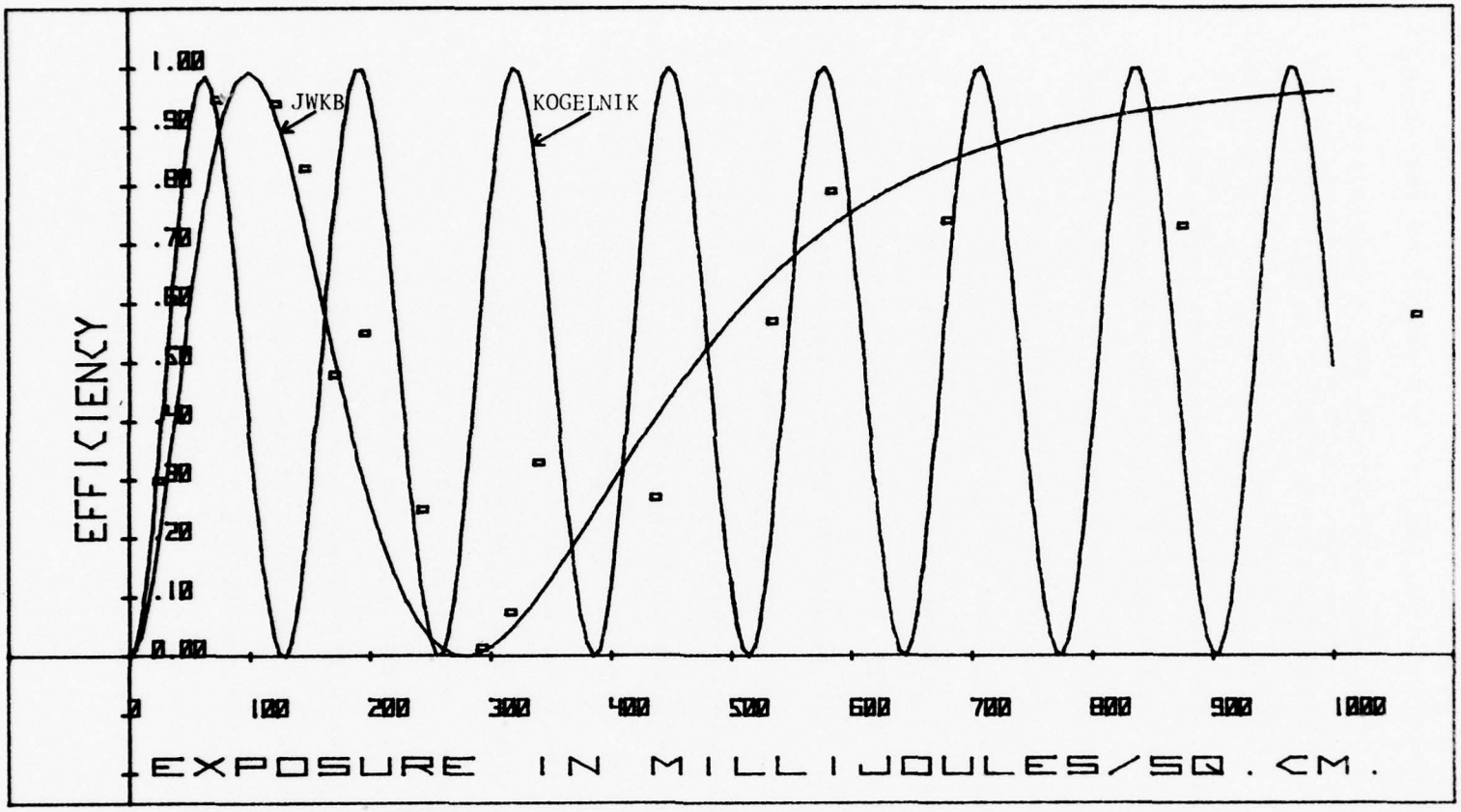

Figure 14. Diffraction Efficiency versus Total Exposure for the ERIM Hologram
The curve labeled "JWKB" is the diffraction efficiency calculated from Eq (159) using the JWKB theory assuming a saturating response of the optical index modulation to exposure. The curve labeled "Kogelnik" is the same calculation assuming the Kogelnik case and a linear optical index modulation response to exposure. The data (represented by squares) is the experimental diffraction efficiency measured at the center of the angular bandwidth (Ref. 6, used by permission).

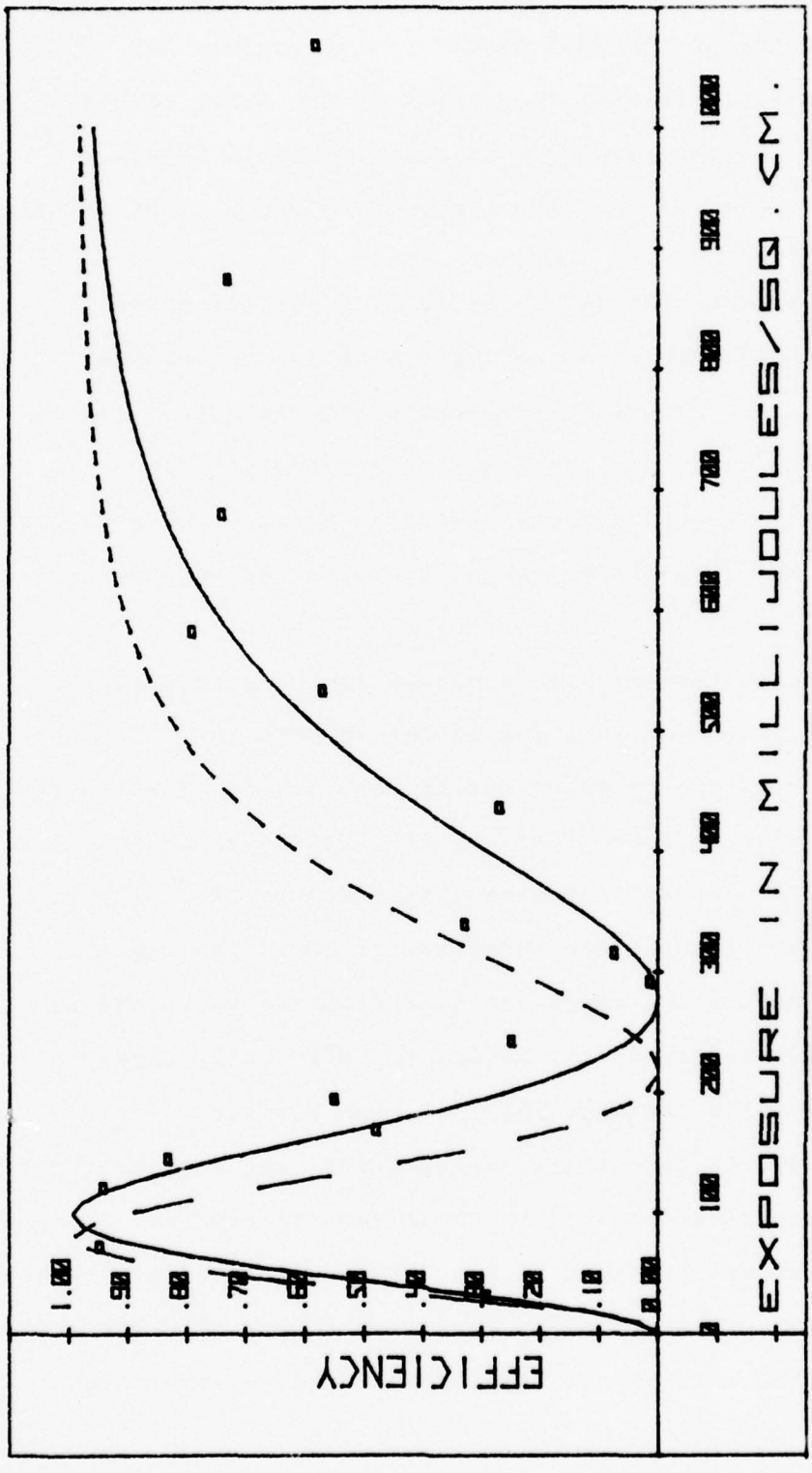

Figure 15. Diffraction Efficiency versus Total Exposure for the ERIM Hologram
The solid curve is the JWKB theory (Eq (159)) assuming a saturating optical index modulation response to exposure. The dashed curve is the Kogelnik theory assuming the same response. In both cases the same parameters determined in Figure 12 were used.

accounted for by the JWKB theory, fully explain the data, particularly near the region of the first zero at 300 mj/cm^2. This result is also indicated in Figure 16, which is a plot of the JWKB theory with and without saturation effects included.

The experimental data plotted in Figure 14 agrees with the JWKB theory in the regions of low and medium exposure. Disagreement is observed for exposures larger than 700 mj/cm^2. For the last two data points (at 875 mj/cm^2 and 1069 mj/cm^2) deviation between the experimental data and the JWKB theory cannot be explained by experimental error.

This deviation at high exposure can be accounted for by three things not included in the JWKB theroy: (1) the absorption of the emulsion during exposure is known to increase with exposure (Ref. 5, 7), (2) the expansion of dichromated gelatin decreases with exposure (Ref. 5, 7), and (3) the transmission hologram formed in the emulsion during exposure due to reflections from the back surface of the emulsion substrate begins to efficiently couple energy from the incident light at high exposure.

In order to test these explanations, the angular sensitivity data obtained by Chang for the exposure of 1069 mj/cm^2 was compared to the JWKB theoretical predictions of Eq (159). These results appear in Figure 17. The solid curve is the JWKB result for S_z=1.353 and an absorption

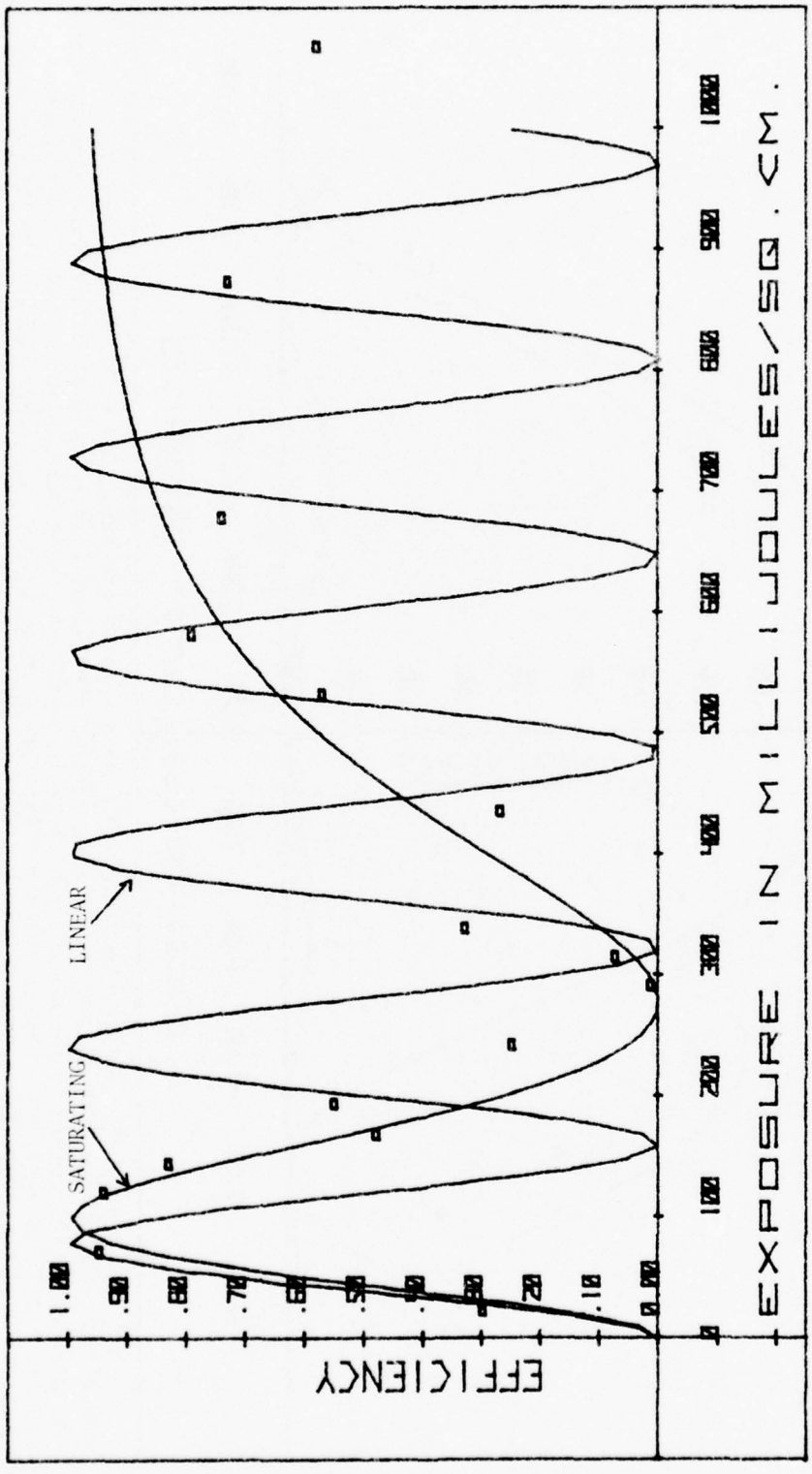

Figure 16. Diffraction Efficiency versus Total Exposure for the ERIM Hologram

The diffraction efficiency is calculated for both curves by Eq (159) using the JWKB theory. In the curve labeled "SATURATING", a saturating index modulation response to exposure is used. In the other curve, a linear response is used. In both curves, the parameters determined in Figure 12 are used.

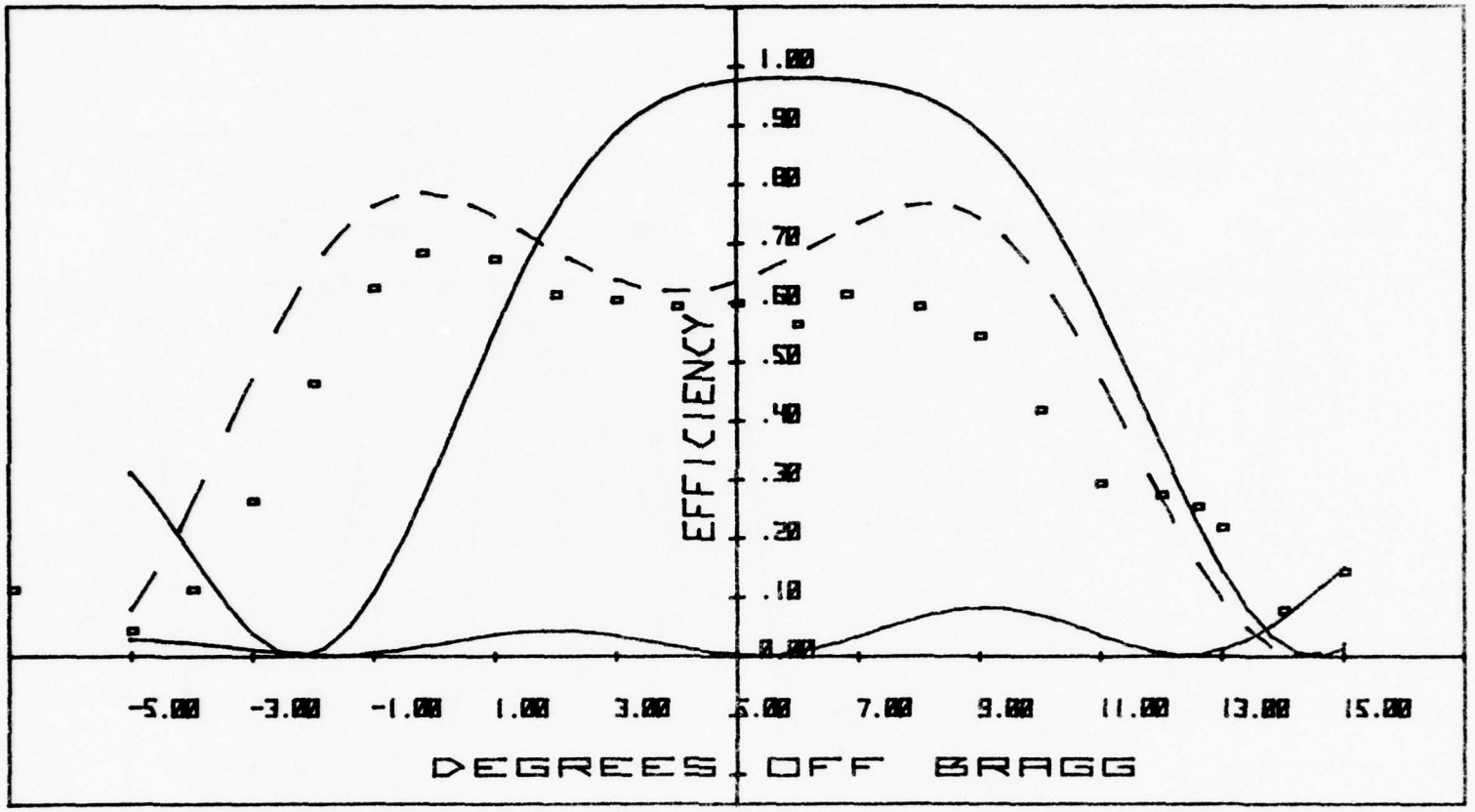

Figure 17. Diffraction Efficiency versus angle-off-Bragg for the ERIM Hologram
The solid curve is the JWKB theory (Eq (159)) in which a saturating index modulation response is used with the parameters determined in Figure 12. The dashed curve is the same calculation for the new parameters $\alpha=4.5\times10^{4}\,m^{-1}$ and $S_z=1.220$. The data (represented by squares) is for an exposure of 1069 millijoules/cm^2 (Ref. 6, used by permission). The lower curve is the same calculation for the hologram formed by reflections from the emulsion substrate surface.

coefficient during exposure of $\alpha = 2.75 \times 10^{4} m^{-1}$. The dashed curve is the JWKB results for an absorption coefficient of $\alpha = 4.5 \times 10^{4} m^{-1}$ and an expansion coefficient of $S_z = 1.220$. It is observed that these values for the parameters α and S_z more closely fit the data and this substantiates the first two reasons for the deviations observed in Figure 14. These effects could be included in the JWKB theory by requiring α and S_z to functions of exposure.

The lower curve plotted in Figure 17 is the diffraction efficiency of a second transmission hologram formed simultaneously with the primary hologram by the reflections of the object and reference beams from the back surface of the emulsion substrate. The diffraction efficiency plotted in Figure 17 is based upon an exposure level of 20% of the total exposure for the primary hologram. The 20% value is determined by the amount of reflection at the back emulsion substrate and is consistent with the angles of incidence of the object and reference beams inside the emulsion and the fact that the reflection occurs within a region of high optical index. The position of the diffraction maxima for the second hologram formed from the reflected object and reference beams accounts for the asymmetry in the experimental data. The order of magnitude of the diffractive losses to this hologram further substantiates the contention that some of the discrepancy

between the JWKB theory and the experimental data may be due to diffraction of the reconstruction light by the second hologram contained in the emulsion.

The effect of the JWKB terms upon the diffraction efficiency is related to the absorption during exposure. The diffraction efficiency as a function of total exposure is plotted in Figure 18 for a family of curves with different absorption coefficients. As the absorption during exposure increases, the first diffraction efficiency maximum occurs at higher exposures. Also, the broadening of the second diffraction efficiency maximum becomes more pronounced due to the greater delaying effects of the JWKB terms.

E. Summary of Results

In this chapter the JWKB theory has been evaluated for two specific transmission holograms for which significant experimental data is available. The first experiment was the polarization exerpiment by Rose and Williamson. The JWKB theory agreed with the diffraction efficiency response to incident wave polarization changes obtained experimentally. It was further predicted that this response was a consequence of the fact that the 649F emulsion is a weak coupler. A different response was predicted for stronger coupling materials. The second experiment was that performed by Chang. In this case, the JWKB theory improved the accuracy

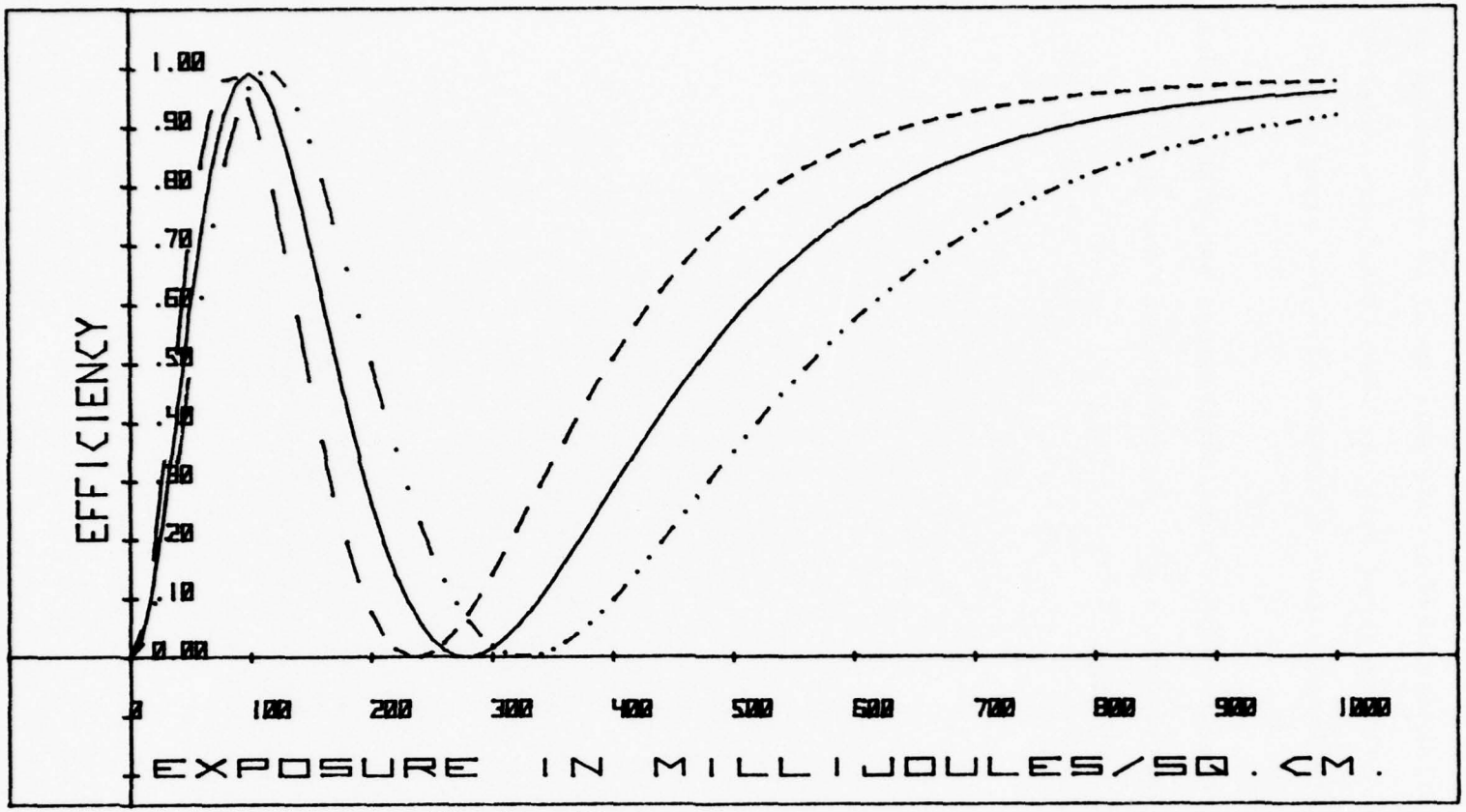

Figure 18. Diffraction Efficiency versus Total Exposure for the ERIM Hologram
The diffraction efficiency is calculated from Eq (159) for saturating index modulation response using the parameters determined in Figure 10. In each curve, a different absorption coefficient during exposure is used. - - - - $\alpha=1.00\times10^{4}m^{-1}$ ——— $\alpha=2.75\times10^{4}m^{-1}$ —·—·· $\alpha=4.5\times10^{4}m^{-1}$

in predicting the diffraction efficiency as a function of exposure. It was shown that the JWKB terms were required in order to reach better agreement with the experimental results.

In the next chapter some conclusions based upon these results are described and recommendations for further work are indicated.

CHAPTER VI

CONCLUSIONS AND RECOMMENDATIONS

In this chapter the major conclusions and accomplishments of the preceding work are reviewed and compared to the objectives set forth for this effort. Recommendations for improvements are made and further research is suggested.

A. Conclusions

The preceding work has provided a theoretical development and a comparison to experimental measurement of the diffraction efficiency of a hologram. An equation for the diffraction efficiency of a hologram has been obtained which relates the diffraction efficiency to the apriori characteristics of: (1) the exposure conditions, (2) the emulsion parameters, and (3) the reconstruction conditions. In short, the objective of this work was obtained.

The analysis presented in this dissertation was based upon a pair of coupled wave equations with variable coeffcients of sufficient generality to permit the determination of the diffraction efficiency of a hologram in cases where previous theories were deficient. These cases include: (1) spherical object, reference, and construction waves, (2) polarization of the reconstruction wave, (3) reconstruction wave vectors out of the plane of incidence of the construtction wave vector, (4) thickness changes of the emulsion during processing, (5) changes in the optical index of the emulsion during processing, (6) variations with depth of the index of refraction and index modulation of the emulsion,

(7) saturation of the index modulation response to exposure, and (8) absorption of the construction waves during exposure.

The spherical nature of the construction and reconstruction waves was accounted for by a spherical wave expansion. This permitted an easy analysis of holographic lenses and other optical elements formed by spherical waves. Previous theories, based upon plane waves, were shown to be a special case of the spherical wave theory.

The polarization of the construction and reconstruction wave vectors was included in the theoretical development by the use of polarization vectors. The polarization of the diffracted wave vector was determined by the scattering theory derived by Tatarskii (Appendix H). This polarization was dependent upon the reconstruction wave polarization and the diffracted wave direction. The results indicate that considering polarization effects in this manner agree with experiment for weakly coupling holograms. Significantly different predictions are expected for strongly coupling holograms, but an experimental verification of this prediction is lacking, so far.

The diffracted wave vector was determined by the gradient of the phase of the diffracted order. The relationship between the diffracted order wave vector, the fringe wave vector, and the reconstruction wave vector was shown to be equivalent to the Bragg condition, when the reconstruction wave vector was in a position of apparent coincidence with the original reference wave vector position.

As a consequence of using polarization vectors to characterize polarization effects and wave vectors to geometrically characterize the construction and reconstruction conditions, the theory was able to handle reconstruction wave vectors out of the plane of incidence of the original object and reference wave vectors.

Thickness changes of the emulsion during processing were included in the theory by a transformation of both the original thickness and the original fringe wave vector. This transformation successfully predicted the experimentally observed shift in the position of the reconstruction wave vector associated with maximum diffraction efficiency. This shift was consistent with a modified Bragg condition involving the transformed fringe wave vector.

Optical index changes of the emulsion during processing were included in the theory by changing the index of refraction of the emulsion after processing. It was shown that such optical index changes should produce a shift in the position of the reconstruction wave vector for which maximum diffraction efficiency occurs.

Variations in optical index and index modulation with depth were related to the exposure and the absorption of the construction waves. A linear index modulation response to exposure was initially used. The variations in hologram characteristics with depth were accounted for by the use of variable coefficients in the pair of coupled wave equations describing the hologram. This set was solved using the JWKB

approximation and evaluated specifically for the boundary conditions of transmission and reflection holograms. It was shown that these results reduce to those of Kogelnik for the case of plane waves and constant coefficients.

The trapezoidal rule was used to compute the JWKB integrals for the case of a transmission hologram. It was found that good agreement between the experimentally measured diffraction efficiency and the theoretically calculated diffraction efficiency required accounting for both (1) saturation of the index modulation response to exposure, and (2) variations of hologram parameters with depth. It was shown that by including both of these factors, experiment and theory agreed except at extremely high exposure levels. This discrepancy was attributed to: (1) the absorption during exposure being a function of exposure, (2) expansion of the emulsion decreasing with exposure, and (3) reflections during exposure from the hologram - air boundary creating a second transmission hologram in the emulsion which depletes the energy of the incoming reconstruction wave.

It was found that the Kogelnik theory in conjunction with both the linear and saturating index modulation response to exposure was insufficient to explain the experimental results of Chang (Ref. 6,7). The JWKB theory combined with the saturating index modulation response to exposure closely matched the experimental data. From this, it was concluded that variations in hologram parameters with depth were responsible for the remaining experimental and theoretical

discrepancy; these effects were accurately accounted for JWKB theory developed in this work.

The shape of the curves for diffraction efficiency versus angle off-Bragg was affected little by the variation in hologram parameters with depth. These variations strongly retarded the response of the diffraction efficiency to exposure, however.

B. Recommendations

One of the significant results of this work has been the agreement between the theory developed in this work and the experimentally measured diffraction efficiency response to reconstruction wave polarization changes (Ref.40). It was indicated that the agreement was a consequence of the weak coupling which typifies Kodak 649F holograms. Strikingly different theoretical results are predicted for dichromated gelatin holograms, which can be strong couplers. In order to more fully test polarization effects predicted in this dissertation, it is recommended that the polarization experiment be repeated for a strongly coupling dichromated gelatin hologram.

An experimental and theoretical evaluation of the theory should be performed for reflection holograms. It is expected that the sensitivity of reflection holograms to hologram parameter variations with depth and changes in thickness should be stronger than those observed in

transmission holograms because the fringe structure for a reflection hologram is more nearly parallel to the emulsion surface. Consequently, the JWKB terms should be even more important. Such an investigation may help reveal why reflection holograms made using dichromated gelatin are not as efficient in practice as corresponding transmission holograms made with the same material.

One should recall that the experimental and theoretical comparisons made in Chapter V were for holograms constructed and reconstructed with plane waves. Consequently, an omission which has occurred during the performance of the work presented in this dissertation is that a theoretical and experimental analysis of the holographic lens has not been performed. The holographic lens was not pursued because too many other interesting avenues of research evolved for which experimental data was available for comparison. All of the tools have been developed to investigate theoretically and experimentally the effects of (1) radius of curvature changes for the reconstruction and construction waves, and (2) exposure tapering across the surface of the emulsion. Also, the theoretical capability now exists to perform a holographic optical lens design starting with the desired operational characteristics and ending up with the proper construction geometry, exposure conditions, and emulsion parameters required to make the lens.

Finally, one other recommendation pertaining to an alternate theoretical approach is in order. With some controversy, it is believed that cracks form in dichromated gelatin emulsion along the fringe planes during processing. These cracks, with their associated air emulsion interfaces, are considered to be responsible for the large refractive index modulation which occurs in dichromated gelatin. Consequently, one might be able to describe theoretically the dichromated gelatin hologram as an interference stack of layers of air and emulsion. The diffraction efficiency would be determined by a calculation of the amplitude and phase relationship between the multiple reflections and transmissions occurring for the incident and diffracted light within this stack.

REFERENCES

1. Alferness, Rodney C. Optical Propagation in Holographic Gratings. The University of Michigan, Ann Arbor, MI (1976) Dissertation.

2. Bogoliubov, N.W. and Y.A. Mitropolsky. Asymptotic Methods in the Theory of Non-Linear Oscillations. (Translated from Russian), Gordon and Breach Science Publishers, New York (1961).

3. Burckhardt, C.B. "Diffraction of Plane Waves in A Sinusoidally Stratified Dielectric Grating", Journal of the Optical Society of America, 56, 1502-1512 (11 Nov 66).

4. Burckhardt, C.B. "Efficiency of a Dielectric Grating", Journal of the Optical Society of America, 57, 601-603 (May 67).

5. Case, Steven K. Multiple Exposure Holography in Volume Materials, The University of Michigan, Ann Arbor, MI (1976) Dissertation.

6. Chang, B.J. and C. Leonard. "Exposure Characteristics of Dichromated Gelatin Holograms", Journal of Optical Society of America, 66, 1063 (10 Oct 76). *(Abstract) Presentation at the annual meeting of the Optical Society of America, Oct 76, Tucson, AZ. Details to be published.*

7. Chang, B.J. "Post-Processing of Developed Dichromated Gelatin Holograms", Optics Communications, 17, 3, 270-271 (June, 1976).

8. Chang, M.T. Holographic Dielectric Cratings: Theory and Practice, (May 1969) California Institute of Technology, Dissertation, AD696577

9. Chang, M.T. and N. George. "Holographic Dielectric Grating: Theory and Practice", Applied Optics, 9, 713-719 (3 Mar 70).

10. Chang, M.T. Applied Optics, 10, 2550 (1970).

11. Curran, R.K. and T.A. Shankoff. "The Mechanism of Hologram Formation in Dichromated Gelatin", Applied Optics, 9, 1651 (1970).

12. Fillmore, G. and J. Tynan. Journal of the Optical Society of America, 61, 199 (1971).

13. Friesem, A.A. Three-Dimensional Recording Media in Holography, University of Michigan, Ann Arbor, MI, Dissertation (1969).

14. Fröman, N. and P.O. Fröman, JWKB Approximation, "Contribution to the Theory", North-Holland Publishing Company, Amsterdam (1965).

15. Gabor, D. and G.W. Stroke. "The Theory of Deep Holograms", Proc. Roy. Soc. Am., 304 275-289 (1968).

16. Hamilton, J.F. "Photographic Grain", Applied Optics, 2, 13-21 (1 Jan 72).

17. Jackson, J.D. Classical Electrodynamics, John Wiley and Sons, Inc., New York (1967).

18. Jennings, W. First Course in Numerical Methods, The MacMillan Co., London (1964).

19. Kermish, D. "Nonuniform Sinusoidally Modulated Dielectric Gratings", Journal of the Optical Society of America, 59, 1409-1414 (11 Nov 69).

20. Klein, W.R. and Bill D. Cook. "Unified Approach to Ultrasonic Light Diffraction", IEEE Transactions on Sonics and Ultrasonics, SU-14, 123-134 (3 Jul 67).

21. Kogelnik, H. "Coupled Wave Theory for Thick Hologram Gratings", Bell System Technical Journal 48, 2909-2947 (1969).

22. Kogelnik, H. "Filter Response of Nonuniform Almost-Periodic Structures", Bell System Technical Journal, 55, 109-126 (1 Jan 76).

23. Kosan, J. Light Sensitive Systems, John Wiley, New York (1965) Chapter 2.

24. Lamberts, R.L "Characteristics of Bleached Photographic Material", Applied Optics, 2, 33-41 (1 Jan 72).

25. Lamberts, R.L. "Optical Path Variations in a Photographic Emulsion", Journal of the Optical Society of America, 60, 1389-1397 (10 Oct 70).

26. Latta, John N. "Analysis of Multiple Hologram Optical Elements with Low Dispersion and Low Aberrations", Applied Optics, 11, 1686-1696 (8 Aug 72).

27. Latta, John N. "New Developments in the Design of Holographic Optics", Seminar in Depth on Application of Geometrical Optics, 27-28 Aug 73, San Diego, CA.

28. Latta, John N. "Computer Based Analysis of Holography Using Ray Tracing", Applied Optics, 10, 2698-2710 (12 Dec 71).

29. Lehmann, M., Lauer, J.P., and J. W. Goodman. "High Efficiency, Low Noise, and Suppression of Photochromic Affects in Bleached Silver Halide Holography", Applied Optics, 9, 1948 (8 Aug 70).

30. Lieth, E.N., Kozma, A., Upatnicks, J., Marks, J., and N. Massey. "Holographic Data Storage in Three-Dimensional Media", Applied Optics, 5, 1303-1311 (8 Aug 66).

31. Lin, S.H. Applied Optics, 8, 963 (1969).

32. Matthews, John W. Theory of Holography, California Institute of Technology, June 1967, Dissertation, AD667189.

33. Mees, C. E. Kenneth, and T.H. James. The Theory of the Photographic Process, 3rd edition, The MacMillan Co., New York (1966).

34. Meyerhofer, D. RCA Review, 33, 33 (Mar 72).

35. Neblette, C.B. Photography, Its Materials and Processes, 6th edition, Van Nostrand Reinhold Co., Cincinnati, OH, 235 (1962).

36. Nering, E.D. Linear Algebra and Matrix Theory, 2nd edition, John Wiley and Sons, Inc., New York (1970).

37. Pressley, R.J. Handbook of Lasers with Selected Data on Optical Technology, The Chemical Rubber Co., Cleveland, OH (1971).

38. Raman, C.V. and N.S. Nath. Proc. Ind. Acad. Sci. A,2, 406-413 (1935).

39. Raman, C.V. and N.S. Nath. Proc. Ind. Acad. Sci. A,3, 75-119 (1936).

40. Rose, H.W., T.L. Williamson and S.A. Collins. "Polarization Effects in Holography", Applied Optics, 9, 2394-2396 (10 Oct 70).

41. Su, S.F., and T.K. Gaylord. "Calculation of Arbitrary-Order Diffraction Efficiencies of Thick Gratings with Arbitrary Shape", Journal of the Optical Society of America, 65, 59-64 (1 Jan 75).

42. Tatarskii, V.I. The Effects of the Turbulent Atmosphere on Wave Propagation, (Translated from Russian), Israel Program for Scientific Translations, Jerusalem (1971). Available from U.S. Department of Commerce, National Technical Information Service, Springfield, VA 22151, TT 68-50464.

43. Uchida, N. "Calculation of Diffraction Efficiency in Hologram Gratings Attenuated along the Direction Perpendicular to the Grating Vector", Journal of the Optical Society of America, 63, 280-287 (3 Mar 73).

44. Williamson, Tom L., Scattering Theory of Holography Diffraction, The Ohio State University (1975) Dissertation.

Preceding Page BLANK - NOT FILMED

APPENDIX A

THE COORDINATES, UNITS, AND WAVE EQUATION

In this appendix, the coordinate system sign convention, and system of units used throughout this dissertation is identified. Then, based upon Maxwell's equations, the wave equation appropriate to holographic diffraction is presented.

1. The Coordinate System.

The coordinate system used throughout this dissertation is assumed to have its origin at the center (point 0 in Figure A-1) of the front surface of the holographic medium. The rectangular coordinate system used is shown in Figure A-1.

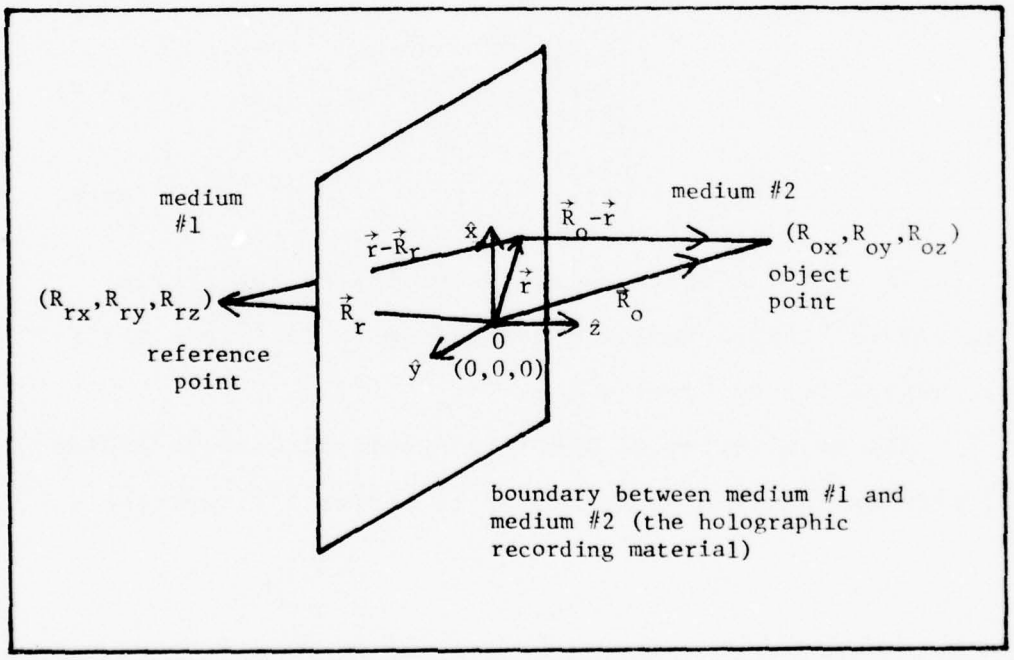

Figure A-1. Coordinate System

The (x,y) plane is defined to be the plane of the front surface of the holographic medium. The $\hat{z}$ direction is normal to this plane and is into the emulsion.

The position vector $\vec{r}$ is the 3-tuple of independent coordinate variables (x,y,z) which defines a point in the coordinate system. $\vec{r}$ is represented by

$$\vec{r} = \begin{bmatrix} x \\ y \\ z \end{bmatrix} \tag{A-1}$$

All functions used throughout this dissertation are functions of the coordinate variables (x,y,z). The object and reference waves used to construct the hologram are assumed to be spherical waves, centered at positions defined by $\vec{R}o$ and $\vec{R}r$, respectively.

$$\vec{R}o = \begin{bmatrix} Rox \\ Roy \\ Roz \end{bmatrix} \tag{A-2}$$

$$\vec{R}r = \begin{bmatrix} Rrx \\ Rry \\ Rrz \end{bmatrix} \tag{A-3}$$

The optical index change occurring at the (x,y,o) interface between medium 1 and medium 2, in Figure A-1 is accounted for by Snell's Law.

The wave vector of the j-th spherical wave in medium 1 propagating from -z toward +z in medium 1 is written as

$$\vec{k}_{1j}^{(+)} = \begin{cases} \dfrac{k_1(\vec{r}-\vec{R}_j)}{|\vec{r}-\vec{R}_j|} ; & R_{jz} \geq 0 \quad \text{diverging spherical wave} \\ \dfrac{-k_1(\vec{r}-\vec{R}_j)}{\vec{r}-\vec{R}_j} ; & R_{jz} < 0 \quad \text{converging spherical wave} \end{cases} \tag{A-4}$$

(+) implies propagation of the wave from -z to +z directions. Where $k_1 = \frac{2\pi n_1}{\lambda_j}$; λj is the free space wavelength of the wave, and n_1 is the optical index in medium number 1.

If the direction of propagation is reversed, i.e., propagation occurs from +z to -z in medium number 2, then

$$\vec{k}_{2j}^{(-)} = \begin{cases} \dfrac{k_2(\vec{r}-\vec{R}_j)}{|\vec{r}-\vec{R}_j|} ; & R_{jz} \geq 0 \quad \text{diverging spherical wave} \\ \dfrac{-k_2(\vec{r}-\vec{R}_j)}{|\vec{r}-\vec{R}_j|} ; & R_{jz} < 0 \quad \text{converging spherical wave} \end{cases} \tag{A-5}$$

and $k_2 = \frac{2\pi n_2}{\lambda j}$.

Eqs (A-4) and (A-5) define the wave vectors for spherical waves. j = o,r,c for object, reference or reconstruction spherical wave vectors, respectively. The values of $\vec{k}_{1j}^{(+)}$ in medium number 2 are determined by Snell's Law at the boundary to be

$$\vec{k}_{2j}^{(+)} = \frac{k_1}{|\vec{r}-\vec{R}_j|}\left[(x-R_{jx})\hat{x}+(y-R_{jy})\hat{y}+(z-R_{jz})\hat{z}\sqrt{1+\left(\frac{n_2^2}{n_1^2}-1\right)\frac{|\vec{r}-\vec{R}_j|^2}{(z-R_{jz})^2}}\right] \tag{A-6}$$

$\vec{k}_{1j}^{(-)}$ is defined in a similar manner except that the direction is reversed and n_1 is interchanged with n_2 in all places.

In the case of the reconstruction wave, $\vec{k}_{2c}$, n_2 is replaced by $n_b(\vec{r})$ which is the optical index of the emulsion after processing given in Appendix B.

Units and the Wave Equation for the Emulsion.

The wave equation used to describe holographic diffraction is derived from Maxwell's equations, which is Gaussian units, are (Ref. 17)

$$\vec{\nabla}\cdot\vec{D} = 0 \qquad \text{(A-7)}$$

$$\vec{\nabla}\cdot\vec{H} = 0 \qquad \text{(A-8)}$$

$$\vec{\nabla}X\vec{E} + \frac{1}{c}\frac{\partial\vec{H}}{\partial t} = 0 \qquad \text{(A-9)}$$

$$\vec{\nabla}X\vec{H} - \frac{\varepsilon}{c}\frac{\partial\vec{E}}{\partial t} - \frac{4\pi\sigma}{c}\vec{E} = 0 \qquad \text{(A-10)}$$

$$\vec{D} = \varepsilon\vec{E} \qquad \text{(A-11)}$$

Since the emulsion is a non-magnetic material and there are no free static charges existing in the material, it has been assumed that $\mu = 1$ and $\rho = 0$ for the hologram emulsion. ε is the dielectric constant of the emulsion and σ is the conductivity of the emulsion after processing (during reconstruction).

The corresponding wave equation for monochromatic light in Gaussian units is

$$\nabla^2 \vec{E} + k^2(\vec{r})\vec{E} + \vec{\nabla}(\vec{\nabla} \ell n \varepsilon \cdot \vec{E}) = 0 \qquad (A\text{-}12)$$

where

$$k^2(\vec{r}) = \frac{\omega^2}{c^2}\left(\varepsilon + \frac{i4\pi\sigma}{\omega}\right) \qquad (A\text{-}13)$$

$k(\vec{r})$ is the wave propagation constant of the material. $k(\vec{r})$ is related to the optical index, $n(\vec{r})$, and the absorption coefficient, $\alpha(\vec{r})$, of the emulsion by

$$k^2(\vec{r}) = k_c^2\left[n^2(\vec{r}) - \frac{i\alpha^2(\vec{r})}{2k_c^2} + \frac{i\, n(\vec{r})\alpha(\vec{r})}{k_c}\right] \qquad (A\text{-}14)$$

where $k_o = \frac{2\pi}{\lambda_o}$ and λo is the free space wavelength of the construction light. It is shown in Appendix B that n and α are functions of $\vec{r}$, hence $k^2 = k^2(\vec{r})$ for the hologram.

APPENDIX B

DERIVATION OF THE WAVE PROPAGATION CONSTANT OF A HOLOGRAM

It is the purpose of this appendix to relate the wave propagation constant, $k(\vec{r})$ to the original hologram construction geometry and exposure conditions. This requires that the optical index, $n(\vec{r})$ and the absorption coefficient, $\alpha(\vec{r})$, be related to the exposure. These terms are determined from the exposure by either a linear response or a saturating response to exposure. First, the exposure of the holographic recording medium to the object and reference waves is derived, then the relationships between optical index, absorption coefficient, and exposure are determined. $k(\vec{r})$ is derived for a hologram and related to $n(\vec{r})$ and $\alpha(\vec{r})$. Finally, the variable coefficients Q_o, Q_{-1}, C_o and C_{-1} appearing in the coupled wave equations are evaluated in terms of $n(\vec{r})$ and $\alpha(\vec{r})$.

1. The Exposure.

The interference intensity pattern between the object and reference spherical waves is calculated using the superposition principle and Beer's Law for absorption in the emulsion during the exposure. This intensity is related to exposure. Only the exposure within the emulsion is of concern since that is what photochemically changes the emulsion.

The electric field of the object and reference waves inside the emulsion (medium number 2) is given by

$$\vec{E}_o(\vec{r}) = E_o(\vec{r})\, e^{i\phi_o(\vec{r})}\, \hat{e}_o \qquad (B\text{-}1)$$

$$\vec{E}_r(\vec{r}) = E_r(\vec{r})\, e^{i\phi_r(\vec{r})}\, \hat{e}_r \qquad (B\text{-}2)$$

in which $\hat{e}_o$ and $\hat{e}_r$ are the unit polarization vectors of the spherical waves derived in Appendix I. $E_o(\vec{r})$ and $\vec{E}r(\vec{r})$ are the real amplitudes of the spherical waves. They account for the amplitude tapering across the emulsion surface.

The total electric field within the emulsion is given by

$$\vec{E}(\vec{r}) = \vec{E}_o(\vec{r}) + \vec{E}_r(\vec{r}) \qquad (B\text{-}3)$$

The intensity is

$$I(\vec{r}) = \vec{E} \cdot \vec{E}^* \qquad (B\text{-}4)$$

which becomes

$$I(r) = E_o E_o^* + E_r E_r^* + \hat{e}_o \cdot \hat{e}_r [E_o E_r^*\, e^{i(\phi_o - \phi_r)} + E_r E_o^*\, e^{-i(\phi_o - \phi_r)}] \qquad (B\text{-}5)$$

since the amplitudes were assumed to be real, this yields

$$I(\vec{r}) = I_o(\vec{r}) + I_r(\vec{r}) + 2\sqrt{I_o(r) I_r(r)}\, \cos\phi\, \hat{e}_o\, \hat{e}_r \qquad (B\text{-}6)$$

where

$$\phi = \phi_o - \phi_r \qquad (B\text{-}7)$$

$Io(\vec{r})$ and $Ir(\vec{r})$ are the intensities of the object and reference waves inside the emulsion. These functions contain the $\frac{1}{|\vec{r}-\vec{R}_j|^2}$ fall-off with position. Any absorption within the emulsion is also included in these terms. $\sqrt{I_o(\vec{r})I_r(\vec{r})}$ is the modulation amplitude for which complete coherence has been assumed. If one would desire to include coherence effects such a term would be contained in this modulation amplitude. $I_o(\vec{r})$ and $I_r(\vec{r})$ are derived starting with the equation

$$I_o(\vec{r})=I_o(\vec{r}'+\vec{L}_o)=I_o(x,y,o)e^{-\alpha|\vec{L}_o|z} \qquad (B-8)$$

and

$$I_o(\vec{r})=I_r(\vec{r}'+\vec{L}_r)=I_r(x,y,o)e^{-\alpha|\vec{L}_r|z} \qquad (B-9)$$

Where r ' is a position vector on the surface of the emulsion and $|\vec{L}_o|$ and $|\vec{L}_r|$ are the slant distances into the emulsion to the point $\vec{r}$ measured from $\vec{r}'$, α is the absorption coefficient of the emulsion during exposure.

The relation between $\vec{r}$, $\vec{r}'$ and $\vec{L}_o$ is shown in Figure B-1.

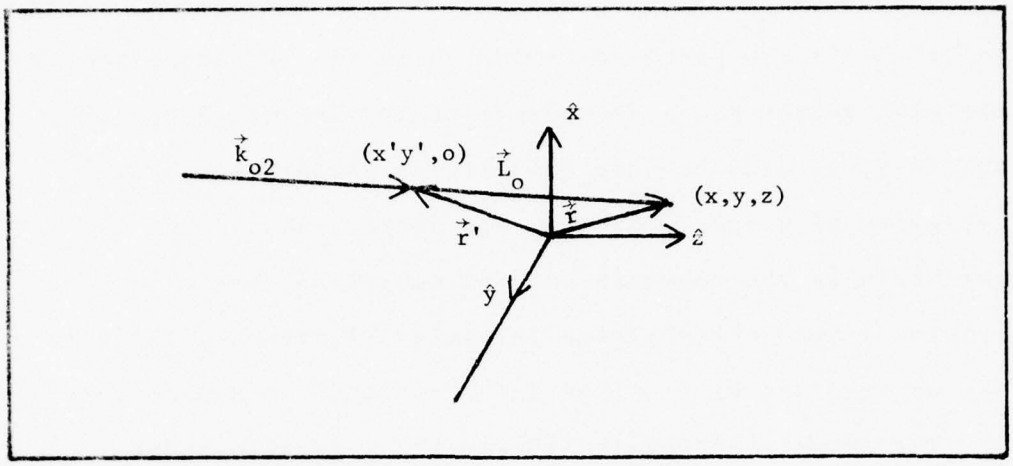

Figure B-1. Relation between $\vec{r}$, $\vec{r}'$ and $\vec{L}_o$

$\vec{L}_o$ is a vector along the object beam wave vector in holographic recording medium, $\vec{k}_{o2}$, whose magnitude is given by

$$L_o = |\vec{L}_o| = \frac{z}{\cos\theta_o} \qquad \text{(B-10)}$$

and similarly for

(B-11)

$\vec{L}_o$ and $\vec{L}_r$ represent the distance along the wave vector at the position (x,y,z) over which absorption has occurred. It is easily shown that

$$\cos\theta_o = \frac{\vec{k}_{o2}\cdot\hat{z}}{|\vec{k}_{o2}|} \qquad \text{(B-12)}$$

and

$$\cos\theta_r = \frac{\vec{k}_{2r}\,\hat{z}}{|\vec{k}_{2r}|} \qquad \text{(B-13)}$$

The vector $\vec{r}'$ is a position vector in the (x,y,o) plane. (x',y',o) is the point of incidence on the (x,y,o) plane of the wave vector k_{1j}. The last equality in Eqs (B-8) and (B-9) is true because the lateral variations in the intensity of a spherical wave are small. Also, the variation in the intensity of the spherical wave with thickness into the emulsion is small. Therefore, (x',y') may be replaced by (x,y) at the position $\vec{r}$, and vice versa.

The intensities of the object and reference waves in the (x,y,o) plane are

$$I_o(x,y,o) = \frac{A_o^2}{|\vec{r}-\vec{R}_o|^2} \qquad \text{(B-14)}$$

and

$$I_r(x,y,o) = \frac{A_r^2}{|\vec{r}-\vec{R}_r|^2} \qquad \text{(B-15)}$$

A_o^2 and A_r^2 are intensities to account for any other emulsion surface exposure variations which might be superimposed over the spherical variations.

Using Eqs(B-8) and (B-9),the exposure of the emulsion is written as

$$E(\vec{r}) = I(\vec{r}) \cdot t = E_b(\vec{r}) + M(\vec{r}) \cos\phi \qquad \text{(B-16)}$$

where $E_b(\vec{r})$ is a background exposure and $M(\vec{r})$ is a modulation to this exposure. t is the exposure time.

The background exposure is written as

$$E_b(\vec{r}) = E_o(\vec{r}) + E_r(\vec{r}) \tag{B-17}$$

Substitution of Eqs (B-8) and (B-9) along with Lo and Lr into Eq (B-17) yields

$$E_b(\vec{r}) = E_b(x,y,o)\left[\frac{I_o(x,y,o)\, e^{-\alpha L_o z} + I_r(x,y,o)\, e^{-\alpha L_r z}}{I_o(x,y,o) + I_r(x,y,o)}\right] \tag{B-18}$$

Defining $\kappa(x,y) = \dfrac{I_r(x,y,o)}{I_o(x,y,o)}$ as the ratio of reference to object beam intensity at the point (x,y) on the surface of the emulsion, Eq (B-18) becomes

$$E_b(\vec{r}) = E_b(x,y,o)\left[\frac{e^{-\alpha L_o z} + \kappa(x,y)\, e^{-\alpha L_r z}}{1 + \kappa(x,y)}\right] \tag{B-19}$$

which can be written as

$$E_b(\vec{r}) = \frac{E(0)R_o^2}{|\vec{r}-\vec{R}_o|}\left[\frac{e^{-\alpha L_o z} + \kappa(x,y)\, e^{-\alpha L_r z}}{1+\kappa(0)}\right] \tag{B-20}$$

in which E(o) is the background exposure at the origin (o,o,o) and $\kappa(o)$ is the ratio of the reference to object beam intensities at the origin during exposure.

The modulation is derived in a similar manner to yield

$$M(r)=\frac{2\sqrt{\kappa(0)}}{1+\kappa(0)}\ \frac{E(0)\ |\vec{R}_o||\vec{R}_r|\ \hat{e}_o\cdot\hat{e}_r}{|\vec{r}-\vec{R}_o||\vec{r}-\vec{R}_r|}\ e^{-\frac{\alpha}{2}(L_o+L_r)z} \qquad \text{(B-21)}$$

Eq (B-21) has been derived assuming an intensity modulation transfer function of unity for the recording material. A modulation transfer function could be included in Eq (B-21) if deemed appropriate.

2. Relation between Hologram Parameters and Exposure.

There are two theories relating exposure to the hologram parameters $n(\vec{r})$ and $\alpha(\vec{r})$. One is a linear response of the hologram parameters to exposure and the other is a saturating response to exposure. These two theories are reviewed in this section.

a. Linear theory.

In this theory, the optical index, after processing, is assumed to respond linearly to exposure such that

$$n(\vec{r}) = n_o+\gamma_n E(\vec{r}) \qquad \text{(B-22)}$$

where γ_n is the slope of the response of the emulsion material and n_o is the unexposed index of the emulsion. Substitution of Eq (B-16) into Eq (B-22) yields

$$n(\vec{r})=n_o+\gamma_n E_b(\vec{r})+\gamma_n M(\vec{r})\cos\phi \qquad \text{(B-23)}$$

which may be written as

$$n(\vec{r})=n_b(\vec{r})+\Delta n(\vec{r})\cos\phi \qquad \text{(B-24)}$$

where

$$n_b(\vec{r}) = n_o + \gamma_n E_b(\vec{r}) \tag{B-25}$$

and

$$\Delta n(\vec{r}) = \gamma_n M(\vec{r}) \tag{B-26}$$

$n_b(r)$ is the background optical index of the emulsion after processing. $\Delta n(\vec{r})$ is the index modulation which occurs in the material.

Similar equations are assumed to hold for the absorption coefficient of the material. These equations are

$$\alpha(\vec{r}) = \alpha_b(\vec{r}) + \Delta\alpha(\vec{r})\cos\phi \tag{B-27}$$

where,

$$\alpha_b(\vec{r}) = \alpha_o + \gamma_\alpha E_b(\vec{r}) \tag{B-28}$$

and,

$$\Delta\alpha(\vec{r}) = \gamma_\alpha M(\vec{r}) \tag{B-29}$$

These equations for the index response of a holographic emulsion have been shown to hold experimentally for bleached 649F holograms at low exposures (Ref. 24,25,44). This is discussed in greater detail in Appendix D, which describes 649F emulsions. The equations for the absorption coefficient response for bleached 649F holograms have not been verified in the literature. Appendix D contains a description of an experiment and results which this author performed which

verify Eqs (B-27) through (B-29) for low and medium exposure values. Dichromated gelatin is believed to respond in a similar manner for low and medium exposure levels (Ref. 6,7).

At high exposure levels ($^{>}800$ mj/cm^2) the linear approximation becomes invalid. Saturation of the index and absorption response occurs. The reasons are described fully in Appendix D for silver halide emulsions and in Appendix E for dichromated gelatin. The next section contains a discussion of the saturation equations.

b. Saturation theory.

In order to include the effect of saturation Eqs (B-25) and (B-26) are modified to be

$$n_b(\vec{r}) = n_o + \delta n_{max}\left(1 - e^{\frac{-E_b(\vec{r})}{D_n}}\right) \qquad (B\text{-}30)$$

and

$$\Delta n(\vec{r}) = \delta n_{max}\left(1 - e^{-\frac{M(\vec{r})}{D_n}}\right) \qquad (B\text{-}31)$$

where D_n is the damping rate of the emulsion response and δn_{max} is the value of index modulation to which the index response of the emulsion assymtotically approaches. At low exposure levels it is related to γ_n by the equation

$$\gamma_n = \frac{\delta n_{max}}{D_n} \qquad (B\text{-}32)$$

For dichromated gelatin, Chang has experimentally determined D_n to be

$$D_n = 95 = 200\, e^{-\frac{C}{6.5}} \quad \text{(millijoules/cm}^2\text{)} \qquad \text{(B-33)}$$

Where C is the concentration in percent by volume of dichromate in the emulsion (Ref. 6,7).

Similar equations hold for the silver halide emulsions for which C is the concentration in percent by volume of silver halide (Ref. 24,25).

The equations for the absorption coefficients of the processed emulsion are assumed to be of the same form.

$$\alpha(\vec{r}) = \alpha_b(\vec{r}) + \Delta\alpha(\vec{r})\cos\phi \qquad \text{(B-34)}$$

$$\alpha_b(\vec{r}) = \alpha_o + \delta\alpha_{max}\left(1 - e^{-\frac{E_b(\vec{r})}{D_\alpha}}\right) \qquad \text{(B-35)}$$

and

$$\Delta\alpha = \delta\alpha_{max}\left(1 - e^{-\frac{M(\vec{r})}{D_\alpha}}\right) \qquad \text{(B-36)}$$

The residual absorption in dichromated gelatin is so small that absorption can be ignored (Ref. 6,7). The residual absorption in bleached 649F holograms cannot be ignored and its tendency to saturate is verified in Appendix D.

The parameters N_o, γ_n, D_n, δn_{max}, α_o, γ_α, D_α and $\delta\alpha_{max}$ can be measured for any emulsion and processing technique. This determines the response of the processed hologram to the exposure conditions. It now remains to relate the wave propagation constant used in the wave equation to those parameters. This is done in the next section.

3. Relation between $k^2(r)$ and material parameters.

In Appendix A, the wave propagation constant for a hologram was seen to be

$$k^2(\vec{r}) = k_o^2 \left[n^2(\vec{r}) - \frac{i\alpha^2(\vec{r})}{k_o^2} + \frac{in(\vec{r})\alpha(\vec{r})}{k_o}\right] \qquad \text{(B-37)}$$

Substitution of Eqs (B-24) and (B-34) into Eq (B-37) yields

$$k^2(\vec{r}) = k_o^2\left[(n_b+\Delta n\cos\phi)^2 - \frac{i(\alpha_b+\Delta\alpha\cos\phi)^2}{k_o^2} + i\left(\frac{(n_b+\Delta n\cos\phi)(\alpha_b+\Delta\alpha\cos\phi)}{k_o}\right)\right] \qquad \text{(B-38)}$$

If the second-order terms Δn^2, $\Delta\alpha^2$, and $\Delta n\Delta\alpha$ are sufficiently small, Eq (B-38) becomes

$$k^2(r) = k_o^2\left(n_b^2 - \frac{\alpha_b^2}{4k_o^2} + \frac{i\, n_b\alpha_b}{k_o}\right) + k_o^2\cos\phi\left[2n_b\Delta n - \frac{2\alpha_b\Delta\alpha}{4k_o^2} + \frac{i}{k_o}(n_b\Delta\alpha + \alpha_b\Delta n)\right] \qquad \text{(B-39)}$$

which may be written as

$$k^2(\vec{r}) = k_2^2(\vec{r}) + k_1^2(\vec{r})\cos\phi \qquad \text{(B-40)}$$

where

$$k_1^2(\bar{r}) = k_o^2 \left[2n_b\Delta n - \frac{2\alpha_b \Delta\alpha}{4b_o^2} + \frac{i}{k_o}(n_b \Delta\alpha + \alpha_b \Delta n)\right] \qquad \text{(B-41)}$$

and

$$k_2^2(\vec{r}) = k_o^2(n_b^2(\vec{r}) - \frac{\alpha_b^2(\vec{r})}{4k_o^2} + \frac{in_b(\vec{r})\alpha_b(\vec{r})}{k_o} \qquad \text{(B-42)}$$

$k_2(\vec{r})$ is the average wave propagation coefficient of the bulk emulsion. $k_1(\vec{r})$ is the amplitude of the sinusoidal modulation of the wave propagation coefficient which gives rise to the coupling between the waves which exist in the hologram. The first term in Eq (B-42) results from the index modulation present in the holographic medium. Such a modulation produces a corresponding modulation of the phase of a wave passing through the material. Therefore, holograms of this sort are called "phase holograms". The second term in Eq (B-42) results from the absorption modulation present in the hologram which also produces a modulation upon the phase of a wave passing through the material. These types of holograms are still called "phase holograms" even though the source of the phase modulation is caused by absorption. The third term is totally imaginary, hence, it produces a modulation upon the amplitude of a wave

passing through the material. These types of holograms have come to be known by the misnomer "absorption holograms", since they typically require a rather high absorption coefficient in order to achieve any coupling.

4. Relation between the hologram parameters and the Coefficients of the coupled wave equations.

The following section contains a derivation of the variable coefficients C_o, C_{-1}, Q_o and Q_{-1} in terms of material parameters.

From Eqs (31) and (38) of Chapter III,

$$C_m = \frac{-i}{2}\left[\frac{k_2^2(\vec{r}) - (\vec{\nabla}\phi_m)^2 + i\vec{\nabla}\cdot\vec{\nabla}\phi_m}{\vec{\nabla}\phi_m \cdot \hat{z}}\right] \qquad \text{(B-43)}$$

and

$$Q_m = \frac{i\, k_1^2(\vec{r})}{4\vec{\nabla}\phi_m \cdot \hat{z}} \qquad \text{(B-44)}$$

For m = 0

$$C_o = \frac{-i}{2}\left[\frac{k_2^2(\vec{r}) - (\vec{\nabla}\phi_o)^2 + i\vec{\nabla}\cdot\vec{\nabla}\phi_o}{\vec{\nabla}\phi_o \cdot \hat{z}}\right] \qquad \text{(B-45)}$$

where

$$\vec{\nabla}\phi_o = \vec{k}_{2c} \qquad \text{(B-46)}$$

$\vec{k}_{2c}$ is the reconstruction wave vector inside the hologram. Substitution of (B-46) into (B-45) yields

$$C_o = -\frac{i}{2}\left[\frac{k_2^2(\vec{r}) - \vec{k}_{2c}\cdot\vec{k}_{2c} + i\vec{\nabla}\cdot\vec{k}_{2c}}{k_c n_b(\vec{r})\cos\theta_c}\right] \tag{B-47}$$

where

$$\vec{k}_{2c}\cdot\vec{k}_{2c} = k_c^2 n_b^2(\vec{r}) \tag{B-48}$$

$k_2^2(\vec{r})$, given by Eq (B-41) and $\vec{k}_{2c}\cdot\vec{k}_{2c}$, Eq (B-48) may be substituted into Eq (B-47) to obtain

$$C_o = -\frac{i}{2}\left[\frac{k_o^2 n_b^2 - \frac{\alpha_b^2}{4} + i\, n_b \alpha_b k_o - k_c^2 n_b^2 + i\vec{\nabla}\cdot\vec{k}_{2c}}{k_c n_b \cos\theta_c}\right] \tag{B-49}$$

which can be written as

$$C_o = \frac{k_o \alpha_b(\vec{r})}{2k_c\cos\theta_c} + \frac{\vec{\nabla}\cdot\vec{k}_{2c}(\vec{r})}{2k_c\cos\theta_c}\,\frac{1}{n_b(\vec{r})} + \frac{i}{2k_c\cos\theta_c}\left[\frac{\alpha_b^2}{4n_b(\vec{r})} - \Delta k^2 n_b^2\right] \tag{B-50}$$

where

$$\Delta k^2 = k_o^2 - k_c^2 \tag{B-51}$$

In a similar manner, the equation for C_{-1} is obtained as follows, starting with Eq (B-43) for m= -1,

$$C_{-1} = \frac{-i}{2}\left[\frac{k_2^2(\vec{r}) - (\vec{\nabla}\phi_{-1})^2 + i\vec{\nabla}\cdot\vec{\nabla}\phi_{-1}}{\vec{\nabla}\phi_{-1}\cdot\hat{z}}\right] \qquad \text{(B-52)}$$

$$\phi_{-1} = \phi_{2c} - \phi = \phi_{2c} - (\phi_{r2} - \phi_{o2}) \qquad \text{(B-53)}$$

hence

$$\vec{\nabla}\phi_{-1} = \vec{K}_{2c} - \vec{K} \qquad \text{(B-54)}$$

where

$$\vec{K} = \vec{k}_{r2} - \vec{k}_{o2} \qquad \text{(B-55)}$$

$\vec{K}$ is the fringe wave vector inside the emulsion, which may be transformed due to processing as discussed in Appendix C. In that case, $\vec{K}$ is replaced by $\vec{K}'$, the transformed fringe fringe wave vector. However, $\vec{K}$ will be used in this Appendix. Substitution of (B-54) into Eq (B-52) yields

$$C_{-1} = \frac{-i}{2}\left[\frac{k_2^2(\vec{r}) - (\vec{k}_{2c} - \vec{K})^2 + i\vec{\nabla}\cdot(\vec{k}_{2c} - \vec{K})}{k_c n_b(\vec{r}) \cos_c - K_z}\right] \qquad \text{(B-56)}$$

which can be written as

$$C_{-1} = \frac{1}{2}\left[\frac{i\left(\frac{\alpha_b^2}{4} - \Delta k^2 n_b^2 + \vec{K}\cdot\vec{K} - 2\vec{k}_{2c}\cdot\vec{K}\right) + n_b\,\alpha_b k_o + \vec{\nabla}\cdot(\vec{k}_{2c} - \vec{K})}{k_c n_b \cos\theta_c - K_z}\right] \tag{B-57}$$

One comment about Eq (B-57) is of interest. The term $\vec{K}\cdot\vec{K} - 2\vec{k}_{2c}\cdot\vec{K}$ is contained in the imaginary part of $C_{-1}(\vec{r})$, therefore, as explained in the text, it contributes to the phase of the diffracted wave. Furthermore, it is dependent upon the reconstruction wave vector $\vec{k}_{2c}$ and its angular relation to the fringe wave vector $\vec{K}$. The condition for phase matching (synchronization) between the incident wave and the diffracted wave is obtained by equating the imaginary parts of C_o and C_{-1} which yields

$$\vec{K}\cdot\vec{K} - 2\vec{k}_{2c}\cdot\vec{K} = \Omega\left[\Delta k^2 n_b^2 - \frac{\alpha_b^2}{4}\right] \tag{B-58}$$

where

$$\Omega = \frac{K_z}{k_{2cz}} \tag{B-59}$$

Eq (B-58) is the condition for phase synchronization between the incident wave and the diffracted wave. By performing the dot product in Eq (B-58), it is seen that there is a cone of angles for which phase matching occurs, defined by the relation,

$$\cos(\vec{k}_{2c}, \vec{K}) = \frac{|\vec{K}|^2 + \Omega\left[\frac{\alpha_b^2}{4} - \Delta k^2 n_b^2\right]}{2k_c n_b |\vec{K}|} \tag{B-60}$$

where $(\vec{k}_{2c},\vec{K})$ defines the angle between the reconstruction wave vector and the fringe wave vector at which phase synchronization should occur. Eq (B-60) is a generalized Bragg condition and $(\vec{k}_{2c},\vec{K})$ is a generalized Bragg angle. It is seen that for the special case of reconstruction with the construction wave length ($\Delta k^2=0$) and in a lossless medium ($\alpha_b^2=0$), that Eq (B-60) reduces to

$$\cos\ (\vec{k}_{2c},\ \vec{K}) = \frac{|\vec{K}|}{2k_c n_b} \tag{B-61}$$

Eq (B-61) is the standard equation for the Bragg angle such that $(\vec{k}_{2c},\vec{K}) = \theta_{Bragg}$.

In a similar manner, by forcing phase synchronization between the incident light and the mth-order diffracted light, a general equation for the mth-order Bragg angle can be obtained. By equating I(Co) and I(Cm) one obtains

$$\cos(\theta_{Bragg}^{(mth\ order)}) = \frac{m|\vec{K}|^2+\Omega[\Delta k^2 n_b^2 - \frac{\alpha_b^2}{4}]}{-2k_c n_b|\vec{K}|} \tag{B-62}$$

For reconstruction wave vectors along the mth-order Bragg angle, given in Eq (B-62) an appropriate set of two couple wave equations can be obtained as was done in the main text for the m=-1 order condition.

The relationship Q_o, and Q_{-1} and the material parameters may be derived in a similar manner as that for the Cm's. Using Eq (B-44) and (B-42) it is seen that

$$Q_o(\vec{r}) = \frac{i\, k_o^2 \left[2n_b \Delta n - \frac{\alpha_b \Delta\alpha}{2k_o^2} + \frac{i}{k_o}(n_b \Delta\alpha + \alpha_b \Delta n)\right]}{4k_c n_b \cos\theta_c} \qquad (B\text{-}63)$$

and

$$Q_{-1}(\vec{r}) = \frac{i\, k_o^2 \left[2n_b \Delta n - \frac{\alpha_b \Delta\alpha}{2k_o^2} + \frac{i}{k_o}(n_b \Delta\alpha + \alpha_b \Delta n)\right]}{4\,(k_c n_b \cos\theta_c - K_z)} \qquad (B\text{-}64)$$

Q_o and Q_{-1} are the coupling coefficients of the coupled wave equations. It is observed from these equations that coupling can occur due to index modulation ($\Delta n \neq 0$) and for absorption modulation ($\Delta\alpha \neq 0$) for a material.

The equations for C_o and C_{-1}, Eqs (B-50) and (B-57), respectively, are used in various locations throuout the text. These equations serve to relate the coefficients of the coupled wave equations to the material parameters α_b, $\Delta\alpha_b$, n_b and Δn_b. Also these equations for C_o and C_{-1} have been shown to relate the reconstruction wave vector to the coupled wave equations, thus, accounting for changes in reconstruction wave vector position.

In Appendices D, E and F the material parameters α_b, $\Delta\alpha$, n_b and Δn are related to the exposure conditions. This will complete the loop between the formation conditions of the hologram and its reconstruction conditions.

APPENDIX C

THE TRANSFORMATION TO ACCOUNT FOR CHANGES IN THICKNESS OF THE EMULSION DURING PROCESSING

The intensity distribution formed by the interference of the object and reference waves is used to expose the emulsion. This induces a latent fringe pattern into the emulsion. This fringe pattern is represented by the fringe wave vector derived in Appendix A.

Since the latent fringes are actually a part of the emulsion, any motion of the emulsion with respect to the substrate during the processing shifts the latent fringe structure. Consequently, the hologram fringe structure after processing may not be identical to the latent fringe structure.

This difference is accounted for theoretically by a transformation of the latent fringe wave vector $\vec{K}$ to the hologram fringe wave vector $\vec{K}'$, by

$$\vec{K}' = \underline{\underline{T}}\vec{K} \qquad \text{(C-1)}$$

$\underline{\underline{T}}$ is the transformation matrix which accounts for changes in the emulsion caused by processing.

The predominate effect upon the emulsion due to processing is a change in thickness. Some development processes cause the emulsions to swell due to absorption of liquids, others cause shrinkage due to fixing and hardening. These

effects are described in Appendix D for the silver halide emulsions and in Appendix E for dichromated gelatins.

Since the emulsion is attached to the substrate by an extremely strong adhesive, lateral motion of the emulsion can be ignored except near the edges of the plate. In most cases, the hologram is constructed near the center of the photographic plate, therefore, the changes in the emulsion due to processing may be described simply as a change in thickness.

The geometry of the change in fringe structure caused by an expansion is shown in Figure (C-1). From this geometry the transformation for an emulsion thickness change is derived.

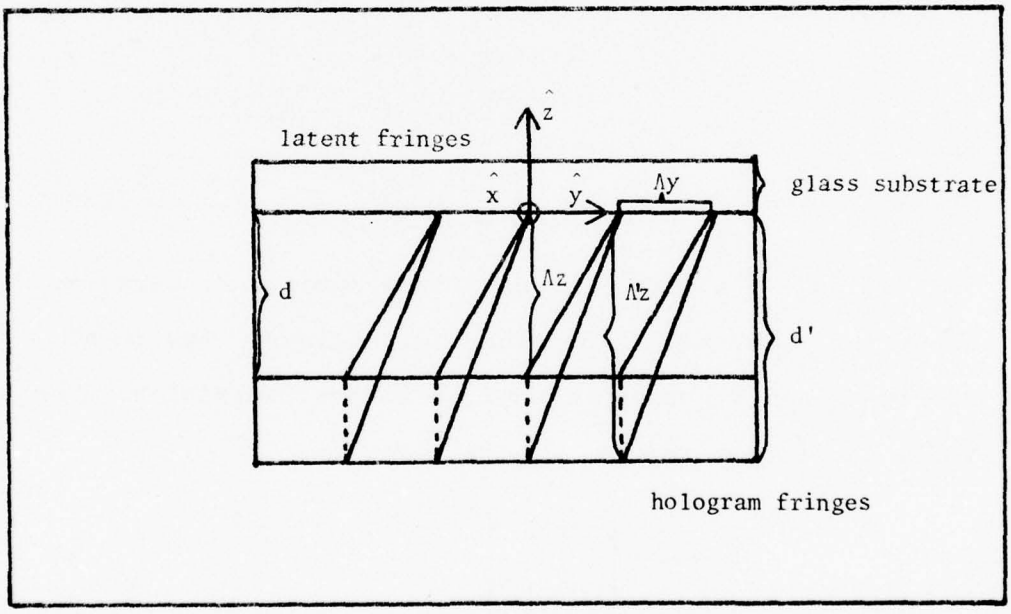

Figure C-1. Fringe Change for Expansions

d' = expanded thickness, d = emulsion thickness during exposure Λ_y = spatial fringe frequency in y direction, Λ_z spatial fringe frequency in z direction, Λ'_z is the spatial frequency of the expanded fringes in the z direction.

Starting with the equation

$$\vec{K} = k_x \hat{x} + k_y \hat{y} + K_z \hat{z} \qquad (C-2)$$

where

$$K_x = \frac{2\pi}{\Lambda_x} \qquad (C-3)$$

$$K_y = \frac{2\pi}{\Lambda_y} \qquad (C-4)$$

$$K_z = \frac{2\pi}{\Lambda_z} \qquad (C-5)$$

and because the expansion or shrinkage is only in the z direction, it is seen that

$$K'_x = K_x = \frac{2\pi}{\Lambda_x} \qquad (C-6)$$

$$K'_y = k_y = \frac{2\pi}{\Lambda_y} \qquad (C-7)$$

and

$$K'_z = \frac{K_z}{S_z} = \frac{2\pi}{S_z \Lambda_z} \qquad (C-8)$$

Λx, Λy, and Λz are the latent fringe spatial frequencies along the x, y, and z coordinate directions. Eqs (C-6) and (C-7) are a consequence of no lateral expansion. Therefore, the transformation, $\underline{\underline{T}}$, is given by,

$$\underline{\underline{T}} = \begin{bmatrix} 1 & 0 & 0 \\ 0 & 1 & 0 \\ 0 & 0 & \frac{1}{S_z} \end{bmatrix} \qquad (C-9)$$

where S_z is the change in thickness factor defined by

$$d' = S_z d \tag{C-10}$$

The effect of thickness changes is inserted into the theory derived in the main body of the dissertation through the variable coefficient C_m, Eq (31), which was determined in Chapter III to be

$$C_m = -\frac{i}{2}\left[\frac{k^2(\vec{r}) - (\vec{\nabla}\phi_m)^2 + i\vec{\nabla}\cdot\vec{\nabla}\phi_m}{\vec{\nabla}\phi_m \cdot \hat{z}}\right] \tag{14}$$

where

$$\phi_m = \phi_{2c} + m(\phi_{r2} - \phi_{o2}) \tag{C-11}$$

$$\vec{\nabla}\phi_m = \vec{\nabla}\phi_{2c} + m(\vec{\nabla}\phi_{r2} - \vec{\nabla}\phi_{o2}) \tag{C-12}$$

but the gradient of the phase is the wave vector, which implies

$$\vec{k}_m = \vec{k}_{c2} + m(\vec{K}) \tag{C-13}$$

$$\vec{K} = \vec{k}_{r2} - \vec{k}_{o2} \tag{C-14}$$

In order to account for thickness changes, $\vec{K}$ is replaced by $\vec{K}'$

$$\vec{k}_m = \vec{k}_{c2} + m\vec{K}' \tag{C-15}$$

Where $\vec{K}'$ represents the wave vector of the hologram fringes defined by Eq (C-1).

APPENDIX D

CHARACTERISTICS OF KODAK 649-F BLEACHED SILVER HALIDE HOLOGRAMS

The purpose of this appendix is to summarize the effects of exposure and processing upon bleached silver halide holograms. It is shown that changes in the thickness, optical index, and absorption occur due to processing.

In this appendix, the characteristics of Kodak 649-F holograms are discussed and the processing procedures used in this dissertation are presented. The exposure and image formation process is reviewed. The development of silver halide is discussed, and the specific processes of (1) development, (2) stop bath, (3) fixing, (4) washing, and (5) bleaching used in this work are described. It is shown that these processes change the thickness, optical index, and absorption coefficient of the emulsion as compared to their values during exposure.

Experimental measurements of the optical index, the absorption coefficient, and the thickness of Kodak 649-F holograms are presented in Appendix F.

1. Kodak 649-F Emulsion.

The Kodak 649-F emulsion is composed of a gelatin in which are colloidally suspended silver halide crystals, usually silver bromide, along with a small percentage of other silver halides and sensitizers. The gelatin has an optical index of 1.535 for Kodak 649-F plates (Ref. 24)

and the silver bromide optical index is 2.25. A typical emulsion contains 20-40% by weight, 5-10% by volume of silver halide (Ref. 8), but the specific amount is not generally known.

The emulsion used in this work is held on an optically flat .040 inch thick glass substrate by a layer of adhesive. Measurements of the emulsion thickness before and after processing are presented in the experimental section of Appendix F.

The following sections describe what happens to this emulsion during exposure and development.

2. Exposure and Image Formation.

Exposure to light causes a change in the grains of silver halide suspended in the emulsion. This change is regarded as the addition to the grain of a "latent image" in the form of an aggregate of silver atoms, perhaps as few as two to four atoms (Ref. 33). The change is latent in the sense that no visible change in the film is observed, but the probability that a chemical change will occur upon development of the grain is great.

The latent image undoubtedly arises due to surface imperfections and surface impurity sites (Ref. 33). The absorption of the light forms electron - hole pairs in the silver halide which somehow combine with the silver ions and other impurity metal ions in combination with pre-existing

electron traps. The electron-hole pairs drift to impurity or lattice imperfections to form aggregates of silver or other metallic impurities and release of halogens (Ref. 33).

The physical process is described by two competing theories: (1) the Gurney-Mott theory and (2) the Mitchell theory. The theories are similar except for the order in which the processes occur.

In the Gurney-Mott theory electrons in the conduction band are thought to be free to move about the crystal. These electrons are provided by absorption of light on or near the crystal surface. They are momentarily trapped at a lattice defect or impurity site on the crystal surface. Thus, the first process to occur, according to this theory, is trapping. The electron is temporarily localized by the trap. The second step is migration of a mobile silver ion to this center and it combines with the electron to form an atom of silver. Because the trap is shallow, the electron may randomly escape the trap due to thermal energy and return to the free state prior to migration. Eventually, on the average, the electron will remain trapped long enough to be joined by a silver ion. The single atom is not stable, but will decompose again into a silver ion and free electron, thus, the cycle of trapping and silver formation is cyclic during exposure. The silver atom acts as an electrode to attract electrons. With the arrival of a second silver ion, a stable two-atom nucleus of molecular silver is formed. Therefore, the third and fourth steps

are trapping and ionic motion resulting in nucleation of molecular silver. Only after nucleation is the process not reversible (Ref. 33).

The Mitchell theory supposed that existing traps must first be deepened by the proximity of a mobile silver ion. The electron arrives at the trap either with, or after, the silver ion, and together they form a silver atom at once, without a further ionic step. The simple silver atom cannot act as a trap for a second photo electron, but must first acquire a second silver ion. If an electron arrives before the escape of the second silver ion, a stable silver speck is formed (Ref. 33).

Therefore, the basic differences between the two theories involve the depth of the traps and the sequence in the arrival of particles.

Regardless, once a stable, two atom speck is formed, its growth occurs by repeated migration to the speck of photo electrons and mobile silver ions. For our purpose, it is not important to know any more detail about the photo chemical processes but only that the latent image is a silver speck of a few atoms.

The development process depends upon the fact that the latent silver with a minimum size of only a few atoms acts as the catalyst for the development of the entire grain (Ref. 16). For this reason, changes in develcped grain

number density determine the eventual optical density of a photograph. In general, for any given development progress, the size of the developed grains varies only slightly. Since only two to four photons are required to form a latent image, the response of the developed film to exposure exhibits almost no threshold effects.

3. Development.

Two kinds of development processes have historically been acknowledged (Ref. 33). These two kinds are: (1) chemical or direct development and (2) physical development. The two processes differ only in the source of silver from which the latent silver speck grows during development. If the source of the silver is from the solid silver halide crystal on which the latent image resides, then this is called direct or chemical development. If the source of silver is from a silver salt results from dissolving the silver halide grains in the emulsion, the process is called physical development (Ref. 16). A misnomer arises because "chemical development" is no more chemical than is "physical development" (Ref. 33).

The two development techniques usually result in different developed particle sizes and shapes. When the developer is a weak solvent for silver halide and contains no additional silver salts, the major portion of development occurs in a reaction at the interface between the latent silver nucleus, the developer, and the remaining silver

halide crystal. Initially, the grain develops nearly uniformly and spherically. As development proceeds, the specks elongate into thickened filaments (Ref. 16).

When the same emulsion is developed in a developer that contains a soluble silver salt or that has a solvent for silver halide, then a mixture of chemical and physical developments occurs. In general, if physical development dominates, the developing latent silver speck, being uniformly surrounded with silver ions, grows spherically or in some regular crystalline shape (Ref. 33). Any number of speculative proposals have been made about the mechanism which leads to the specific shape and size of the developed silver grain, but none has been completely verified experimentally (Ref. 16). There are two general viewpoints, both of which have been partially verified by experiment:

(1) Development is an electro-chemical process in which the latent image and developing silver act as an electrode- the process is auto-catalytic.

(2) The other emphasizes the importance of adsorption and assumes the reduction is propagated as a catalytic reaction at the triple interface between silver, silver halide, and developer (Ref. 16).

Both concepts can be interpreted as extensions of the Gurney-Mott or the Mitchell latent image theories, with the electrons being supplied by the developer rather than by

absorption. In general, the electrode mechanism is less successful than the absorption mechanism in accounting for the kinetics of development. It is possible that the triple interface mechanism (adsorption mechanism) dominates in the early stages, when the latent image nucleus is too small to be an effective electrode and the semi-conductor properties of the crystal dominate. The electrode mechanism is more important in the later states (Ref. 16). The search for the cause of filament formation in chemically developed emulsion is an elusive problem to date.

4. Development of 649-F in D-19. The Kodak 649-F hologram is most commonly developed in D-19. This section contains a description of the characteristics of the constituents in D-19 in order to get a better understanding of the effects of development upon the physical and optical characteristics of the emulsion. D-19 consists of the following compounds:

(1) Water [50°]500cc

(2) Elon 2.0 grams

(3) Sodium Sulfite 90.0 grams

(4) Hydroquinone 8.0 grams

(5) Potassium Bromide 5.0 grams

(6) Sodium Carbonate 52.5 grams

(7) Cold water to make 1.0 liter

Elon and hydroquinone are common reducers or developers. The sodium sulfite is a weak solvent for silver halide and a preserver. It reacts with oxidized developer so that the development process does not reverse by oxidation of silver to silver ions. The potassium bromide decreases the fog rate and also decreases the rate of growth in lower-exposure regions. These effects were first pointed out by Hurter and Drifield (Ref. 33).

The halide ion, potassium bromide, can influence the development in several ways. Excess halide is adsorbed and, thus, interferes with the developer. Further, this decreases the thermodynamic activity of the silver, which may be particularly important in fog reduction. The ion also reduces the rate of solution of the silver halide in the developer causing a more direct development.

Sodium carbonate is an alkali to control the pH of the solution (Ref. 33).

The constituents of D-19 indicate that is is very close to a direct developer, but the presence of a weak silver halide solvent (sodium sulfite) implies that a small degree of physical development occurs. Therefore, the shape of the developed silver grains should be nearly spherical and non-filamentary. Indeed, the size of the developed grains has been measured by Chang to be about 500Å and the shape has been determined to be a slightly elongated sphere (Ref. 8).

5. The Stop Bath. The stop bath is usually an acid rinse designed to neutralize any alkaline developer remaining in the emulsion. It rapidly lowers pH to a level at which development ceases (Ref. 33). It can be preceded by a quick rinse in water to reduce the effect of pH shock changes on the emulsion gelatin (Ref. 33). It further serves to preserve the acidity of the fixing bath (Ref. 33). The stop bath used in this work was acetic acid.

6. Fixation. The purpose of the fix is to remove all of the undeveloped silver halide and sensitizer from the emulsion so that further exposure and darkening does not result. The silver halides are only very slightly soluble in water, so the fix must create a soluble silver salt which can be removed by washing.

The following fixing mixture was used:

0.	Water	60 cc
1.	Sodium Thiosulfate (Hypo)	240 grams
2.	Sodium Sulfite	15 grams
3.	Acetic Acid (28%)	48 cc
4.	Boric Acid	7.5 grams
5.	Potassium Alum	15 grams
6.	Cold water to make	1 liter

The fixing reaction proceeds as follows,

$$Na_2(S_2O_3) \xrightarrow{water} 2Na^+ + S_2O_3^{--}$$

$$AgBr + 2S_2O_3^{--} \longrightarrow Ag(S_2O_3)_2^{-3} + Br^-$$

$$3Na^+ + (Ag(S_2O_3)_2)^{-3} \longrightarrow Na_3(Ag(S_2O_3)_2)$$

$Na_3(Ag(S_2O_3)_2)$ is silver thiosulfate and is soluble in water. It is removed by washing.

The concentration of hypo must be kept high so that $Ag(SO_3)$ exists only in a transitory role because the complex $NaAg(S_2O_3)$ is not soluble in water. Thiosulfate attacks metallic silver chemically in the presence of any dissolved oxygen, oxidized developer, or other oxidizing agents. The sodium sulfite is added to reduce these reactions. The acetic acid, boric acid, and potassium alum are hardeners. The sodium sulfite prevents the decomposition of thiosulfate by the acids. Potassium alum ($Al_2(SO_4)_3K_2SO_4$-chloride) is a hardening agent. The hardening process is presumably due to a reaction of Al^{+++} ions, free or adsorbed hydrous alumina, and the COO^- groups of the gelatin, forming cross linkage between chain molecules. This shrinks and hardens the gelatin. The degree of hardening depends on the pH of the solution determined by the concentration of the acid, sulfite, and alum (pH 4-6 required) (Ref. 35). Boric acid increases the useful hardening life of potassium alum baths and reduces sludge (Ref. 35).

7. Washing. The washing removes the soluble thiosulfate, the hypo, and other substances from the emulsion. This wash is critical since the unremoved compounds will degrade the hologram quality. It is in the washing stage that most of the silver halide not changed to silver is removed. This leaves gaps in the emulsion. These gaps are reduced by further shrinkage of the emulsion. The two major sources of shrinkage are hardening and removal of a silver halide. Clearly, the fixer and associated washing have the most pronounced effect upon the emulsion in terms of shrinkage and changes in the optical properties of the emulsion.

8. Bleaching. After washing, the development process is finished. The emulsion contains an image of the interference pattern between the object and reference waves. This image is composed of metallic silver embedded in the emulsion. Because of the strong absorption of metallic silver the hologram diffraction process is very inefficient. In order to increase the efficiency of the hologram, bleaching the silver image is required. The bleaching process used in this dissertation is described in the literature (Ref. 29). The bleaching changes the metallic silver to silver bromide, leaving non-soluble cuprous-bromide in the emulsion. Therefore, the result is a dielectric hologram with transparent silver bromide particles forming the fringe structure in the hologram.

9. Conclusions. The thickness and optical properties of bleached Kodak 649-F holograms are significantly different from those properties prior to processing.

Development changed the silver halide to silver. Fixing removes all of the undeveloped silver halide, leaving the silver image. Fixing has caused a shrinkage of the emulsion. This changes the optical index by removing particles of optical index 2.25 in unexposed, undeveloped regions. Since the exposure is periodic, equal areas of light and dark, it is expected that almost 50% of the silver halide is unexposed. Therefore, the index is significantly reduced from the index during exposure when all of the silver halide particles were present.

The bleaching converts the image from silver to silver halide.

It is expected that the development process used on Kodak 649-F should cause a shrinkage, change the optical index, and change the loss coefficient of the material from the values prior to processing. These conclusions are experimentally verified in Appendix F.

APPENDIX E

CHARACTERISTICS OF DICHROMATED GELATIN HOLOGRAMS

The purpose of this appendix is to review some current thought on the processes which occur in dichromated gelatin and to present some results of the measurement of the optical index modulation response to exposure for dichromated gelatin.

Dichromated gelatin is a photographic emulsion (Ref. 10,11,12,23,31,34) in which a water solution of a dichromate salt, such as ammonium dichromate $[(NH_4)_2Cr_2O_7]$ is allowed to saturate a gelatin and dry. This emulsion is then exposed and processed to become a hologram.

The exact mechanism of hologram formation in dichromated gelatin is poorly understood. Curran and Shankoff (Ref. 11) have hypothesized that swift dehydration during processing the water swollen gelatin layer by isopropanol causes large strains between unhardened (or unexposed) regions and hardened (or exposed) regions. This strain causes the gelatin to crack along fringe planes where photo-initiated cross-linking has caused hardening of the gelatin layer. It is further postulated that the refractive index differential between the air in the crack in the gelatin creates the large refractive index modulation which the material seems to exhibit (Ref. 11).

Chang has (Ref. 6,7) experimentally determined the optical index modulation response of dichromated gelatin to exposure for a transmission hologram to be

$$\Delta n = \Delta n_{max}(1-e^{-\frac{E}{D}}) \qquad (E-1)$$

Where Δn_{max} is the maximum possible index modulation, E is the total exposure (millijoules/cm^2) and D is the rapidity of decay in the exposure sensitivity. Δn_{max} and D are greatly affected by processing conditions. Under a given processing condition, however, they are only dependent on the concentration of the sensitizer solution. Chang, under a controlled processing condition, determined Δn_{max} and D which are given by

$$D = 95+200\ e^{-\frac{c}{6.5}} \quad (\text{millijoules/cm}^2) \qquad (E-2)$$

and

$$\Delta n_{max} = 0.064\ (1-e^{-\frac{c}{3.0}}) \qquad (E-3)$$

where C is the concentration of sensitizer solution in percent. Chang used Kogelnik's theory to determine D. He hypothesized that for E<<D that a linear response of optical index modulation to exposure should occur such that

$$\Delta n = \gamma_n E \qquad (E-4)$$

Therefore, D can be determined from (E-1) and (E-4) by working backwards through the Kogelnik theory for several

values of diffraction efficiency in the low exposure regions. The optical index modulation response of dichromated gelatin to exposure measured by Chang (Ref. 6,7) is used in the theory discussed in the result section of Chapter V.

Hardened dichromated gelatin is a dielectric material that is essentially lossless after development and as a result, volume holograms made from this material are very efficient. Consequently, the absorption coefficient, and absorption modulation can be assumed to be zero. The bulk optical index after processing is also independent of exposure. Another interesting characteristic of the dichromated gelatin hologram is the reprocessibility; the optical index modulation of processed holograms can be either enhanced or diminished by redeveloping with a proper simple post-processing technique (Ref. 7).

The thickness of a processed dichromated gelatin hologram strongly depends on the concentration of sensitizer solution, the relative humidity and temperature of processing room, and exposure level. Under the controlled environments (i.e., relative humidity 40% and temperature 75%F), the thickness of the holograms is generally swollen. However, the relative swelling decreases as either the concentration of sensitizer solution or the exposure increases.

The thickness change of dichromated gelatin holograms as a function of not only a number of processing parameters but also hologram types is a rather complicated problem. But the thickness of dichromated gelatin hologram can be controlled by either baking over a hot plate or drying in a vacuum chamber.

APPENDIX F

EXPERIMENTAL RESULTS FOR THE LOSS COEFFICIENT, OPTICAL INDEX, AND THICKNESS OF BLEACHED KODAK 694-F EMULSION

Two experiments performed by this worker are presented in this appendix: (1) the measurement of the loss coefficient of bleached 649-F emulsion as a function of exposure, and (2) the measurement of the thickness of undeveloped and unbleached 649-F, of developed and unbleached 649-F, and of developed and bleached 649-F. The results of a third experiment performed by Williamson (Ref. 44) are presented for the measurement of the optical index of refraction of bleached 649-F emulsion as a function of exposure. The purpose of these experiments was to verify the theoretical assumptions made in this dissertation as to the response of bleached 649-F to exposure and to determine the amount of change in thickness occurring in 649-F emulsion due to processing.

1. Measurement of the Loss of Bleached 649-F Emulsion. Five plates of 649-F Kodak emulsion were exposed to a Helium-Neon Laser intensity source as shown in Figure F-1.

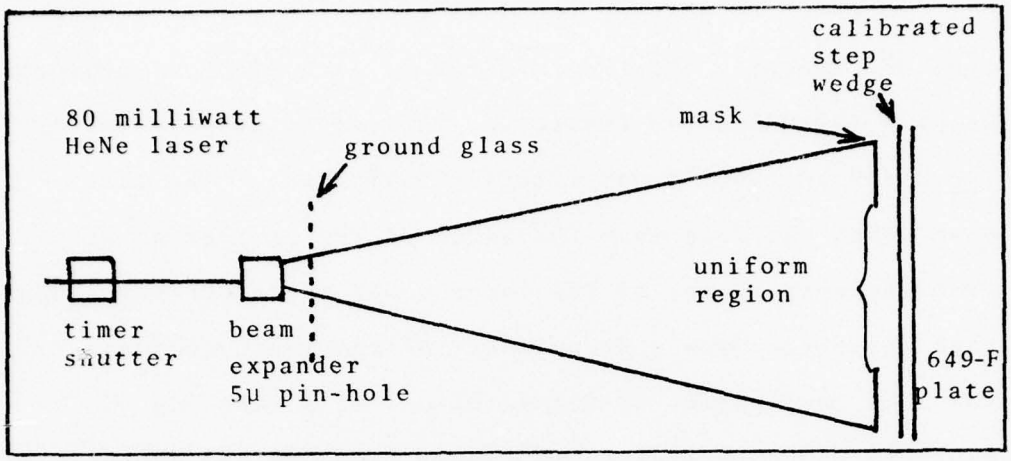

Figure F-1 . Exposure of 649-F Plates

The pin-hole beam expander provided a uniform source of light to expose the step-wedge and film. A ground glass screen was used to disrupt the spatial and temporal coherence of the laser in order to obtain a more uniform exposure. The variance of intensity in the uniform region was less than 3%. A Kodak calibrated transmission step-wedge (Catalog Number 152-3422) was used to vary the exposure on the 649-F emulsion so that a range of known exposures could be photographed on each of the five plates. By varying the choice of steps used and by varying the shutter-timer, the exposure was changed over a range from 4 millijoules/cm^2 up to 2500 millijoules/cm^2.

After exposure, the plates were processed and bleached according to the procedures discussed in Appendix D. Plates #1, #2, and #3 were processed on one day and plates #4 and #5 were processed three weeks later in the same manner.

In order to measure the loss of each plate as a function of exposure, the transmission of each step was measured using a 401-C Spectra Physics calibrated laser power meter (Accurate to ±10%, precise to ±1 millijoule). The laser beam width was less than the width of the photograph steps. From the measurement of the laser power transmitted through each wedge and from a measurement of the incident power, the loss coefficient (1-transmission) as a function of exposure was determined. This loss includes the Fresnell losses, absorption and scattering.

The loss coefficient as a function of exposure is presented in Figure F-2. It is concluded by observation of the data in Figure F-2 that the loss coefficient of the bleached 649-F emulsion is proportional to the exposure for a significant exposure region, but that saturation occurs at the higher exposures.

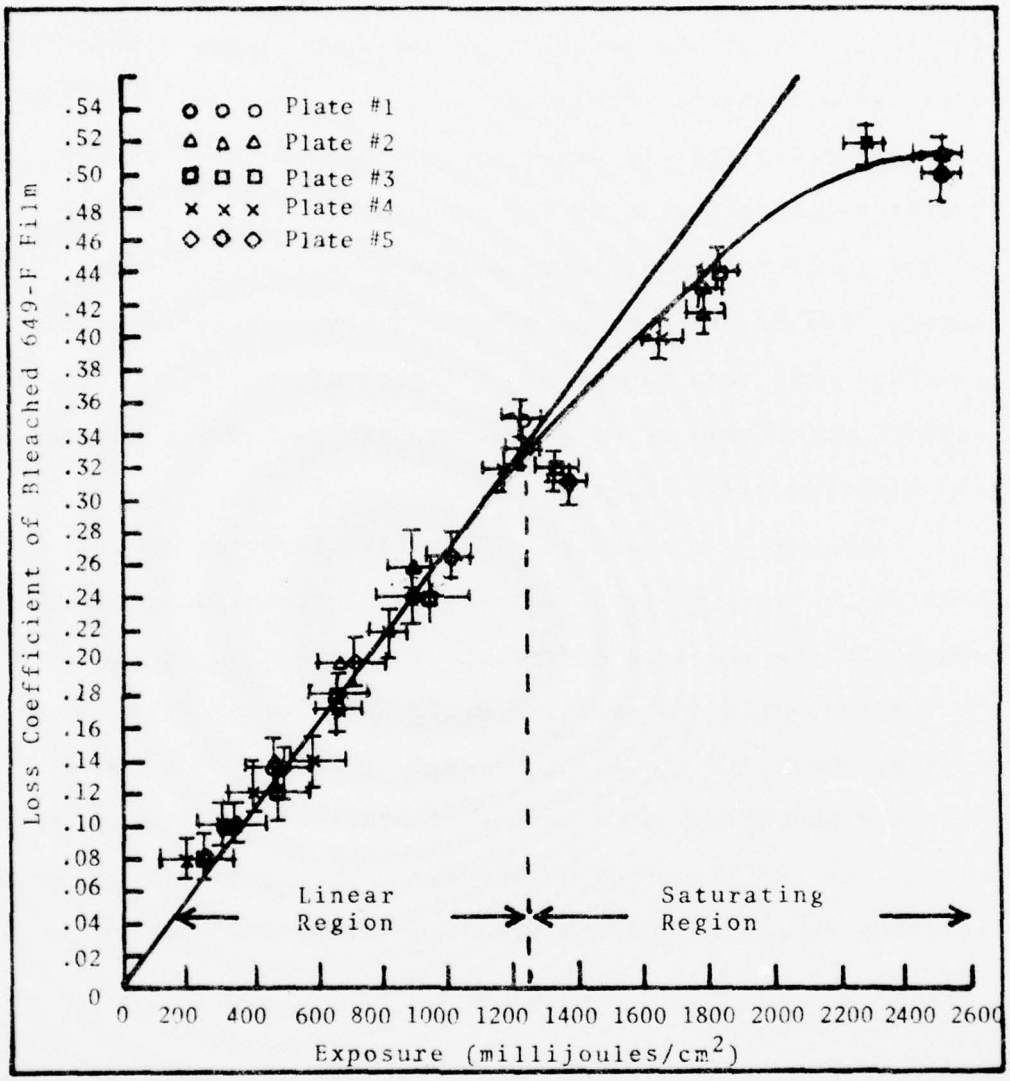

Figure F-2
Loss Coefficient of Bleached 649-F versus Exposure

2. The Thickness Measurement. In order to measure the thickness change due to the processing of 649-F emulsion, the thickness of the emulsion was measured using a scanning electron microscope (SEM).

Several plates of undeveloped 649-F emulsion were broken by impact using an awl and hammer. Small samples of the fractured plates were collected which had clean edges. The clean edges resulted from the propagation of a fracture away from the point of impact of the awl. Similar samples were taken of developed and unbleached, and developed and bleached 649-F emulsion.

Each sample was coated with a 100A layer of gold in a sputter chamber and mounted using an electrically conductive cement in the electron microscope chamber. The sample could be rotated until the emulsion could be observed from a point of view normal to the fracture edge. Figure F-3 shows a Polaroid photograph of a sample of bleached 649-F emulsion taken from the TV screen of the SEM. The emulsion, including an adhesive layer, and the glass substrate are clearly visible.

AD-A041 537 AIR FORCE INST OF TECH WRIGHT-PATTERSON AFB OHIO SCH--ETC F/G 20/6
THE THEORY OF DIFFRACTION FROM A HOLOGRAPHIC LENS.(U)
MAY 77 D D YOUNG

UNCLASSIFIED AFIT/DS/PH/76-4 AFAL-TR-76-270 NL

3 OF 3
AD
A041537

END

DATE
FILMED
8-77

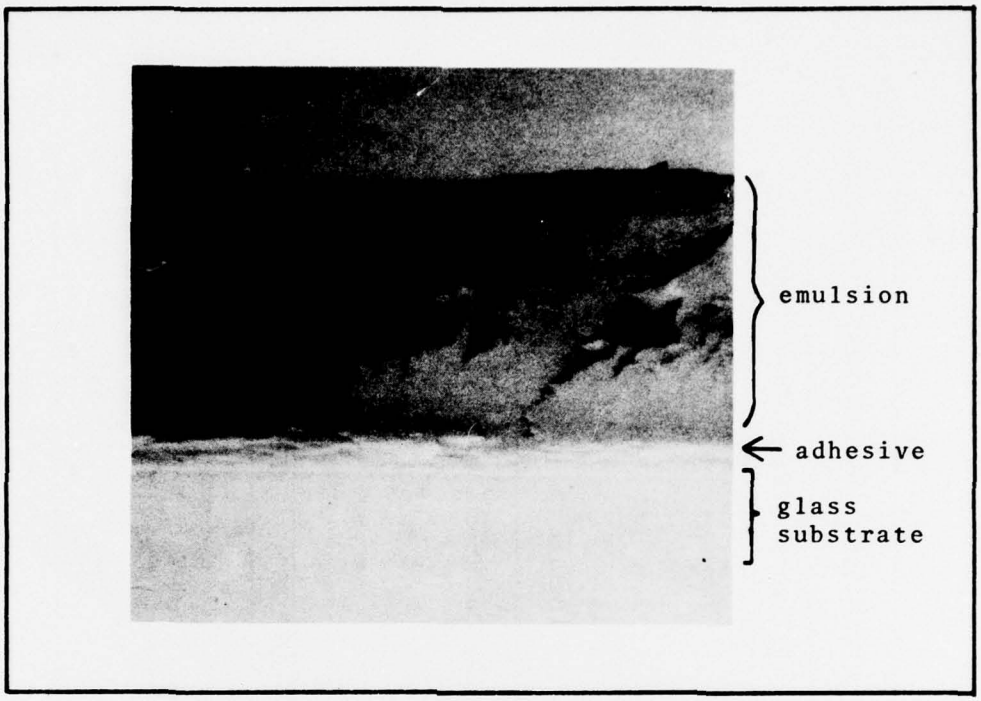

Figure F-3. Bleached 649-F Emulsion Magnification 2750X.

By observing several samples at different positions, a variety of thickness measurements were taken of both developed and bleached, developed and unbleached, and unexposed, unprocessed 649-F emulsion. Table F-I presents the data for these three cases.

TABLE F-I

DEVELOPED AND BLEACHED		DEVELOPED AND UNBLEACHED		UNDEVELOPED, UNBLEACHED	
Sample No.	Thickness	Sample No.	Thickness	Sample No.	Thickness
1	13.4μ	1	13.4μ	1	17.8μ
2	13.6μ	2	13.5μ	2	17.8μ
3	13.9μ	3	13.2μ	3	17.5μ
4	13.8μ	4	13.8μ	4	17.5μ
5	13.2μ	5	13.6μ	5	17.3μ

Table F-II contains the average thickness and average deviation of the thickness for the data in Table F-I.

TABLE F-II

	AVERAGE THICKNESS	AVERAGE DEVIATION
Unexposed, Undeveloped 649-F	17.6μ	±.2μ
Developed and Unbleached 649-F	13.5μ	±.2μ
Developed and Bleached 649-F	13.6μ	±.2μ

It is concluded that the bleaching process has no effect upon the thickness since the developed and unbleached emulsion has the same thickness within experimental error as the developed and bleached emulsion. The development process has the greatest effect causing a shrinkage of about 4μ. This is to be expected because of the fixing and hardening process used in development. Since no lateral motion or tearing of the emulsion was observed at the glass substrate, it is concluded that the processing effects only the thickness of the emulsion.

3. Optical Index of Bleached 649-F. Williamson has measured the optical index of bleached 649-F emulsion, therefore, it was unnecessary to perform this measurement in this dissertation. The data obtained by Williamson is repeated here in order to show that the assumptions concerning the response of the optical index to exposure used in this dissertation are valid. Figure F-4 shows this data obtained by Williamson for the optical index of bleached 649-F emulsion versus exposure. Again, a linear region and a saturating region are observed.

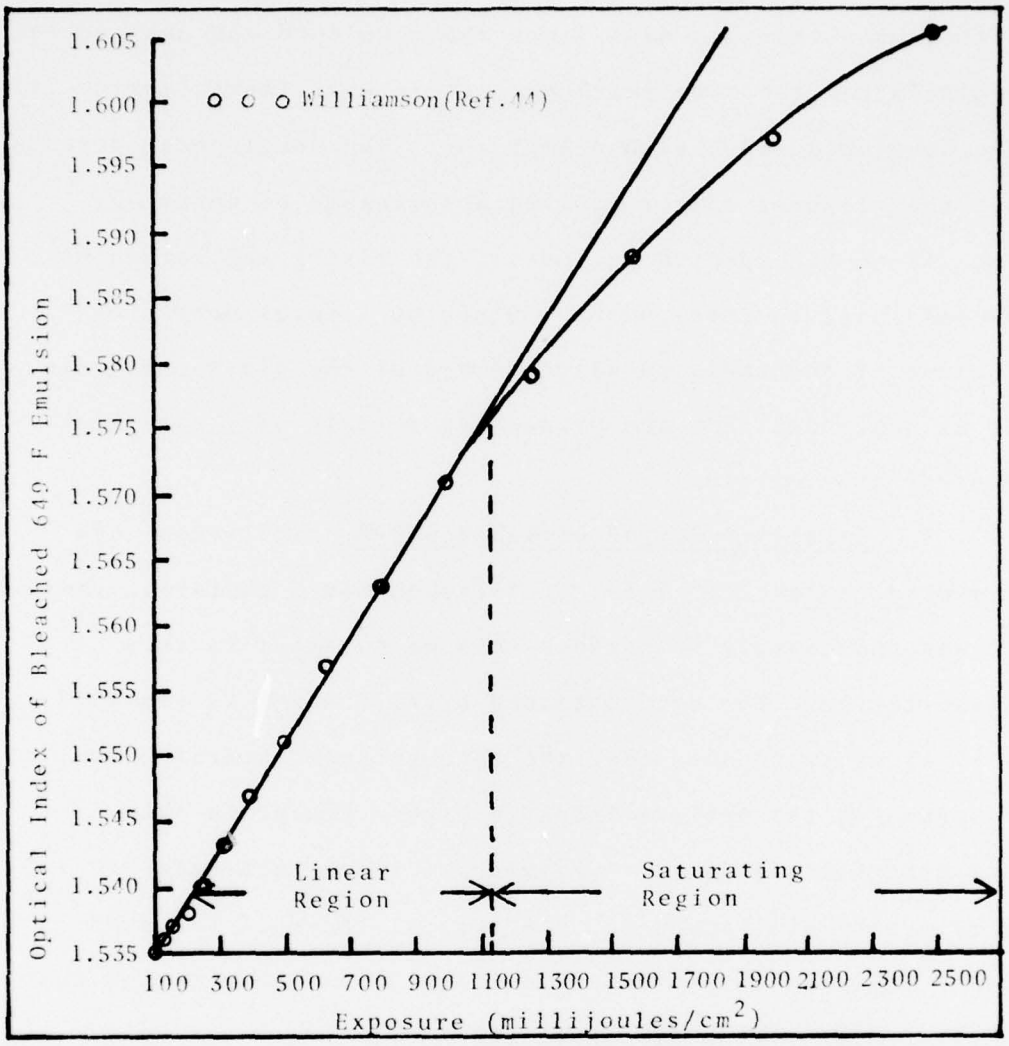

Figure F-4. Optical Index of Bleached 649-F Emulsion versus Exposure

APPENDIX G

ALTERNATE SOLUTION TO THE COUPLED WAVE EQUATIONS

This appendix contains an alternate solution to the coupled wave equations of Chapter III for a thick hologram based upon Green's Functions.

Eqs (54) and (55), Chapter IV, may be written in matrix notation as

$$\frac{d}{dz}\begin{pmatrix} V_o \\ V_{-1} \end{pmatrix} = \frac{d\vec{v}}{dz} = \begin{pmatrix} -C_o & Q_o \\ Q_{-1} & -C_{-1} \end{pmatrix}\begin{pmatrix} V_o \\ V_{-1} \end{pmatrix} = \underline{\underline{M}}\vec{v} \tag{G-1}$$

The off diagonal terms in $\underline{\underline{M}}$ are the coupling terms. The eigenvalues of $\underline{\underline{M}}$ are

$$\lambda_{\pm}(z) = -\frac{1}{2}(C_o + C_{-1}) \pm \sqrt{\frac{1}{4}(C_o - C_{-1})^2 + Q_o Q_{-1}} \tag{G-2}$$

These eigenvalues are very similar to the dominate terms in the JWKB solution in Chapter III. It is seen that

$$\lambda_{\pm}(z) = \gamma_{\pm}(z) \tag{G-3}$$

where $\gamma_{\pm}(z)$ is given by Eq (106), Chpater IV. The equality holds provided all derivatives in $\gamma_{\pm}(z)$ are neglected. Therefore, $\lambda_{\pm}(z)$ would be the zero-order JWKB solutions, that is, the solutions for the constant coefficient case.

By finding an appropriate set of eiven-vectors, $\underline{\underline{M}}$ is transformed to a nearly diagonal matrix, starting with the transformation

$$\vec{r} = P^{-1}\vec{\nu} \tag{G-4}$$

Eq (G-1) becomes

$$\frac{d\vec{r}}{dz} = \underline{\underline{\Lambda}}\vec{r} - \underline{\underline{P}}^{-1}\frac{d\underline{\underline{P}}}{dz}\vec{r} \tag{G-5}$$

where

$$\underline{\underline{\Lambda}} = \begin{bmatrix} \lambda_+(z) & 0 \\ 0 & \lambda_-(z) \end{bmatrix} = \underline{\underline{P}}^{-1}\underline{\underline{M}}\,\underline{\underline{P}} \tag{G-6}$$

and

$$\underline{\underline{P}} = \begin{bmatrix} A^+ & A^- \\ 1 & 1 \end{bmatrix} \tag{G-7}$$

$$\underline{\underline{P}}^{-1} = \frac{Q_{-1}}{A^+A^-(\lambda_- - \lambda_+)}\begin{bmatrix} 1 & -A^- \\ -1 & +A^+ \end{bmatrix} \tag{G-8}$$

where

$$A^+ = \frac{Q_{-1}}{C_- + \lambda_+} \tag{G-9}$$

and

$$A^- = \frac{Q_{-1}}{C_- + \lambda_-} \tag{G-10}$$

Eq (G-5) is of the form

$$\frac{d\vec{r}}{dz} = [\underline{\underline{D}} + \underline{\underline{U}}]\vec{r} \tag{G-11}$$

where $\underline{\underline{D}}$ is a diagonal matrix and $\underline{\underline{U}}$ is an off-diagonal matrix.

$$\underline{\underline{D}} = \begin{bmatrix} \lambda_+ - \frac{dA^+}{dz} & \frac{Q_{-1}}{A^+A^-(\lambda_- - \lambda_+)} \\ 0 & \lambda_- + \frac{dA^-}{dz} \end{bmatrix} \qquad \begin{matrix} 0 \\ \frac{Q_{-1}}{A^+A^-(\lambda_- - \lambda_+)} \end{matrix} \tag{G-12}$$

and

$$\underline{\underline{U}} = \frac{Q_{-1}}{A^+A^-(\lambda_- - \lambda_+)} \begin{bmatrix} 0 & -\frac{dA^-}{dz} \\ \frac{dA^+}{dz} & 0 \end{bmatrix} \tag{G-13}$$

Eq (G-11) is solved by Green's Functions to be

$$\vec{r} = \int_{-\infty}^{\infty} \underline{\underline{G}}(z,t)\ \underline{\underline{U}}(t)\vec{r}(t)dt \tag{G-14}$$

where $\underline{\underline{G}}$ is the Green's Function matrix operator determined by the solution of the equation,

$$\left[\frac{d}{dz}\ \underline{\underline{I}} - \underline{\underline{D}}\right]\ \underline{\underline{G}}(z,t) = \delta(z-t)\ \underline{\underline{I}} \tag{G-15}$$

which yields

$$\underline{\underline{G}}(z,t) = e^{\int_o^z D(\xi)d\xi}\left[\theta(z-t)\underline{\underline{I}} - \theta(-t)\underline{\underline{I}} + \underline{\underline{U}}^{-1}(t)\delta(t)\right] \tag{G-16}$$

where $\theta(t)$ is a step function defined by

$$\theta(t) = \begin{cases} +1 & ;\ t \geq 0 \\ 0 & ;\ t < 0 \end{cases} \tag{G-17}$$

Upon substitution of Eq (G-16) into Eq (G-14), the Green's Function solution is

$$\vec{r}(z) = e^{\int_o^z \underline{\underline{D}}(\xi)d\xi} [\vec{r}(0) + \int_o^z \underline{\underline{U}}(t)\vec{r}(t)dt] \tag{G-18}$$

Eq (G-18) may be solved by a perturbation technique to yield the closed form solution

$$\vec{r}(z) = e^{\int_o^z \underline{\underline{D}}(\xi)\, d\xi} [\underline{\underline{I}} + \int_{x_1=0}^{z} \int_{x_2=0}^{x_1} \underline{\underline{B}}(x_1,x_2)dx_2dx_1 +$$

$$\int_{x_{-1}}^{z} \int_{x_2=x_3}^{x_2} \int_{x_4=0}^{x_3} \underline{\underline{B}}(x_1,x_2)\underline{\underline{B}}(X_3,x_4)dx_4 dx_1 + \int\int\int\int\int\int_{x_1=\cdots=x_6}^{zx_1\cdots x_5} \underline{\underline{B}}\,\underline{\underline{B}}\,\underline{\underline{B}}\, dx_6 \cdots dx_1, + \ldots] \vec{r}(o) \tag{G-19}$$

where,

$$\underline{\underline{B}}(\xi,\eta) = e^{\int_o^\xi \underline{\underline{D}}(\gamma)d\gamma} \underline{\underline{U}}(\eta)\, e^{\int_o^\eta \underline{\underline{D}}(\gamma)d\gamma} \tag{G-20}$$

If $1 >> |\underline{\underline{B}}|\, z^2 >> |\underline{\underline{B}}|^2 z^4$, then only the first term need be kept in Eq (G-19). This yields the approximate solution

$$\vec{r} \approx e^{\tilde{\underline{\underline{D}}}(z)} \vec{r}(o) \tag{G-21}$$

where

$$\tilde{\underline{\underline{D}}}(z) = \int_o^z \underline{\underline{D}}(\xi)d\xi \tag{G-22}$$

From Eq (G-4), the solution becomes

$$\vec{\nu} = \underline{P}\, e^{\tilde{\underline{D}}}\, \underline{P}^{-1}(o)\ \nu(o) \tag{G-23}$$

using Eq (G-7) and G-8 for

$$\vec{\nu} = \begin{matrix} V_o(z) \\ V_{-1}(z) \end{matrix} = \frac{Q_{-1}(o)}{\lambda_+(o)-\lambda_-(o)} \begin{bmatrix} A^+ e^{\tilde{D}_{11}} - A^- e^{\tilde{D}_{22}} & -A^+A^-(o)e^{\tilde{D}_{11}} + A^-A^+(o)e^{\tilde{D}_{22}} \\ e^{\tilde{D}_{11}} - e^{\tilde{D}_{22}} & -A^-(o)e^{\tilde{D}_{11}} + A^+(o)e^{\tilde{D}_{22}} \end{bmatrix} \vec{\nu}(o) \tag{G-24}$$

where

$$D_{11} = \lambda_+(z) - \frac{dA^+}{dz}\,\frac{Q_{-1}}{\lambda_+ - \lambda_-} \tag{G-25}$$

$$D_{22} = \lambda_-(z) - \frac{dA^-}{dz}\,\frac{Q_{-1}}{\lambda_+ - \lambda_-} \tag{G-26}$$

In conclusion, it appears that the Green's Function technique is very similar to the JWKB approximation technique. The solutions are identical in 0-order terms and very nearly identical in first-order terms.

A complete application of the boundary conditions for a transmission and reflection hologram is not presented, but results very similar to the JWKB solution are obtained. The technique using Green's Function has been included in order to illustrate the similarity between it and the JWKB solution.

APPENDIX H

DERIVATION OF THE POLARIZATION OF THE WAVE DIFFRACTED BY A HOLOGRAM

The equation for the scattered electric field amplitude from an elemental volume of scatterers is given by

$$\vec{E}_s(\vec{r}) = \frac{k^2}{4\pi} \int_v \frac{e^{ik_1|\vec{r}-\vec{r}'|}}{|\vec{r}-\vec{r}|} \varepsilon_1(\vec{r}')[\hat{n}x\vec{E}_o(\vec{r}')x\hat{n}]d\vec{r}' \qquad \text{(H-1)}$$

Eq (H-1) is taken from Tatarskii's book on atmospheric transmission (Ref. 42). $\vec{E}_o$ is the incident electric field at position $\vec{r}'$ from a source at $\vec{R}$. $\varepsilon_1(\vec{r}')$ is the dielectric constant. This relation is shown in Figure H-1. $\hat{n}$ and $\hat{M}$ are unit vectors. $\hat{M}$ is the direction of the incident wave vector at $\vec{r}'$, and $\hat{n}$ is the direction of the diffracted wave vector.

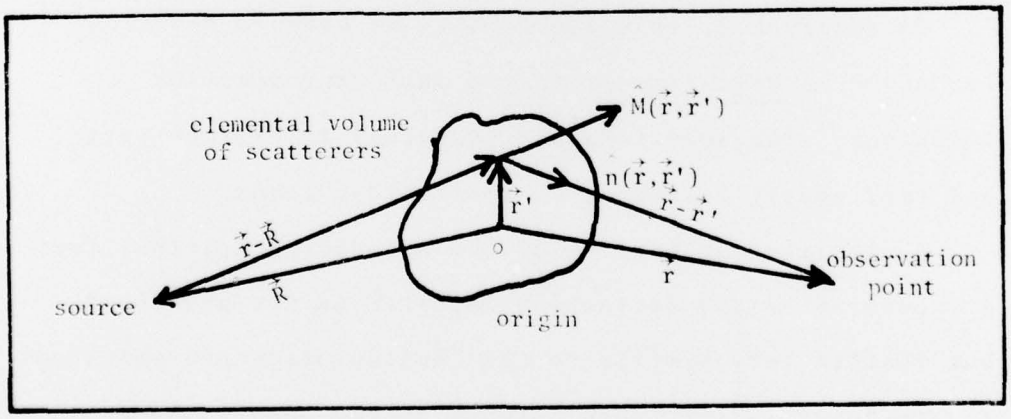

Figure H-1. Relationship of Vectors in the Scattering Process

For a hologram, the diffracted wave vector is determined from the incident wave vector direction by the relation

$$\vec{k}_m = \vec{k}_{2c} + m\vec{K} \tag{H-2}$$

The incident electric field amplitude for the reconstruction wave can be written

$$\vec{E}_{2c} = A_{2c}(\vec{r}', \vec{R}_c)\hat{e}_c(\vec{r}')e^{i\phi_c(\vec{r}')} \tag{H-3}$$

Eqs (H-2) and (H-3) may be substituted into Eq (H-1) to yield the electric field amplitude diffracted into the mth order

$$\vec{E}_m(\vec{r}) = \frac{k_c^2}{4\pi}\int \frac{e^{ik_c|\vec{r}-\vec{r}'|}}{|\vec{r}-\vec{r}'|}\varepsilon_1(\vec{r}')A_{2c}(\vec{r}', \vec{R}_c)e^{i\phi_c(\vec{r}')}[\hat{k}_m x \hat{e}_c x \hat{k}_m]d^3\vec{r}' \tag{H-4}$$

If the scattering volume is taken to be a very small volume surrounding a single hologram fringe, then as the first approximation, the $\hat{e}_c$ and $\hat{k}_m$ are independent of position, $\vec{r}'$, and may be removed from the integral. Therefore, Eq (H-4) becomes

$$\vec{E}_m(\vec{r}) = \vec{e}_m E_m(\vec{r}) \tag{H-5}$$

where

$$\vec{e}_m = \hat{k}_m x \hat{e}_c x \hat{k}_m \tag{H-6}$$

and

$$E_m(\vec{r}) = \frac{k_c^2}{4\pi} \int_V \frac{e^{ik_c|\vec{r}-\vec{r}'|}}{|\vec{r}-\vec{r}'|} \varepsilon_1(\vec{r}') A_{2c}(\vec{r}', \vec{R}_c) e^{i\phi_c(\vec{r}')} d^3\vec{r}' \tag{H-7}$$

$\vec{e}_m$ is the polarization direction of the scattered light into the mth diffracted order. $E_m(\vec{r})$ is the diffraction amplitude to be calculated in the main body of the dissertation using coupled wave theory.

Of particular concern is the evaluation of the dot product, $\hat{e}_o \cdot \hat{e}_{-1}$, between the polarizations of the zero-order and the first-diffracted order. This is accomplished using Eq (H-6), but first, Eq (H-6) must be normalized.

$$|\vec{e}_m| = |\hat{k}_m \times \hat{e}_c \times \hat{k}_m| \tag{H-8}$$

using the vector identity

$$\vec{A} \times \vec{B} \times \vec{C} = (\vec{A}\cdot\vec{C})\vec{B} - (\vec{A}\cdot\vec{B})\vec{C} \tag{H-9}$$

$$|\hat{k}_m \times \hat{e}_c \times \hat{k}_m| = |\hat{e}_c - (\hat{k}_m \hat{e}_c)\hat{k}_m| \tag{H-10}$$

The right hand side of Eq (H-10) becomes

$$|\hat{e}_c - (\hat{k}_m \hat{e}_c)\hat{k}_m| = \sqrt{1-2(\hat{k}_m\cdot\hat{e}_c)^2 + (\hat{e}_c\cdot\hat{k}_m)^2} = \sqrt{1-\cos^2(\hat{e}_c,\hat{k}_m)} \tag{H-11}$$

$$|\vec{e}_m| = |\sin\Psi_m| \tag{H-12}$$

where Ψ_m is the angle between the wave vector of the mth diffracted order and the incident polarization.

Therefore, the unit polarization vector for the mth diffracted order becomes

$$\hat{e}_m = \frac{\hat{k}_m \times \hat{e}_c \times \hat{k}_m}{|\sin\Psi_m|} \tag{H-13}$$

using the fact that $\hat{e}_c = \hat{e}_o$ and identity (H-9), the dot product becomes

$$\hat{e}_o \cdot \hat{e}_{-1} = \frac{\hat{e}_o \cdot (\hat{e}_o - (\hat{k}_{-1} \cdot \hat{e}_o)\hat{k}_{-1})}{|\sin\Psi_{-1}|} \tag{H-14}$$

therefore,

$$\hat{e}_o \cdot \hat{e}_{-1} = |\sin\Psi_{-1}| \tag{H-15}$$

Eq (H-15) is used in Chpater III in the derivation of the coupled wave equations which describe holographic diffraction. While Kogelnik included a polarization term $\hat{e}_o \cdot \hat{e}_{-1}$ in his coupled wave equations, he did not derive an expression relating it to known quantities. Ψ_{-1} is a known, apriori angle. It is the angle between the incident wave polarization vector and the wave vector of the diffracted light. The incident polarization is a given quantity and the diffracted wave vector is determined from Eq (H-2) for m=-1.

APPENDIX I

REPRESENTATION OF THE POLARIZATION OF A SPHERICAL WAVE

It has been assumed in Appendix A that the object (o), reference (r), and reconstruction (c) waves are spherical waves emanating from pin-holes. In practice, the polarization of these spherical waves is determined by a polarizing element located at some point in the wave prior to diffraction at the pin-hole. This is shown schematically in Figure I-1. It is assumed that a wave is incident upon the pin-hole and is propagating in the $-\vec{R}_j$ direction, where $\vec{R}_j$ is the vector to the position of the jth-pin-hole with respect to the coordinates defined in Appendix A.

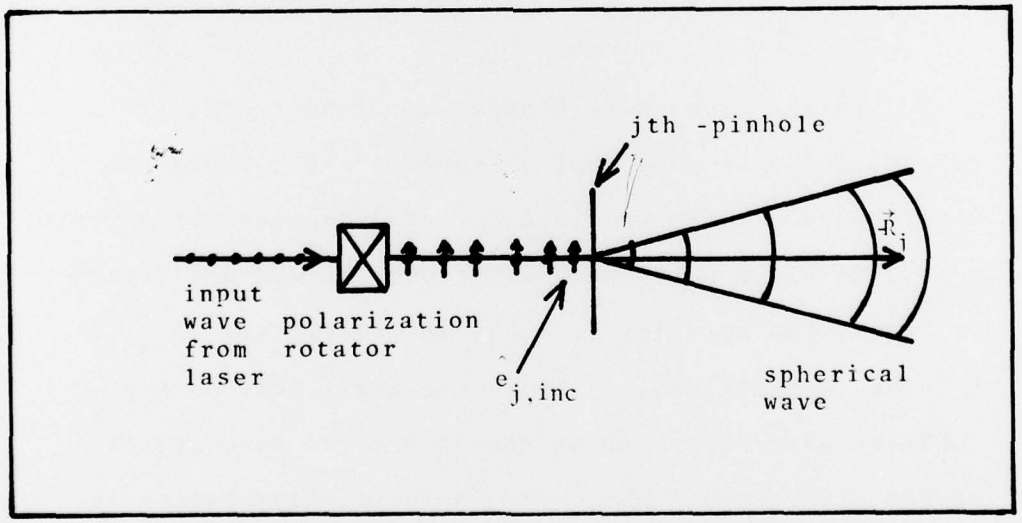

Figure I-1. Polarization of Spherical Wave

The polarization of the spherical wave diffracted by the pin-hole is determined by the polarization of the plane wave incident upon the pin-hole. This polarization is determined by Eq (H-13), developed in Appendix H, to be

$$\hat{e}_j = \frac{\hat{k}_j \times \hat{e}_{j,inc} \times \hat{k}_j}{|\sin(\hat{e}_{j,inc}, \hat{k}_j)} \qquad \text{(I-1)}$$

where j refers to the j=o, r, c spherical waves, $\hat{e}_{j,inc}$ is the unit polarization vector of the plane wave incident upon the jth pin-hole defined with respect to the $\hat{x}'$, $\hat{y}'$, $-\vec{R}_j$) coordinate system in Figure I-2.

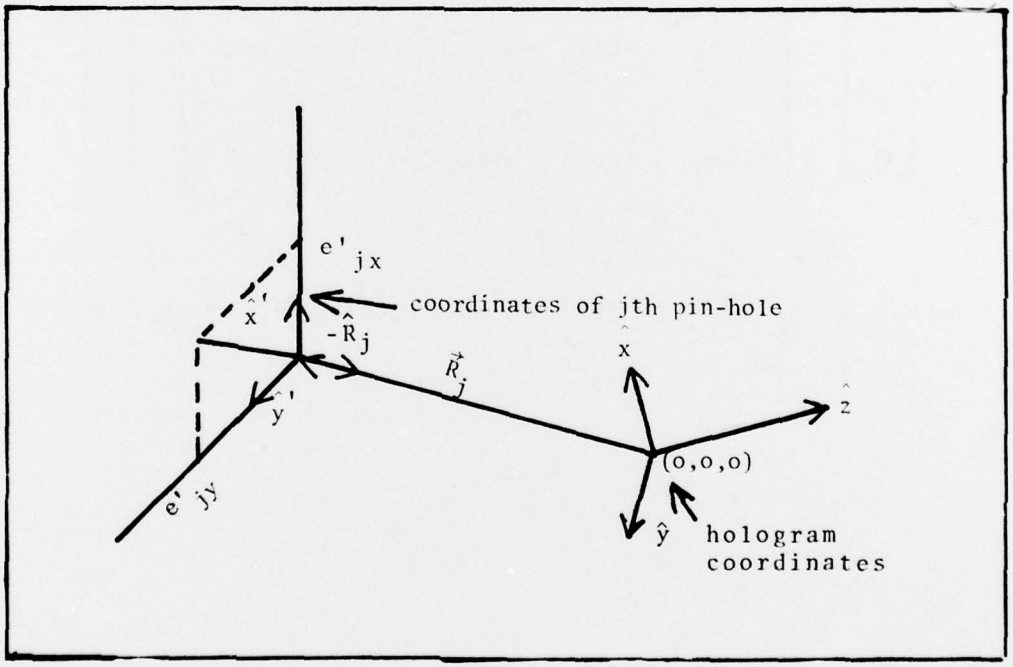

Figure I-2. The Coordinates of the Polarization of the Plane Wave Incident at the jth Pin-hole

Since $\hat{e}_{j,inc}$ is normal to the jth pin-hole, it is defined by two polarization components e'_{jx} and e'_{jy} shown in Figure I-2. $\vec{k}_j$ is defined with respect to the (x,y,z) coordinates to be

$$\vec{k}_j = \frac{k_j(\vec{r}-\vec{R}_j)}{|\vec{r}-\vec{R}_j|} \tag{I-2}$$

In order to evaluate Eq (I-1), $\hat{e}_{j,inc}$ needs to be transformed from the $(\hat{x}', \hat{y}', -\hat{R}_j)$ coordinate system to the (x,y,z) system, this is accomplished by a two rotations of the basis (x,y,z). This basis transformation is

$$\begin{bmatrix} \hat{x}' \\ \hat{y}' \\ -\hat{R}_j \end{bmatrix} = \begin{bmatrix} \cos\Psi_j & \sin\Psi_j \sin\phi_j & -\sin\Psi_j\cos\phi_j \\ 0 & \cos\phi_j & \sin\phi_j \\ \sin\phi_j & -\cos\Psi_j \sin\phi_j & \cos\Psi_j \cos\phi_j \end{bmatrix} \begin{bmatrix} \hat{x} \\ \hat{y} \\ \hat{z} \end{bmatrix} \tag{I-3}$$

where Ψ_j, and ϕ_j, are defined in Figure I-3. $\phi_j > 0$ for $-R_{jy} > 0$ and $\Psi_j > 0$ for $-R_{xj} > 0$.

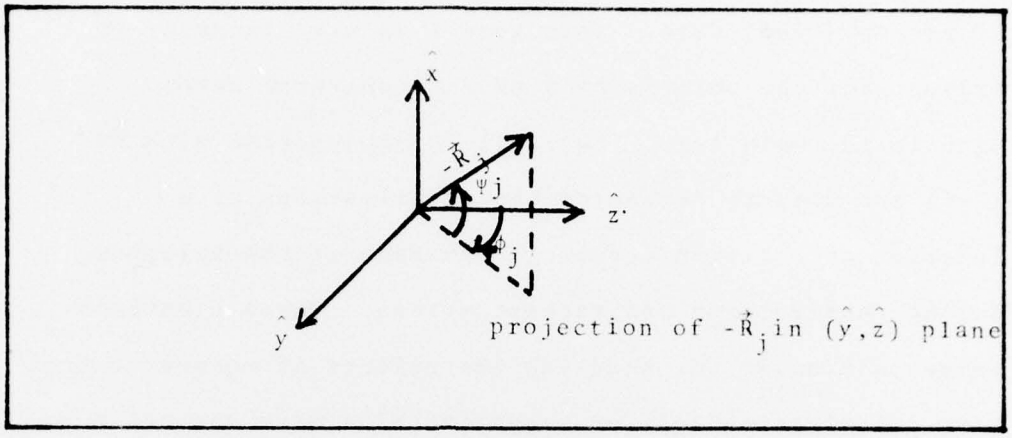

Figure I-3. Definition of ϕ_j and Ψ_j

From Figure I-3, it is clear that

$$\sin\Psi_j = \frac{-R_{jx}}{|\vec{R}_j|} \tag{I-4}$$

$$\sin\phi_j = \frac{-R_{jy}}{\sqrt{R_{jy}^2+R_{jz}^2}} \tag{I-5}$$

From Figure I-2, the equation for $\hat{e}_{j,inc}$ is obtained to be

$$\hat{e}_{j,inc} = e'_{jx}\,\hat{x}' + e'_{jy}\,\hat{y}' \tag{I-6}$$

$e_j'_x$ and $e_j'_y$ are given quantities. By substitution of Eq (I-5) for $\hat{x}'$ and $\hat{y}'$ into Eq (I06), the Eq for $\hat{e}_{j,inc}$ in terms of the $(\hat{x},\hat{y},\hat{z})$ basis is obtained,

$$\hat{e}_{j,inc} = \hat{x}[e_j'_y\cos\Psi_j] + \hat{y}[e_j'_x\sin\Psi_j\sin\phi_j + e'_{jy}\cos\phi_j] + \hat{z}[-e'_{jx}\sin\Psi_j\cos\phi_j + e'_{jy}\sin\phi_j] \tag{I-7}$$

which can be used in Eq (I-1) to determine the polarization of the spherical wave. This result is used in order to account for the polarization of the spherical waves used in the main text. Eq (I-1) in conjunction with Eq (I-7) are used to determine the polarizations as a function of position across the surface of the hologram during construction and reconstruction. These equations serve as a basis for handling the effects of reconstruction wave polarization and for reconstruction wave vectors out of the plane of incidence of the original object and reference wave vectors.

☆ U. S. GOVERNMENT PRINTING OFFICE: 1977 — 757-001/472